NETWORK DYNAMICS IN ANALOG FLUIDIC SYSTEMS

A THESIS

Presented to

The Faculty of the Graduate Division

By

Allan James Lake

In Partial Fulfillment

of the Requirements for the Degree

Master of Science

in Mechanical Engineering

Georgia Institute of Technology

March 1973

NETWORK DYNAMICS IN ANALOG FLUIDIC SYSTEMS

Approved:

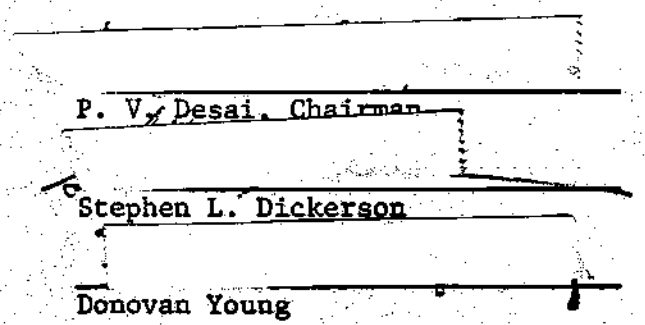

P. V. Desai, Chairman

Stephen L. Dickerson

Donovan Young

Date approved by Chairman: March 8, 1973

ACKNOWLEDGMENTS

My heartfelt thanks to Dr. Perry Desai for his patience and guidance, to my wife, Linda, for her good humor and encouragement, and to my parents, to whom I owe everything.

TABLE OF CONTENTS

TABLE OF CONTENTS (Continued)

LIST OF ILLUSTRATIONS

LIST OF ILLUSTRATIONS (Continued)

LIST OF ILLUSTRATIONS (Continued)

LIST OF ILLUSTRATIONS (Concluded)

NOMENCLATURE

A	area
C_c	control capacitance
C_l	load capacitance
C_o	output capacitance
d	diameter
G	amplitude ratio
g	acceleration due to gravity
K_a	amplifier gain constant
L_c	control inductance
L_o	output inductance
l	connecting line length
l_c	interaction region length
M	magnitude ratio
P_c	control pressure
P_i	input pressure
q	flow rate
R_c	control resistance
R_l	load resistance
R_o	output resistance
r	radius
s	Laplace operator
t_d	transport delay constant
v	velocity of sound

v_c	average fluid velocity in interaction region
v_t	average fluid velocity in connecting line
Z_c	control impedance
Z_l	load impedance
Z_o	output impedance
μ	absolute viscosity
ξ	damping ratio
ρ	density
ϕ	phase angle
ω	angular frequency
ω_p	pole break frequency
ω_z	zero break frequency

SUMMARY

The absence of the series capacitor and inductor causes sizeable difficulties in the design of analog fluidic networks. In general, systems directly analogous to passive R-L-C electrical networks cannot be used. An effective procedure consists of combining in series known basic networks which generate elementary or component transfer functions.

This study is concerned with the dynamic analysis and physical implementation of basic analog fluidic networks. A previously validated electrical equivalent model of the vented proportional amplifier is used in the derivation of network transfer functions. The model serves to represent the dynamics of the amplifier and its associated connectors. Simplified transfer functions, which neglect amplifier and connector dynamics, are also presented and analyzed. Pole-Zero locations in terms of system parameters, a discussion of limits on their positioning and generalized Bode and Pole-Zero diagrams are given. From the unsimplified transfer functions, the degradation of simplified transfer function performance at higher frequencies has been discerned.

The dynamic testing of a few selected networks has been conducted in order to demonstrate the relative accuracies of simplified and unsimplified transfer functions. An important conclusion has been that the capacitance and path length of necessary connectors between network elements prevents accurate implementation of many useful transfer functions.

CHAPTER I

INTRODUCTION

1.1 Analog Fluidic Networks

Since its introduction in 1959 by the Diamond Ordnance Fuze Laboratories (now the Harry Diamond Laboratories), fluidics technology has matured considerably. Digital applications in particular have grown from the stage of feasibility demonstration to successful use in industry.

Analog fluidics has not fared as well, commercial applications at present being far from plentiful. Initial problems involved components; it took several years before analog fluidic amplifiers with workable characteristics could be designed and mass produced. At present, such devices are readily available.

Given these components and their major advantages of reliability, safety in explosive environments, and resistance to high temperatures and radiation, it is surprising that analog fluidics is not experiencing more applications. One significant obstacle is the complex nature of fluid systems analysis.

Analog fluidic amplifiers are, in general, distributed parameter, nonlinear, coupled, multiport elements. To consider them in their total complexity is a staggering problem. The use of graphical characteristics for nonlinear, static analysis and linear electrical equivalent circuits for small signal dynamic analysis have proved to be

successful approaches.

Even with these techniques, obstacles for the network designer still exist. Implementing a specific transfer function is not a straightforward matter of adopting the well established electrical R-L-C network. Fluidic counterparts of two very basic electronic components do not exist--the series capacitor and the inductor.

Briefly, a fluidic capacitor stores energy by virtue of the compressibility of the fluid medium (usually air). Ambient pressure being the network ground potential, all fluidic capacitors are in parallel to ground. Fluidic inductance is a consequence of the inertia of the medium. However, air is both viscous and compressible. Viscosity generates fluidic resistance and compressibility fluidic capacitance. Since these latter effects are typically more significant than the effects of inertia, it is impossible to produce a fluidic component whose dominant characteristic is inductance. For these reasons, transfer function implementation and the design of complex analog fluidic systems have been something of an art, until recently, have proceeded on an intuitive basis.

Boddy[1] has presented an analysis of fluidic networks to implement certain elementary transfer functions, a combination of which results in more complex configurations. Theoretically, any rational, finite transfer function containing no more zeros than poles and having only left hand plane poles may be produced by his method. This paper, however, provides only one network each to generate several elementary transfer functions. Other networks often exist which

prove more satisfactory in certain circumstances. Furthermore, Boddy's amplifier model does not include such dynamic characteristics as transport delay and inductive and capacitive effects. Consequently, the network transfer functions yield no information on the degradation of system performance with increasing frequency due to amplifier dynamics.

Parker and Addy[2] have also presented networks for the implementation of elementary transfer functions. However, the few networks which they presented cannot be combined to make all arbitrary configurations. For example, no transfer functions with either complex poles or complex zeros can be implemented. In addition, amplifier dynamics are neglected.

Another approach to the problem is taken by Doherty.[3] He uses high gain "gain blocks" and fluidic "operational amplifiers" and presents a generalized approach to transfer function implementation. These specialized components tend to exhibit excessive phase lags at higher frequencies and are quite expensive at the present time. They will not be considered here.

Other networks[4,5,6,7] have appeared from time to time for the implementation of certain transfer functions, by and large as minor components of more complex systems. Without exception, these presentations share the previously discussed shortcomings, namely the neglect of amplifier dynamics and lack of provision for the generation of many pole-zero configurations.

1.2 Statement of the Problem

This study is intended to be a more comprehensive treatment of

the problem of fluidic transfer function implementation, with Boddy's approach as a basis. A literature search has produced many additional networks, some of these being singularly useful. These are analyzed to augment the options of the network designer. An electrical equivalent of the vented beam deflection amplifier is utilized to describe amplifier and associated connector dynamics. A "complete transfer function" is then derived for each network. At low frequencies and for small geometries, amplifier dynamics may be neglected and a simplified transfer function is assumed to adequately represent system performance. This transfer function is referred to as the "reduced transfer function" and is presented for each network.

A Bode plot and a Pole-Zero diagram for each reduced transfer function is given. In addition, a discussion of Pole-Zero placement limitations is included. The reduced transfer function is the transfer function to be implemented. The complete transfer function is capable of describing the degradation of reduced transfer function performance at higher frequencies due to amplifier and connecting line dynamics.

CHAPTER II

THE VENTED BEAM DEFLECTION AMPLIFIER

2.1 The Basic Amplifier Geometry

The amplifier considered in this analysis is of vented beam deflection type with or without center dump. It is perhaps the most widely used analog fluidic amplifier because of its many desirable characteristics (large linear range, high pressure gain, high signal to noise ratio and relative independence of input characteristics on output loading). In addition, beam deflection amplifiers have either single sided or push-pull capabilities.

In Figures 1a and 1b, respectively, are shown diagrams of vented proportional amplifiers without and with the center dump. The power jet is controlled by the control jets by virtue of a momentum interchange mechanism. The power jet is deflected toward one output port or the other in response to pressure inputs. In this analysis only pressure amplification is of concern. A load, i. e. some restrictions of the output flow, causes a pressure build-up in the output ports. The center dump allows stable operation at large loads.

2.2 The Lumped Parameter Model

Figure 2 shows a lumped-parameter electrical equivalent circuit of the vented proporational amplifier without the center dump, as

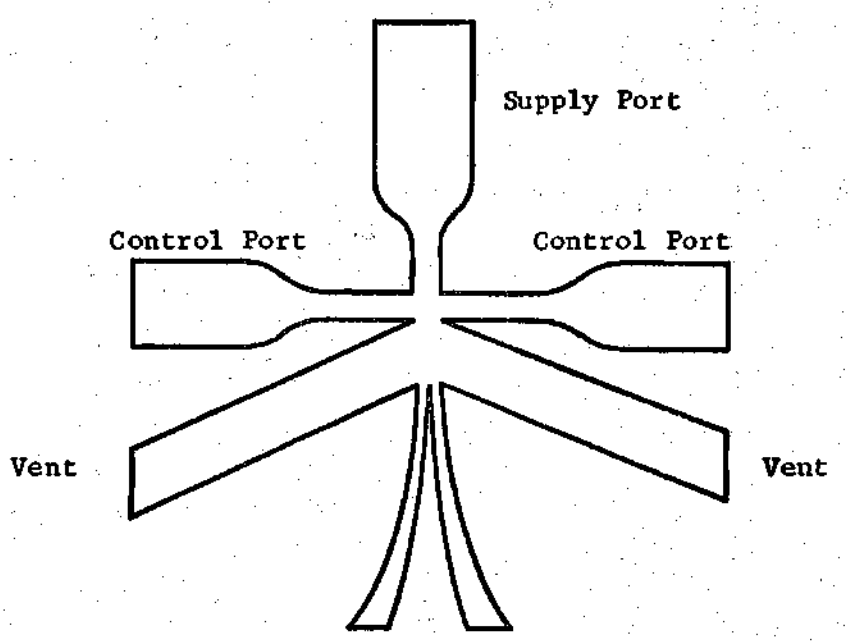

Figure 1a. The Vented Proportional Amplifier.

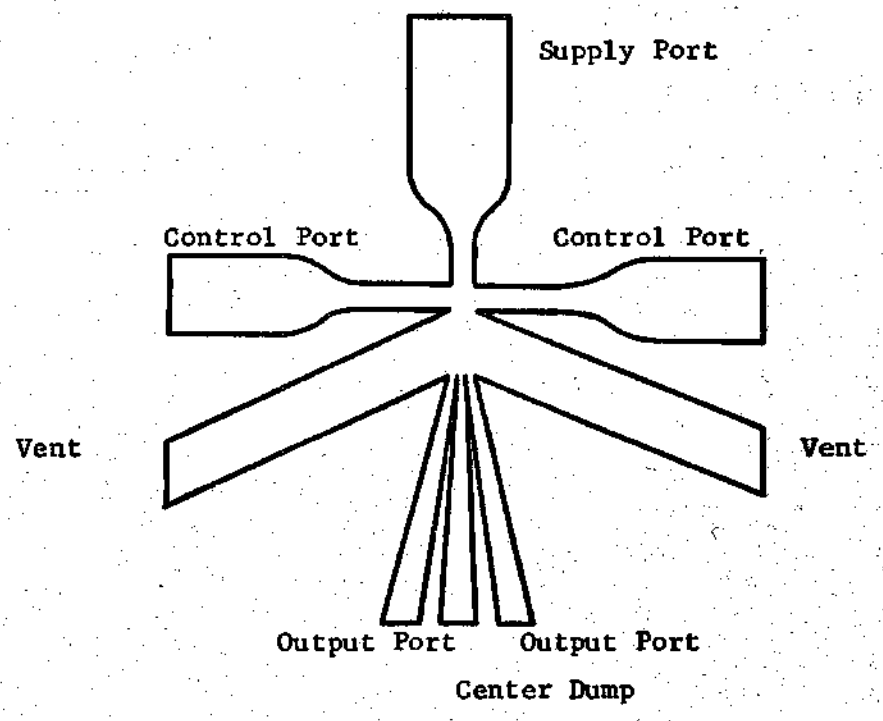

Figure 1b. The Center Dump Proportional Amplifier.

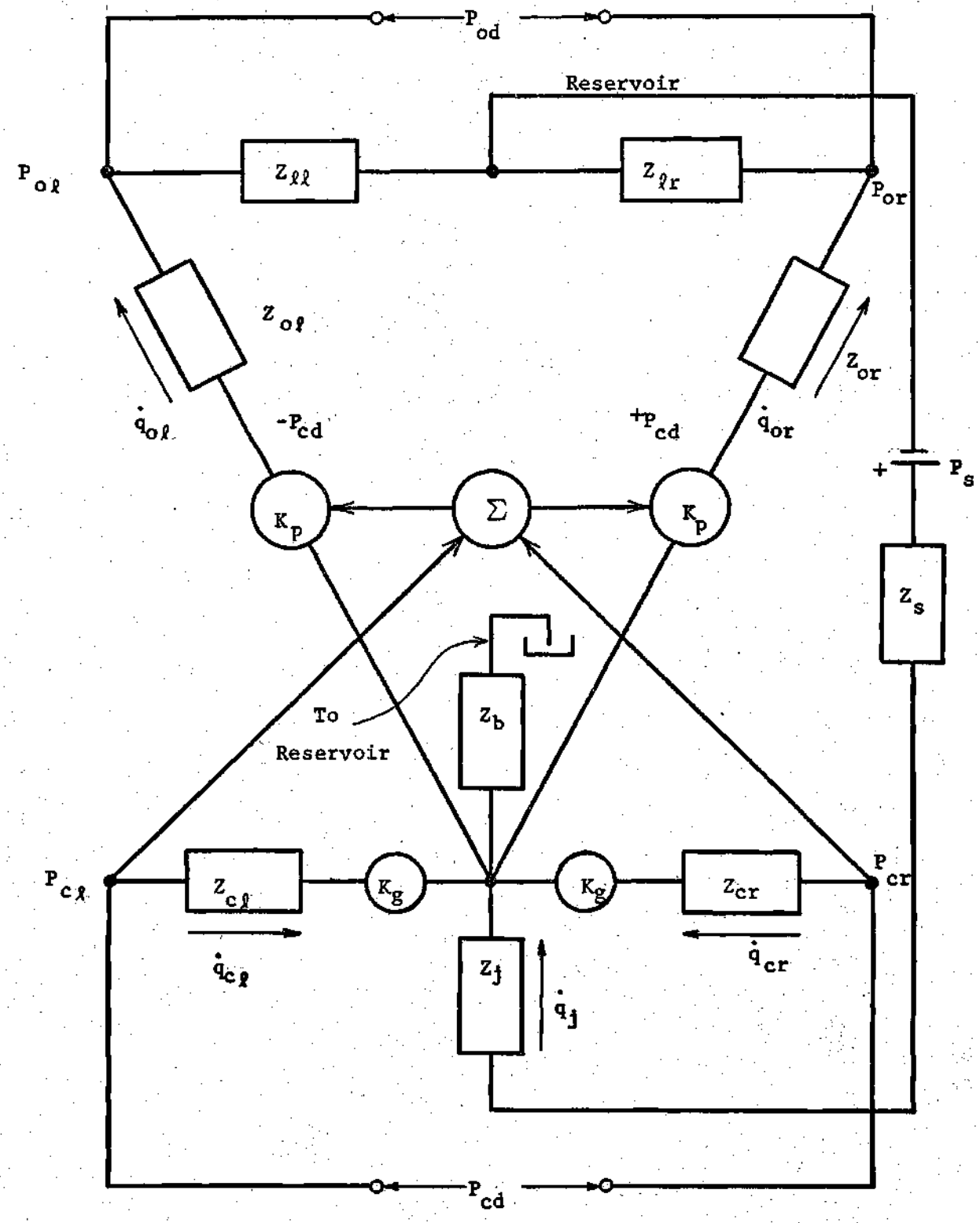

Figure 2. A Lumped Electrical Model for the Vented Jet-Interaction Amplifier.

proposed by Belsterling.[8] Each significant component and parameter in the proportional amplifier is represented and the layout is in direct analogy to the physical device. The lumped-parameter model is valid for low operating frequencies and for relatively small geometries. The present analysis is restricted to such a lumped parameter model of the amplifier, which is applicable to most analog fluidic systems. The analysis for the center dump configuration proceeds along similar lines.

In Figure 2, Z_s is the internal impedance of the voltage or pressure source. $Z_{c\ell}$, Z_{cr}, $Z_{o\ell}$, and Z_{or}, are respectively the left and right input and output impedances of the amplifier. Z_j is the power nozzle impedance and Z_b is the bleed port impedance. $Z_{\ell\ell}$ and $Z_{\ell r}$ are the parallel to ground load impedances on the left and right outputs respectively. K_g is the zero impedance voltage generator due to suction caused by power jet entrainment. K_p is the amplification factor of the device. P_{cd} and P_{od} are respectively the input and output differential signals.

Even in well designed vented amplifiers, a small amount of internal feedback exists. That is, back up pressure in the output legs due to loading affects the interaction between control and power jet streams. This effect is small and is neglected here.

The model is quite general, save for the lumped parameter assumption and the neglect of internal feedback. Each of the circuit parameters is nonlinear. If the nonlinearities were known a complete description of amplifier behavior would become available. Unfortunately,

the nonlinearities are not easily described and a linearized model for small variations about an operating point must be used.

Using Δ to indicate small incremental changes, the equations for the left and right output circuits may be written by inspection as

$$P_s = \dot{q}_j\ (Z_s + Z_j) - K_p\ P_{cd} + (\dot{q}_o - \Delta\dot{q}_o)\ (Z_{o\ell} + Z_{\ell\ell}) \tag{2.1}$$

for the left branch, and

$$P_s = \dot{q}_j\ (Z_s + Z_j) + K_p\ P_{cd} + (\dot{q}_{or} - \Delta\dot{q}_{or})\ (Z_{or} + Z_{\ell r}) \tag{2.2}$$

for the right branch.

In general, for symmetrical operation

$$\Delta P_{c\ell} = \Delta P_{cr} = \Delta P_c,\ \Delta\dot{q}_{c\ell} = \Delta\dot{q}_{cr} = \Delta\dot{q}_c \text{ and } Z_{c\ell} = Z_{cr} = Z_c. \tag{2.3}$$

A substitution of equations (2.3) into equations (2.1) and (2.2) yields

$$2\Delta P_c = 2\Delta\dot{q}_c\ Z_c. \tag{2.4}$$

For the control circuits, the equations become

$$P_{c\ell} + \Delta P_{c\ell} = (\dot{q}_{c\ell} + \Delta\dot{q}_{c\ell})\ Z_{c\ell} - (\dot{q}_j + \Delta\dot{q}_j)\ Z_j\ K_g \tag{2.5}$$

for the left branch, and

$$P_{cr} - \Delta P_{cr} = (\dot{q}_{cr} - \Delta\dot{q}_{cr})\ Z_{cr} - (\dot{q}_j + \Delta\dot{q}_j)\ Z_j\ K_g \tag{2.6}$$

for the right branch.

In general, for symmetrical operation,

$$\Delta P_{c\ell} = \Delta P_{cr} = \Delta P_c,\ \Delta \dot{q}_{c\ell} = \Delta \dot{q}_{cr} = \Delta \dot{q}_c \text{ and } Z_{c\ell} = Z_{cr} = Z_c. \qquad (2.7)$$

Substitution of equations (2.7) into equation (2.5) and (2.6) gives

$$2\Delta P_c = 2\Delta \dot{q}_c Z_c. \qquad (2.8)$$

A linearized electrical circuit representing these equations (2.4) and (2.8) may be drawn directly, as shown in Figure 3. Note that the linearized, incremental circuit eliminates bias or reference conditions at null state, the supply pressure, and the bleed impedance.

At low frequencies, when inductive and capacitive effects are negligible, each impedance in the model may be approximated by a pure resistance. At higher frequencies, the circuit in Figure 4 must be used. Here each impedance is represented by a resistor, a capacitor, and an inductor. The e^{-st_d} term is included to represent pure transport delay in the amplifier and its associated connectors. L_c, C_c, and R_c are the inductance, capacitance and resistance, respectively, of the input connectors and control ports combined. The inductor is in series, while the resistor and capacitor are in parallel to ground as they act between the input pressure and ambient. L_o, C_o and R_o are the inductance, capacitance and resistance, respectively, of the output connectors and ports combined. Here both the inductor and the resistor are in series, while the capacitor, as always, is in shunt to ground. The load resistance and capacitance are in shunt to ground, loads typically being the input connectors and

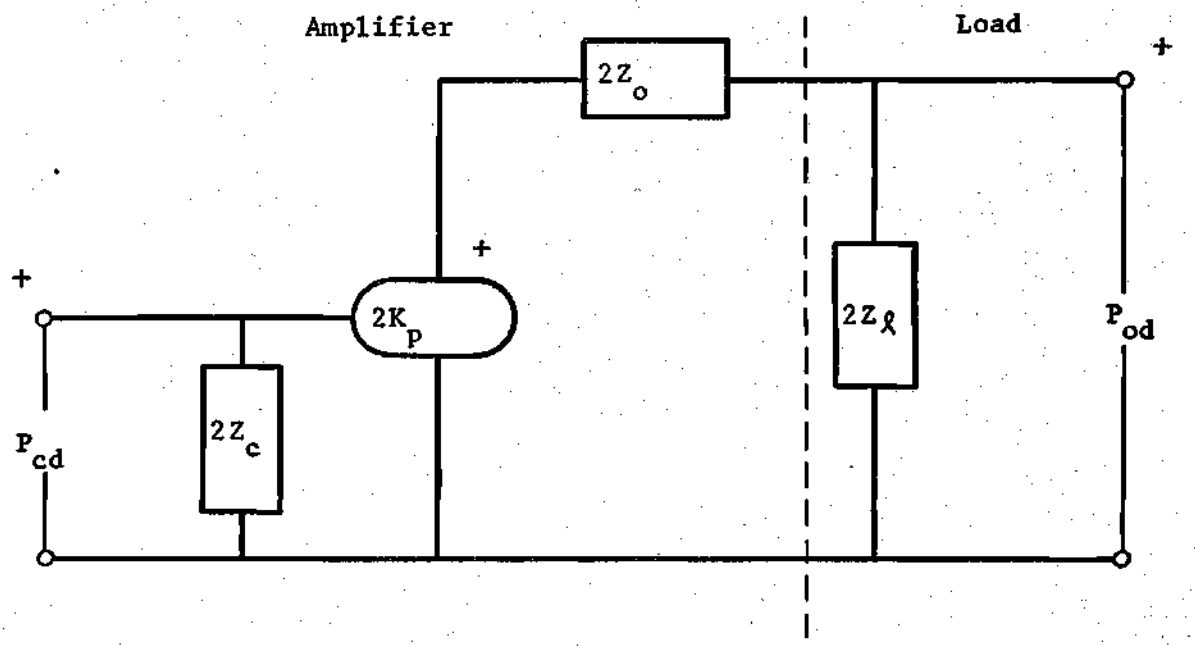

Figure 3. Linearized Small-Signal Equivalent Circuit for the Vented Jet-Interaction Amplifier (Valid for Static and Low Frequency Behavior).

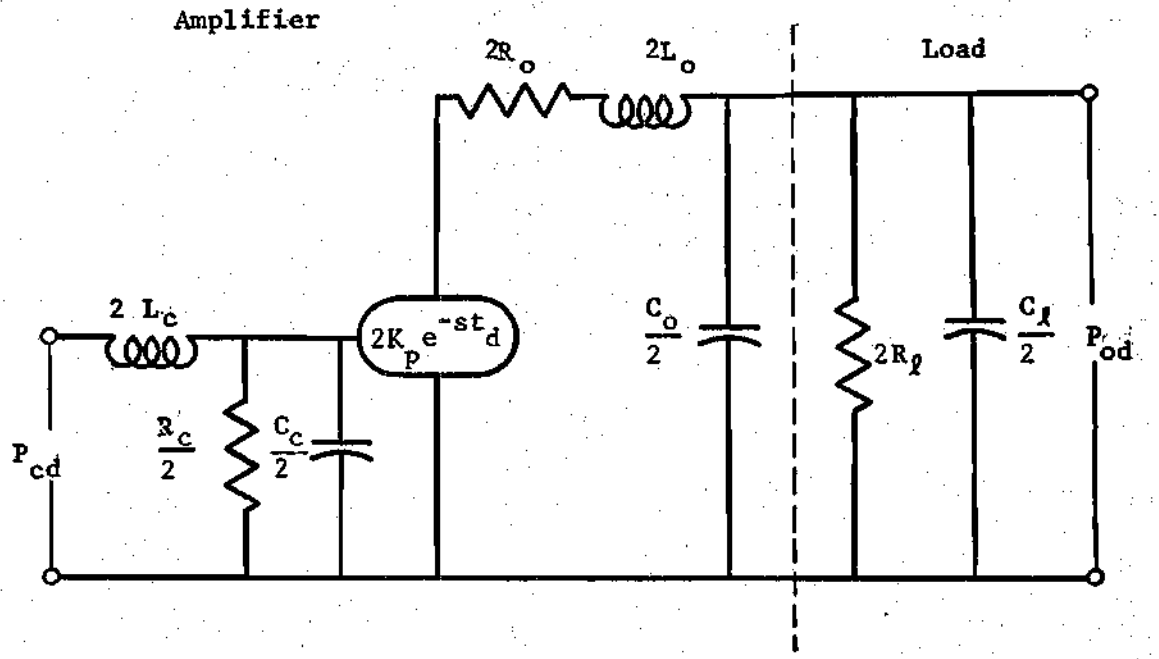

Figure 4. Linearized Small-Signal Equivalent Circuit for Vented Jet-Interaction Amplifier (Valid to 400 Hz).

ports of another amplifier, fluidic resistors venting to ambient, or both.

2.2.1 Resistance

Fluidic resistance is due to fluid friction. In laminar flow elements or in connecting lines resistance is linear, with pressure drop being directly proportional to flow rate. In amplifier control and output ports, resistance is nonlinear.

R_c is the resistance of the input connectors and control ports combined. The port resistance is that due to turbulent flow and its value is obtained from an experimentally derived curve of input pressure versus flow at a constant bias level, the value needed being the slope of this curve at the operating point pressure. The input connector resistance is obtained from the Hagen-Poiseuille equation

$$R = \frac{\Delta P}{\Delta \dot{q}} = \frac{128\mu}{\pi d^4} \qquad (2.9)$$

where μ is the fluid viscosity and d is the line inside diameter.

R_o is the combined resistance of the output port and connector. The output port resistance is the slope of the output pressure versus flow curve at a fixed control signal. R_ℓ is the resistance of the load resistor and its associated connector. The load resistor may be a laminar flow element or the turbulent control port of a second amplifier.

2.2.2 Capacitance

A fluidic capacitor is a volume, either an incidental connector

volume or an external one intentionally placed. The isothermal relation for capacitance is given as $C = V/P_{abs}$. The operating point absolute pressure in the volume is used in its evaluation.

It might appear that at higher frequencies the adiabatic expression for capacitance, $C = V/k\ P_{abs}$, is more realistic. However, Rohman and Grogan[10] have demonstrated that the isothermal assumption is more accurate due to the relatively large flow rates through pneumatic capacitors.

2.2.3 Inductance

Fluidic inductance is given by $L = \frac{\rho \ell}{A_{eff}}$ where ρ is fluid density, ℓ is inductor length and A_{eff} is effective inductor area, usually taken as

$$A_{eff} = \frac{A_{in} - A_{out}}{\ell n\ (A_{in}/A_{out})} \qquad (2.10)$$

In a connecting line, $A_{eff} = A$, the cross sectional area of the connector.

2.2.4 Pressure Amplification Factor

The pressure amplification factor K_p is the slope of the output differential pressure versus control differential pressure curve at a constant output flow. This is the maximum pressure gain that an amplifier could deliver if there were no loading effects. K_p must be experimentally determined.

2.2.5 The Transport Delay Constant

In fluidic systems, it takes a finite period of time for a pressure signal to traverse the distance between input and output. In a transmission line, the signal travels at the velocity of sound in the

fluid medium plus the mean velocity of the medium. In the interaction region of a proportional amplifier, the signal travels only at the average velocity of the fluid in the interaction region. An expression may thus be written for signal transmission time through an amplifier-connecting line system as

$$t_d = \frac{\ell}{v + v_t} + \frac{\ell_c}{v_c} \quad , \tag{2.11}$$

where t_d = total signal transmission time,

ℓ = connecting line length,

ℓ_c = characteristic length of interaction region,

v = velocity of sound in transmission line,

v_t = average velocity of fluid in the transmission line,

and v_c = average velocity of fluid in interaction region.

Since three jets of different average velocities meet in the interaction chamber, exact expressions for ℓ_c and v_c are difficult to determine. A good approximation is to use the average velocity of the power jet for v_c and the distance from the power nozzle to the opposite side of the interaction chamber as ℓ_c. v_c can be calculated from the nozzle dimensions and a measurement of supply flow rate at the operating point supply pressure. The transfer function for pure transport delay is

$$\frac{\theta_o}{\theta_i} = e^{-st_d} = e^{-j\omega t_d} = t_d - j \sin t_d \tag{2.12}$$

The phase angle is

$$\phi = -\tan^{-1}\left(\frac{\sin\omega t_d}{\cos\omega t_d}\right) = -\omega t_d. \qquad (2.13)$$

The gain is constant at unity.

A generalized plot of magnitude G and phase ϕ versus frequency for the phase transport delay transfer function is shown in Figure 5. Phase lag due to transport delay is seen to increase linearly with frequency.

The lumped electrical equivalent amplifier model presented in Figure 4 has been experimentally validated to above 400 Hz[11]. A comparison is now made of lumped parameter capacitive and inductive reactances to demonstrate that for the geometries and frequencies of interest in this analysis, inductance may be neglected. Fluidic inductance for a connecting line was previously defined as $L = \frac{\rho \ell}{A}$. Typical values are $\rho = 1.15 \times 10^{-7} \frac{\text{lbf - sec}^2}{\text{in}^4}$, $A = .0123\ \text{in}^2$, and $\ell = 6$ in. Inductive reactance is given by $X_L = \omega L$. At $\omega = 100$ Hz or 628 rad/sec, $X_L = 3.52 \times 10^{-2} \frac{\text{lbf - sec}}{\text{in}^5}$.

Fluidic capacitance was defined previously as $C = \frac{V}{P_{abs}}$. The volume of the above inductor is $V = .0738\ \text{in}^3$. At $P_{abs} = 14.7 \frac{\text{lbf}}{\text{in}^2}$, $C = 5.02 \times 10^{-3} \frac{\text{in}^5}{\text{lbf}}$. Capacitive reactance is given by $X_c = \frac{1}{\omega C}$. At $\omega = 628$ rad/sec, $X_c = 3.17 \times 10^{-1} \frac{\text{lbf - sec}}{\text{in}^5}$. The ratio of inductive to capacitive reactance is then $\frac{X_L}{X_C} = \frac{3.52 \times 10^{-2}}{3.17 \times 10^{-1}} = 0.11$.

An examination of the relations for inductive and capacitive reactances shows that increasing line length as well as frequency increases X_L, while decreasing X_C. For a typical network, a serious degradation of system performance will occur by 100 Hz due to transport

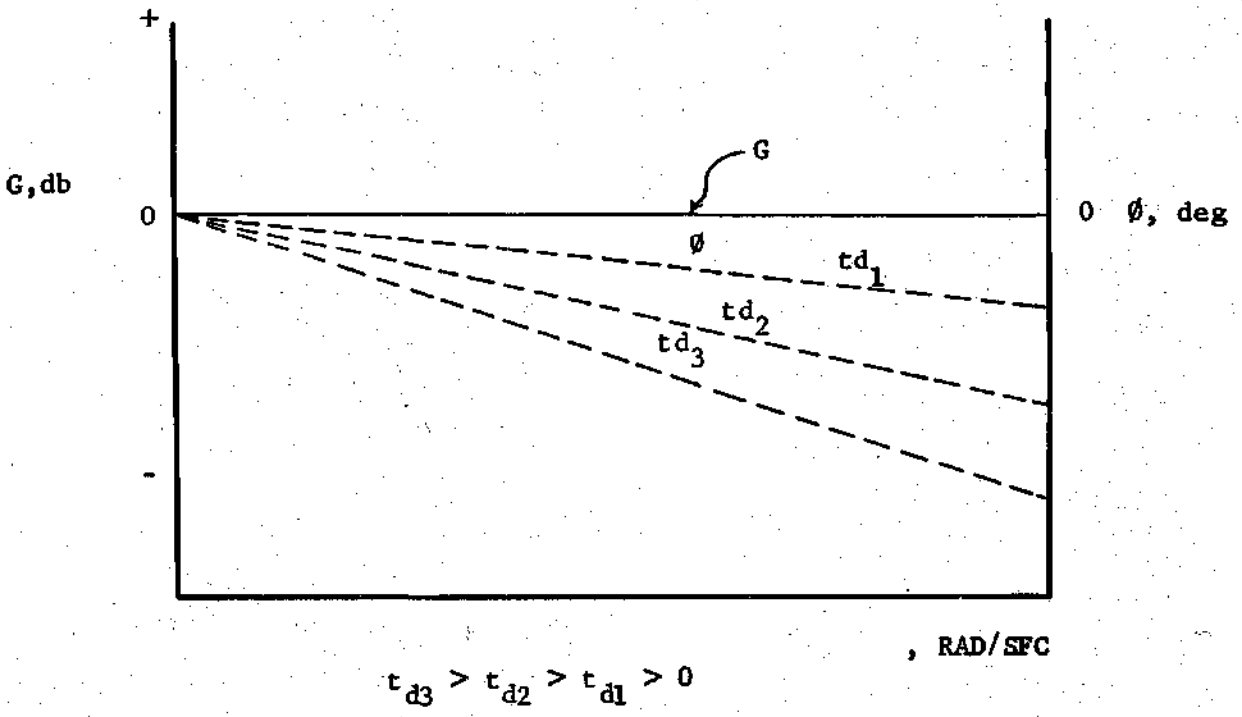

Figure 5. Magnitude and Phase Versus Frequency for e^{-st_d} with t_d as a Parameter.

delay. In addition, the 6 in connector length used in the above calculations is a large value. An untypically high X_L/X_C ratio is then obtained. The ratio is still low enough to justify the neglect of inductance, but will be considered as the upper limit of negligible inductance. In the remaining part of this study, inductive effects are not included.

2.4 The Amplifier Transfer Function

A schematic of the amplifier circuit without inductance is shown in Figure 6. Derivation of the amplifier transfer function can now be obtained in a straightforward manner. Use of loop equations in Figure 7 gives

$$P_{cd} \, (2 \, K_p e^{-st_d}) - P_{od} = 2\dot{q}_o \, R_o. \tag{2.14}$$

Application of flow balance gives

$$\dot{q}_o = \frac{C_o}{2} \, s \, P_{od} + \frac{P_{od}}{R_\ell} + \frac{C_\ell}{2} \, s \, P_{od}. \tag{2.15}$$

A combination of equations (2.14) and (2.15) gives

$$2 \, P_{cd} \, K_p e^{-st_d} = 2 \, P_{od} \, R_o \left[\left(\frac{C_o + C_\ell}{2} \right) s + \frac{1}{2R_o} + \frac{1}{2R_\ell} \right]$$

or

$$\frac{P_{od}}{P_{cd}} = \frac{2K_p \, R_\ell}{R_o + R_\ell} \left[\frac{e^{-st_d}}{\left(\frac{2C_t \, R_o \, R_\ell}{R_o + R_\ell} \right) s + 1} \right], \tag{2.16}$$

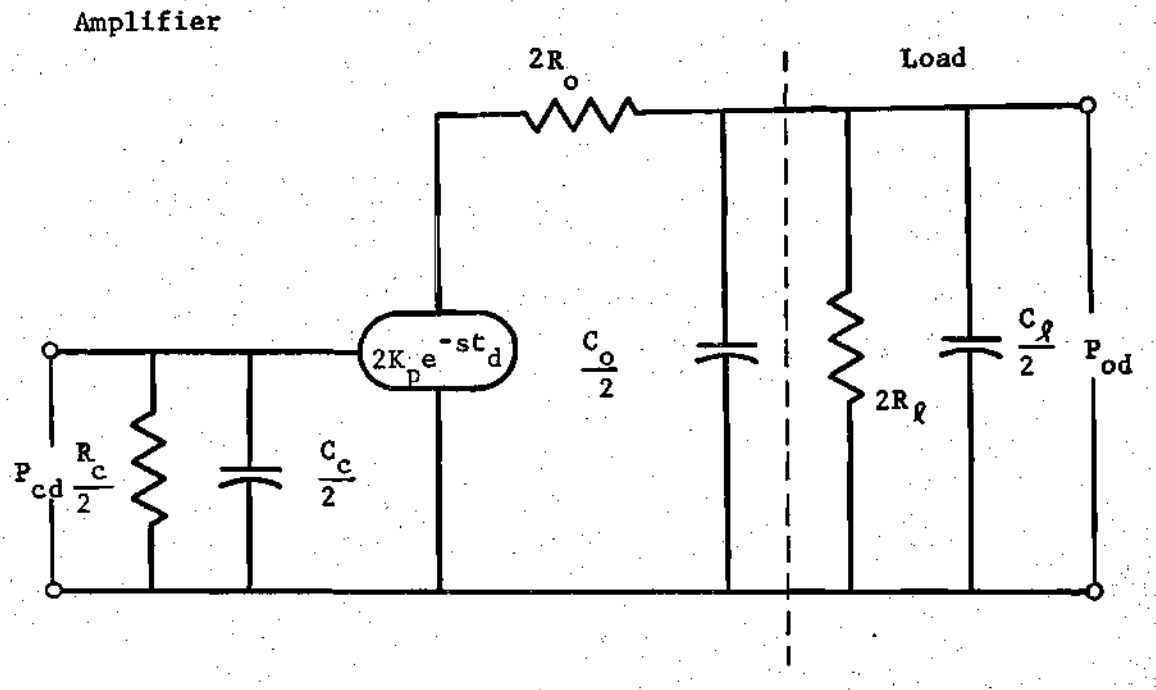

Figure 6. Amplifier Equivalent Circuit (Neglecting Inductance).

or

$$\frac{P_{od}}{P_{cd}} = \frac{K_a e^{-st_d}}{s/\omega_{pa} + 1} \quad ,$$

where

$$K_a = \frac{2K_p R_\ell}{R_o + R_\ell} \quad , \quad \omega_{pa} = \frac{R_o + R_\ell}{2C_t(R_o + R_\ell)}$$

and

$$C_t = C_o + C_\ell \quad .$$

K_a is called the overall amplifier gain constant. This scaler constant becomes the amplifier transfer function when amplifier dynamics may be totally neglected. It may be noted that

a) The transfer function consists of a constant multiplied by a first order lag and a pure transport delay;

b) typically $C_t << 1$ and $R_o << R_\ell$, giving $\omega_{pa} >> 1$, which implies that attenuation of amplifier output occurs only at higher frequencies;

c) at $\omega = 0$, the transfer function consists of the scaler constant K_a;

d) as $R_\ell \longrightarrow \infty$, $K_a \longrightarrow 2K_p$, giving the deadhead gain of $2K_p$;

e) output connector capacitance and resistance and transport delay for the entire amplifier-connecting line system are

included in the amplifier transfer function, and

f) the input parameters R_c and C_c are not included. They are included in the input network that precedes the amplifier.

CHAPTER III

ANALYTICAL DEVELOPMENT OF BASIC FLUIDIC NETWORKS

3.1 Preliminary Comments

This chapter is devoted to a detailed analysis of a few basic networks, the results obtained being called upon for use in later sections.

A complete transfer function is derived for each network using the previously discussed linearized electrical equivalent model of the vented proportional amplifier. This gives an accurate picture of network behavior up to the frequency limitations of the amplifier model. A reduced transfer function is obtained from the complete transfer function by neglecting the capacitances of the control port and output port, C_c and C_o respectively, and by neglecting transport delay, t_d. These assumptions are reasonable when connector volumes are small in comparison to external capacitors in the netowrk, and when operating frequencies are low, together with small geometries.

The presence of control capacitance, C_c, can cause slight inaccuracies in the break frequency expressions of the reduced transfer function. For this reason, some of the discussion of pole-zero positioning limitations is somewhat academic. In addition, physical limitations of the amplifier may cause further restrictions on pole-zero positioning. Amplifier matching requirements may demand some network resistors with specific values. If these resistors are contained in

expressions for poles and zeros, further restrictions are effected.

In a typical design situation, network resistors, capacitors and amplifier gains have been selected to locate reduced transfer function poles and zeros as desired. The complete transfer function is then obtained for a given physical implementation of the reduced transfer function and serves to provide information on the performance degradation of reduced transfer functions at higher frequencies.

In the presentation of the first five networks, the development is kept straightforward and readily understandable. The fifth network, namely the integrator or lag-lead configuration, has certain pecularities which have been used in later sections. The presence of more than one amplifier in this network necessitates the introduction of subscripts on certain system parameters. In addition, ambiguities exist as to whether an intermediate connector volume should be lumped with the output plus load capacitance of the preceding amplifier, C_{t1}, or with the input capicatance of the following, C_{c2}. Another difficulty is the absence of a single unique signal path. More than one transport delay constant is then necessary.

In networks with multiple amplifiers, a general convention is adopted by denoting as a primary subscript the number of the amplifier associated with a particular parameter. Secondary subscripts indicate the number of the associated port. For example, in Figure 17, R_{c11} is the resistance of port 1 of amplifier 1 and its associated connector.

When two amplifiers are staged and the total output of the first is used as the input to the second, the convention is to consider the

output network of the first as being the input network of the second, R_L equal to infinity, and C_o equal to zero. The first amplifier transfer function then becomes $2K_{p1}e^{-st_{d1}}$. The first amplifier pole disappears as the output capacitance of the first, C_{01}, is now zero, intermediate connector capacitance being considered part of the control circuit capacitance of the second amplifier, C_{c2}. The first amplifier output port resistance, R_{01}, is now a series resistor in the input circuit of the second amplifier. The resistance of the intermediate connector is included in R_{c2}.

Whenever two amplifiers are staged with an intermediate load present, the first amplifier transfer function has been expressed in the standard form

$$\frac{P_{od}}{P_{cd}} = \frac{K_{a1}\, e^{-st_{d1}}}{s/\omega_{pa1} + 1} \quad ,$$

where

$$K_{a1} = \frac{2K_{p1}\, R_1}{R_{01} + R_1} \quad , \tag{3.1}$$

and

$$\omega_{pa1} = \frac{R_{01} + R_1}{2C_{t1}\, R_{01}\, R_1} \quad .$$

All parameters are as previously defined, with R_{01} being the first amplifier output port resistance plus the resistance of the intermediate connector up to the loading point, and C_{t1} being the load capacitance

plus the capacitance of the intermediate connector up to the loading point.

In configurations with more than one amplifier, it is necessary to use a separate transport delay constant for each unique signal path. These signal paths have been defined in the derivation of the complete transfer functions.

3.2 Network 1 -- The Passive Lag

The fluidic schematic for network 1 and the electrical equivalent are shown in Figures 7a and 7b respectively. Viewing the electrical equivalent and applying Kirchoff's Laws yields

$$\dot{q} = \dot{q}_1 + \dot{q}_2 \quad , \tag{3.2}$$

where

$$\dot{q} = \frac{P_1 - P_0}{R_1} \quad , \quad \dot{q}_1 = C_s P_0 \quad , \tag{3.3}$$

and

$$\dot{q}_2 = \frac{P_0}{R_c} \quad .$$

A combination of equations (3.2) and (3.3) gives

$$\frac{P_0}{P_1} = \frac{1/R_1 \left(\frac{1}{R_c} + \frac{1}{R_1} \right)}{\left(\frac{C}{\frac{1}{R_c} + \frac{1}{R_1}} \right) s + 1} \quad . \tag{3.4}$$

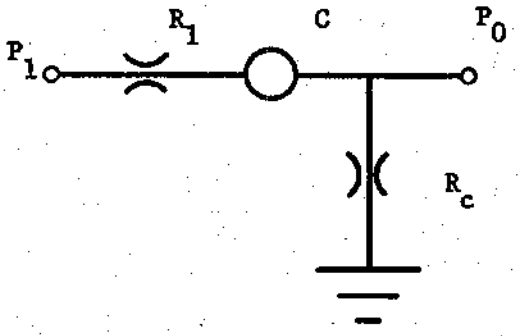

Figure 7a. Network 1 Schematic.

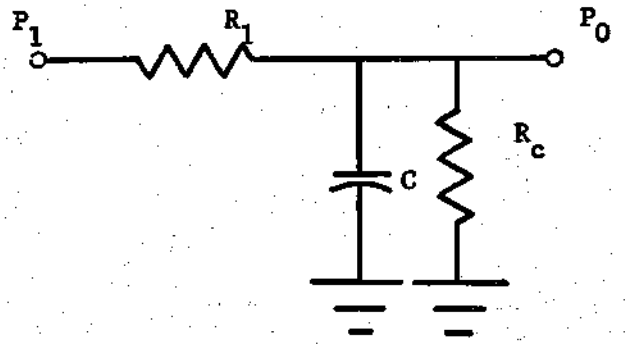

Figure 7b. Network 1 Electrical Equivalent.

The inclusion of transport delay gives

$$\frac{P_0}{P_1} = \frac{1/R_1 \left(\frac{1}{R_c} + \frac{1}{R_1} \right) e^{-st_d}}{\left(\frac{C}{\frac{1}{R_c} + \frac{1}{R_1}} \right) s + 1} \tag{3.5}$$

This is the complete transfer function for network 1. If the geometry is small transport delay may be neglected i. e. $t_d = 0$, and the reduced transfer may be written as

$$\frac{P_0}{P_1} = \frac{K}{s/\omega_p + 1} \quad , \tag{3.6}$$

where

$$K = \frac{1}{R_1 \left(\frac{1}{R_c} + \frac{1}{R_1} \right)} \quad ,$$

and

$$\omega_p = \frac{1}{R_1 C} + \frac{1}{R_c C} \quad . \tag{3.7}$$

It can be seen from equation (3.7) that the pole can be located anywhere on the real axis of the left hand plane. In addition, K, the overall system gain, is less than unity, as R_1 is typically significantly greater than R_c. A generalized pole-zero diagram and a Bode plot which indicate these results are shown respectively in Figures 8a and 8b.

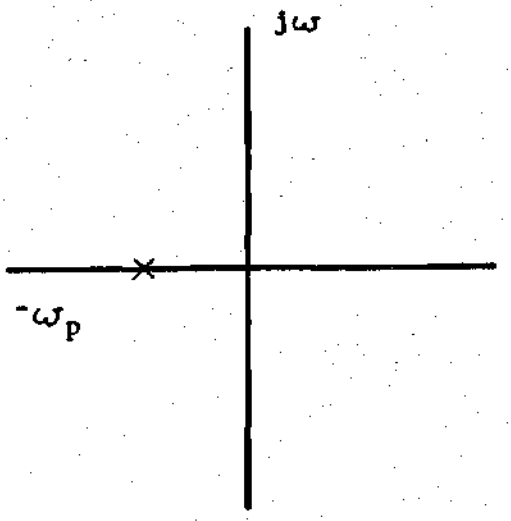

Figure 8a. Network 1 Pole - Zero Diagram.

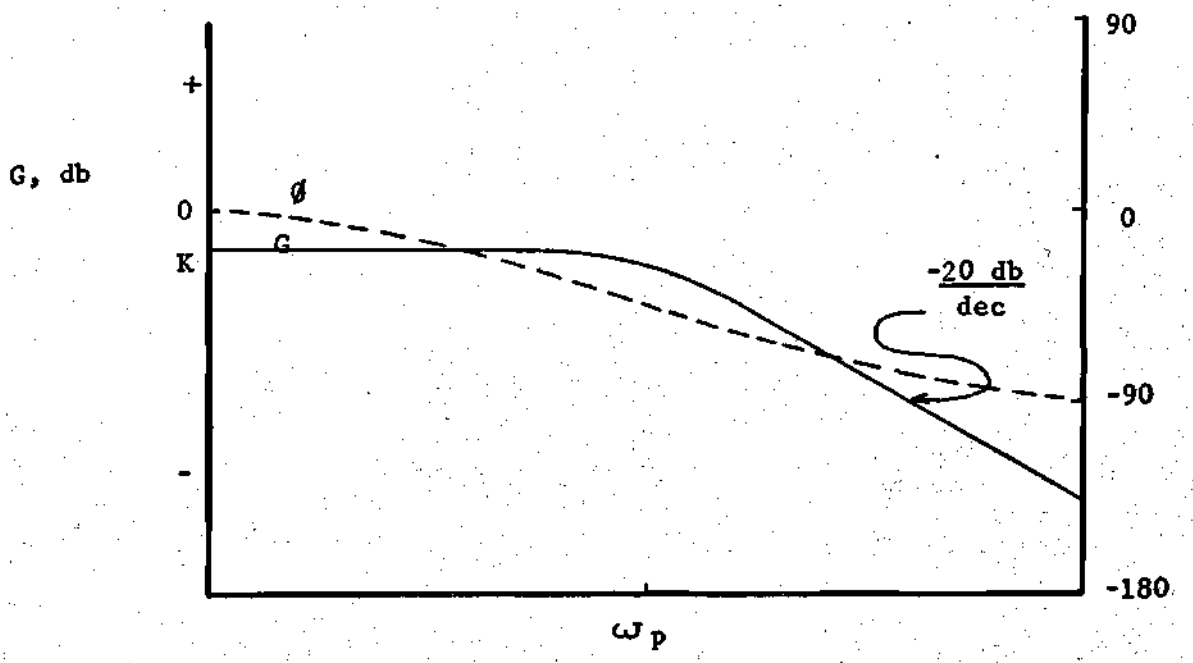

Frequency on Log Scale

Figure 8b. Network 1 Bode Plot.

3.3 Network 2 - The Differential Input Lag

The fluidic schematic and electrical equivalent for both the left and right hand input network are shown in Figures 9a and 9b, respectively. Viewing the electrical equivalent and applying a flow balance gives

$$\frac{P_1^+ - P_{c1}}{R} = CsP_{c1} + \frac{P_{c1}}{R_c} + C_c sP_{c1}, \tag{3.8}$$

or

$$P_{c1} = \frac{P_1^+}{R(C + C_c)s + \frac{R}{R_c} + 1}. \tag{3.9}$$

Similarly

$$P_{c2} = \frac{P_1^-}{R(C + C_c)s + \frac{R}{R_c} + 1}. \tag{3.10}$$

Equations (3.9) and (3.10) may be combined to obtain

$$P_{cd} = \frac{2P_1^+}{R(C + C_c)s + \frac{R}{R_c} + 1}, \tag{3.11}$$

with

$$P_{cd} = P_{c1} - P_{c2} \text{ and } P_1^+ = -P_1^-. \tag{3.12}$$

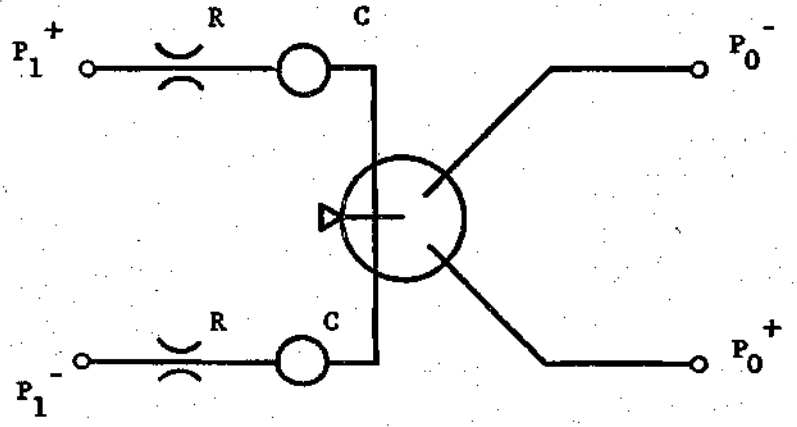

Figure 9a. Network 2 Schematic.

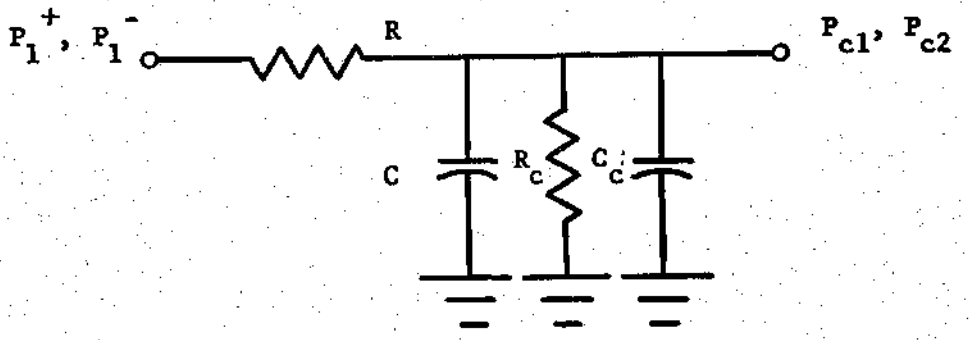

Figure 9b. Network 2 Left and Right Hand Input Electrical Equivalent.

A use of the relation

$$P_{1d} = 2P_1^+ \quad , \tag{3.13}$$

given the total input transfer function as

$$\frac{P_{cd}}{P_{1d}} = \frac{1/R \left(\frac{1}{R} + \frac{1}{R_c} \right)}{\left(\frac{C + C_c}{\frac{1}{R} + \frac{1}{R_c}} \right) s + 1} \quad . \tag{3.14}$$

Since

$$\frac{P_{od}}{P_{1d}} = \frac{P_{cd}}{P_{1d}} \times \frac{P_{od}}{P_{cd}} \quad , \tag{3.15}$$

and since the amplifier transfer function is

$$\frac{P_{od}}{P_{cd}} = \frac{K_a e^{-st_d}}{s/\omega_{pa} + 1} \quad , \tag{3.16}$$

the complete transfer function is written as

$$\frac{P_{od}}{P_{1d}} = \frac{1/R \left(\frac{1}{R_c} + \frac{1}{R} \right)}{\left(\frac{C + C_c}{\frac{1}{R_c} + \frac{1}{R}} \right) s + 1} \quad \frac{K_a e^{-st_d}}{s/\omega_{pa} + 1} \tag{3.17}$$

If the system geometry is such that $C_c \ll 1$ and $t_d \ll 1$, then the reduced transfer function adequately represents system behavior. It can

be written as

$$\frac{P_{od}}{P_{1d}} = K_a K \left(\frac{1}{s/\omega_p + 1} \right) , \tag{3.18}$$

where

$$K = \frac{1}{R \left(\frac{1}{R_c} + \frac{1}{R} \right)}$$

and

$$\omega_p = \frac{1}{R_c} + \frac{1}{R_c C} \tag{3.19}$$

The pole can be located anywhere on the real axis of the left hand plane. As in network 1, K is typically less than unity. However, the overall system gain $K_a K$ is normally greater than unity. A generalized pole-zero diagram and a Bode plot are shown in Figures 10a and 10b respectively.

3.4 Network 3 - The Lag-Lead

A fluidic schematic and electrical equivalents for left and right inputs are shown respectively in Figures 11a, 11b and 11c. Viewing the left hand electrical equivalent, a flow balance gives

$$\frac{P_1 - P_{c1}}{R_1} = C_s P_{c1} + \frac{P_{c1}}{R_c} + C_c s P_{c1}, \tag{3.20}$$

or

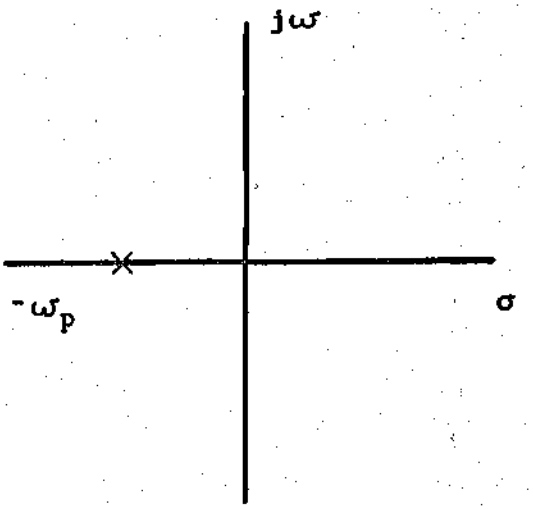

Figure 10a. Network 2 Pole-Zero Diagram

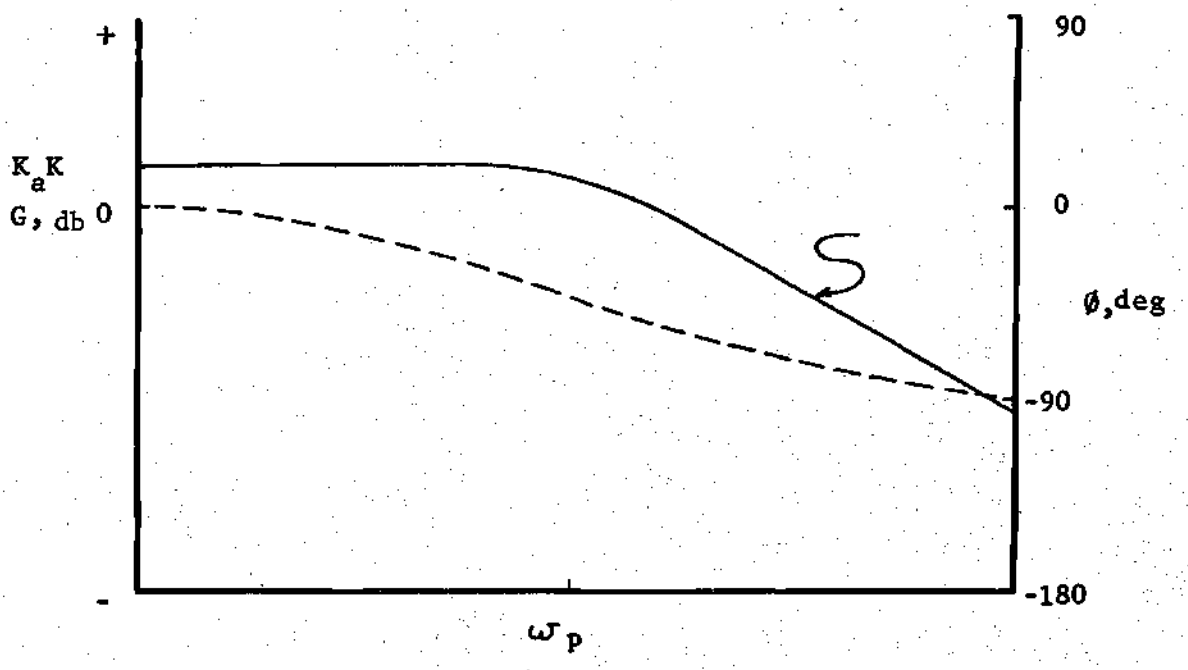

Figure 10b. Network 2 Bode Plot.

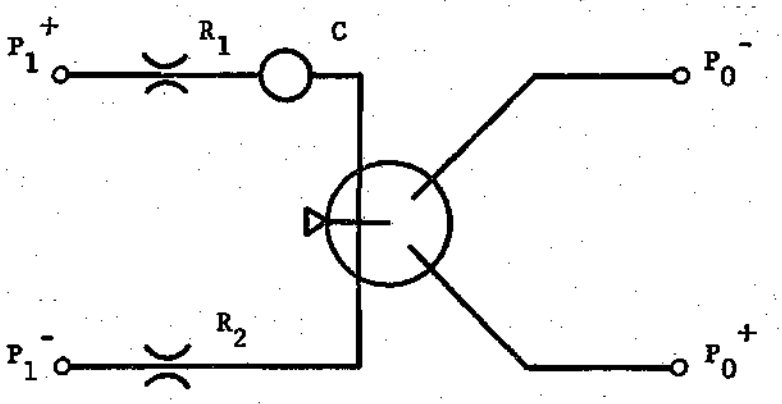

Figure 11a. Network 3 Schematic.

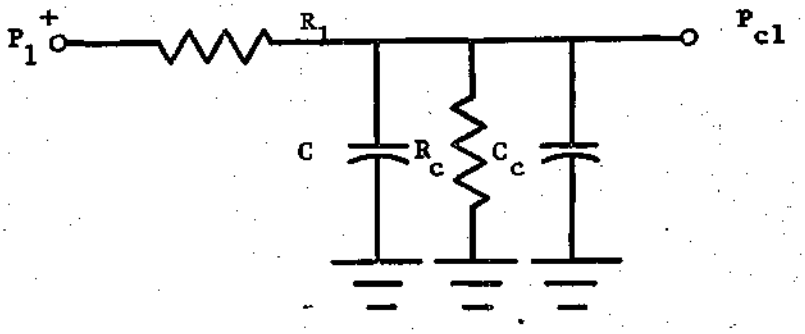

Figure 11b. Network 3 Left Hand Input Electrical Equivalent.

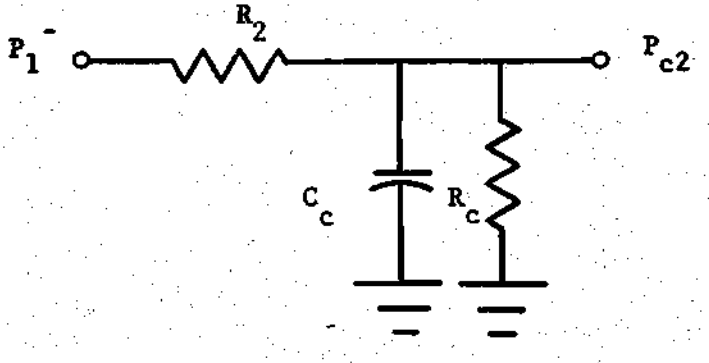

Figure 11c. Network 3 Right Hand Input Electrical Equivalent.

$$P_{c1} = \frac{P_1}{R\,(C + C_c)\,s + \frac{R_1}{R_c} + 1} \quad . \tag{3.21}$$

Viewing the right hand electrical equivalent, a flow balance gives

$$\frac{P_1 - P_{c2}}{R_c} = \frac{P_{c1}}{R_c} + C_c\, s P_{c1}, \tag{3.22}$$

or

$$P_{c2} = \frac{P_1}{R_2\, C_c\, s + \frac{R_2}{R_c} + 1} \quad . \tag{3.23}$$

Using equations (3.12) and (3.13) gives

$$\frac{P_{cd}}{P_{1d}} = \frac{\left[R_1\,(C + C_c)\,s + \frac{R_1}{R_c} + 1\right] + \left[R_2\, C_c\, s + \frac{R_2}{R_c} + 1\right]}{2\left[R_1\,(C + C_c)\,s + \frac{R_1}{R_c} + 1\right]\left[R_2\, C_c\, s + \frac{R_2}{R_c} + 1\right]} \quad . \tag{3.24}$$

Using equations (3.15) and (3.16), the complete transfer function may be written as

$$\frac{P_{od}}{P_{1d}} = \frac{\frac{1}{R_1}\left(\frac{1}{R_c} + \frac{1}{R_2}\right) + \frac{1}{R_2}\left(\frac{1}{R_c} + \frac{1}{R_1}\right)}{2\left(\frac{1}{R_c} + \frac{1}{R_1}\right)\left(\frac{1}{R_c} + \frac{1}{R_2}\right)} \quad x$$

$$\frac{\dfrac{(C + C_c)/R_2 + C_c/R_1}{\dfrac{1}{R_1}\left(\dfrac{1}{R_c} + \dfrac{1}{R_2}\right) + \dfrac{1}{R_2}\left(\dfrac{1}{R_c} + \dfrac{1}{R_1}\right)}\, s + 1}{\left[\left(\dfrac{C + C_c}{\dfrac{1}{R_c} + \dfrac{1}{R_1}}\right) s + 1\right]\left[\dfrac{C_c}{\dfrac{1}{R_c} + \dfrac{1}{R_2}}\, s + 1\right]} \quad x$$

$$\frac{K_a e^{-st_d}}{s/\omega_{pa} + 1} \quad . \tag{3.25}$$

If the geometry is such that $C_c << C$, $C_t << 1$ and $td << 1$, then the reduced transfer function adequately represents system response. It may be written as

$$\frac{P_{od}}{P_{1d}} = K_a K \left(\frac{s/\omega_z + 1}{s/\omega_p + 1}\right), \tag{3.26}$$

where

$$K = \frac{\dfrac{1}{R_1}\left(\dfrac{1}{R_c} + \dfrac{1}{R_2}\right) + \dfrac{1}{R_2}\left(\dfrac{1}{R_c} + \dfrac{1}{R_1}\right)}{\left(\dfrac{1}{R_c} + \dfrac{1}{R_1}\right)\left(\dfrac{1}{R_c} + \dfrac{1}{R_2}\right)}, \tag{3.27}$$

$$\omega_p = \frac{1}{R_1 C} + \frac{1}{R_c C},$$

and

$$\omega_z = \frac{R_2}{C}\left[\frac{1}{R_1}\left(\frac{1}{R_c} + \frac{1}{R_2}\right) + \frac{1}{R_2}\left(\frac{1}{R_c} + \frac{1}{R_1}\right)\right],$$

or

$$\omega_z = \omega_p + \frac{1}{R_1 C}\left(\frac{R_2}{R_c} + 1\right) .$$

It can be seen from equation (3.27) that the break frequency of the zero is always greater than that of the pole. The zero can be located anywhere on the real axis of the left hand plane. The zero always lies to the left of the pole. The positions of the pole and zero are not completely independent. For example, since R_c, the amphfer central part resistance cannot be varied for a specific geometry, a given location of the pole fixes the R_1C product. The only parameter available for the positioning of ω_z is R_2. Increasing R_2 can locate ω_z as far to the left as desired. However decreasing R_2 can only bring ω_z as far to the right as the point $\omega_z = \omega_p + \frac{1}{R_1 C}$.

A generalized pole-zero diagram and a Bode plot for this transfer function are shown in Figures 12a and 12b respectively. Note in the Bode plot the lag-lead characteristics of this network. The phase lag reaches its maximum between the break frequencies of the pole and the zero, and finally returns to zero at high frequencies. The amplitude ratio plot, level at low frequencies, starts to decrease at a rate of 20 db/dec when the break frequency of the pole is reached, then levels off again after the break frequency of the zero.

3.5 Network 4 - The Lead-Lag or The Differentiator

The fluidic schematic and left and right side input electrical equivalents are shown in Figures 13a, 13b and 13c, respectively.

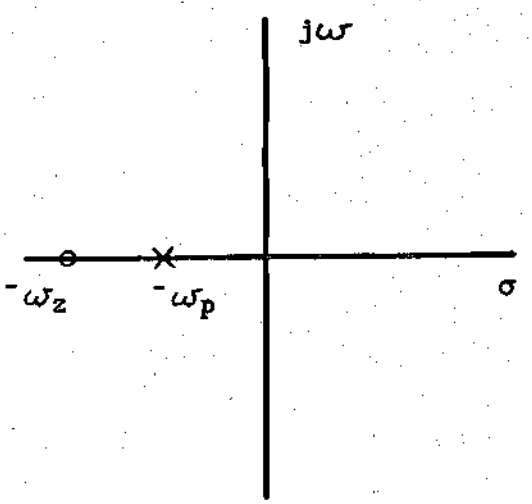

Figure 12a. Network 3 Pole Zero Diagram.

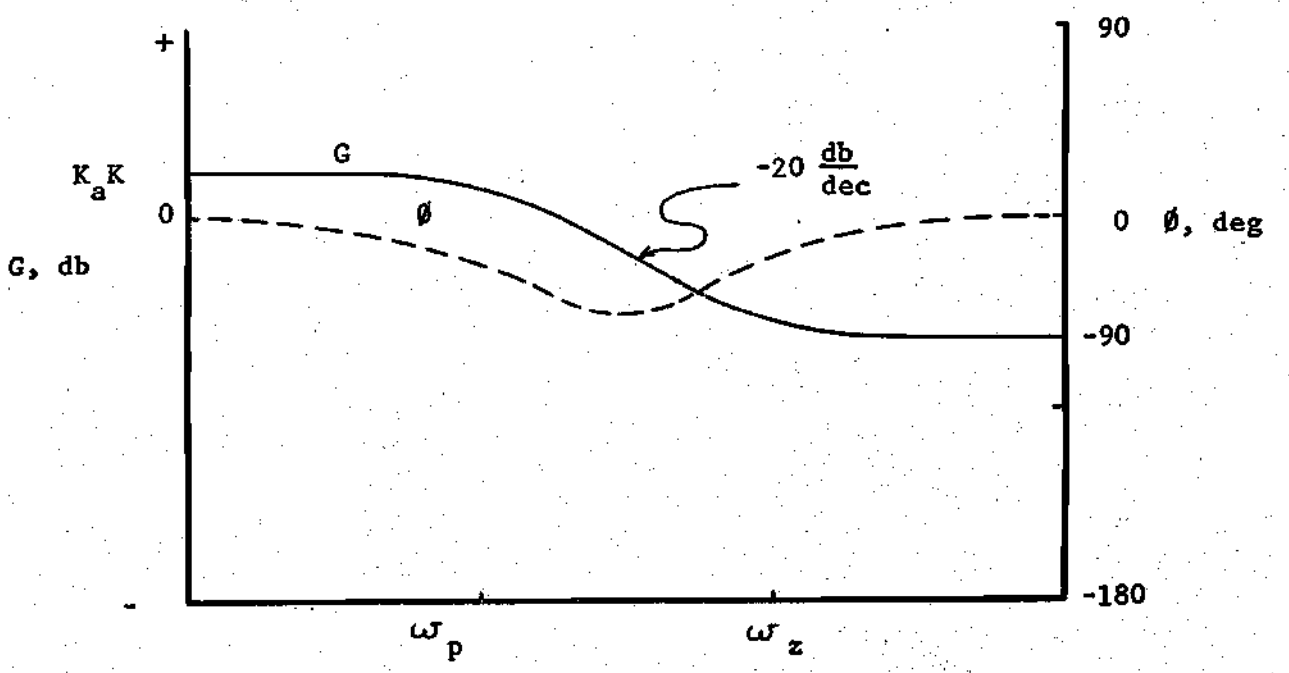

Figure 12b. Network 3 Bode Plot.

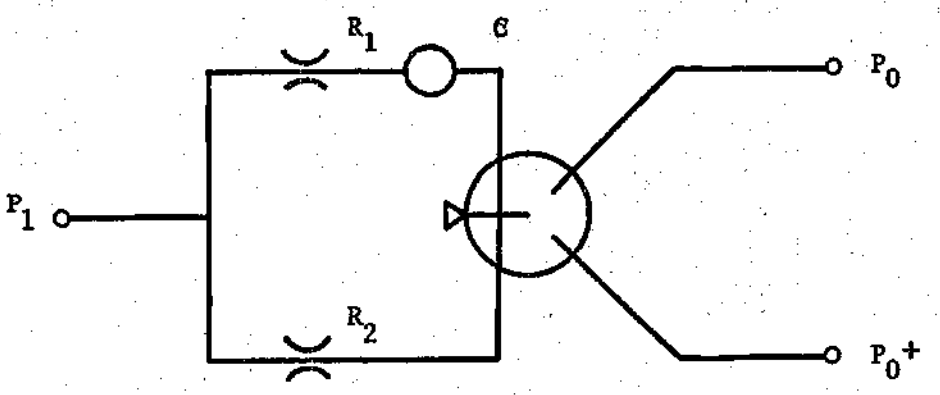

Figure 13a. Network 4 Schematic.

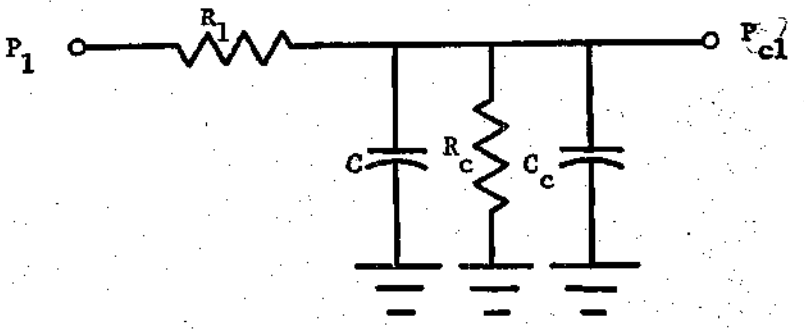

Figure 13b. Network 4 Left Hand Input Electrical Equivalent.

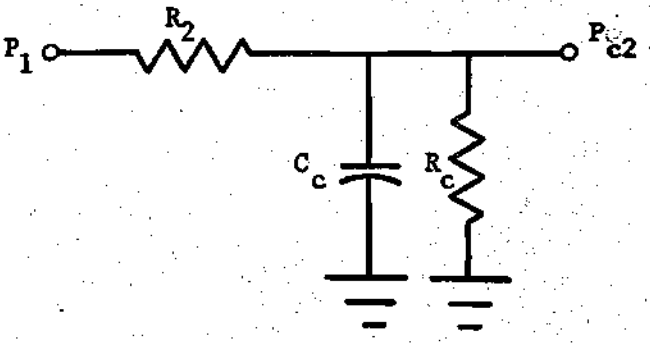

Figure 13c. Network 4 Right Hand Input Electrical Equivalent.

Viewing the left hand equivalent, a flow balance gives

$$\frac{P_1 - P_{c1}}{R_1} = C\ P_{c1} + \frac{P_{c1}}{R_c} + C_c\ s\ P_{c1}, \tag{3.28}$$

or

$$P_{c1} = \frac{P_1}{R_1\ (C + C_c)\ s + \frac{R_1}{R_c} + 1} . \tag{3.29}$$

Viewing the right hand electrical input, again a flow balance gives

$$\frac{P_1 - P_{c2}}{R_2} = \frac{P_{c1}}{R_c} + C_c\ P_{c1} , \tag{3.30}$$

or

$$P_{c2} = \frac{P_1}{R_2\ C_c\ s + \frac{R_2}{R_c} + 1} . \tag{3.31}$$

Thus

$$P_{cd} = P_{c1} - P_{c2} =$$

$$\frac{P_1}{R_1\ (C + C_c)\ s + \frac{R_1}{R_c} + 1} - \frac{P_1}{R_2\ C_c\ s + \frac{R_2}{R_c} + 1} , \tag{3.32}$$

or

$$\frac{P_{cd}}{P_1} = \frac{\left[R_2 C_c s + \frac{R_2}{R_c} + 1\right] - \left[R_1 (C + C_c) s + \frac{R_1}{R_c} + 1\right]}{\left[R_1 (C + C_c) s + \frac{R_1}{R_c} + 1\right] \left[R_2 C_c s + \frac{R_2}{R_c} + 1\right]} \quad . \quad (3.33)$$

With the inclusion of the amplifier transfer function, the complete transfer function for the network may be written as

$$\frac{P_{od}}{P_1} = \frac{\frac{1}{R_2}\left(\frac{1}{R_c} + \frac{1}{R_1}\right) - \frac{1}{R_1}\left(\frac{1}{R_c} + \frac{1}{R_2}\right)}{\left(\frac{1}{R_c} + \frac{1}{R_1}\right)\left(\frac{1}{R_c} + \frac{1}{R_2}\right)} \times$$

$$\frac{\frac{(C + C_c)}{R_2} - \frac{C_c}{R_1}}{\frac{1}{P_2}\left(\frac{1}{R_c} + \frac{1}{R_1}\right) - \frac{1}{R_1}\left(\frac{1}{R_c} + \frac{1}{R_2}\right)} s + 1 \times$$

$$\left[\frac{C + C_c}{\left(\frac{1}{R_c} + \frac{1}{R_1}\right)} s + 1\right]\left[\frac{C_c}{\frac{1}{R_c} + \frac{1}{R_2}} s + 1\right]$$

$$\frac{K_a e^{-st_d}}{s/\omega_{pa} + 1} \quad . \quad (3.34)$$

When circumstances are such that C_c C_0 and t_d may be neglected, the reduced transfer function adequately represents network response. It may be written as

$$\frac{P_{od}}{P_1} = K_a K \left(\frac{s/\omega_z + 1}{s/\omega_p + 1}\right) \quad , \quad (3.35)$$

where

$$K = \frac{\frac{1}{R_2}\left(\frac{1}{R_c} + \frac{1}{R_1}\right) - \frac{1}{R_1}\left(\frac{1}{R_c} + \frac{1}{R_2}\right)}{\left(\frac{1}{R_c} + \frac{1}{R_1}\right)\left(\frac{1}{R_c} + \frac{1}{R_2}\right)} ,$$

$$\omega_p = \frac{1}{R_c C} + \frac{1}{R_1 C} , \qquad (3.36)$$

$$\omega_z = \frac{R_z}{C}\left[\frac{1}{R_2}\left(\frac{1}{R_c} + \frac{1}{R_1}\right) - \frac{1}{R_1}\left(\frac{1}{R_c} + \frac{1}{R_2}\right)\right] ,$$

or

$$\omega_z = \omega_p - \frac{1}{R_1 C}\left(\frac{R_2}{R_c} + 1\right)$$

The pole can be located anywhere on the real axis of the left hand plane. The zero always lies to the right of the pole. As in the previous network, the positions of the pole and zero are not completely independent. Since R_c cannot be conveniently varied, a given location of the pole fixes the R_1C product. The only parameter available for controlling the zero location is R_2. By increasing R_2, the zero can be moved as far to the right as desired, but decreasing R_2 only permits the zero to be located as far to the left as the point given by

$$\omega_z = \omega_p - \frac{1}{R_1 C} = \frac{1}{R_c C} . \qquad (3.37)$$

For this network, there are three basic pole-zero configurations. The first, shown in the pole-zero diagram and the Bode plot of Figures 14a

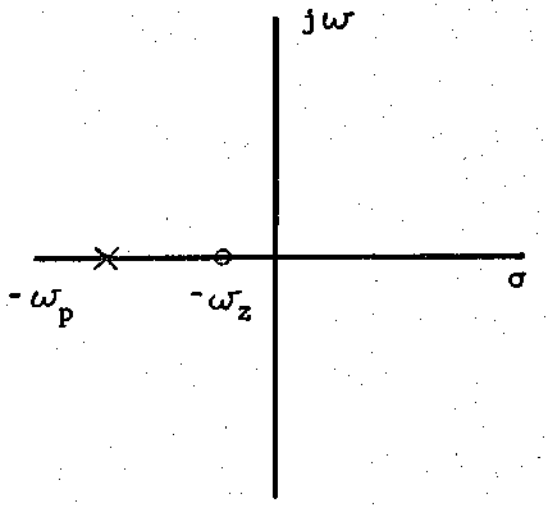

Figure 14a. Network 4 Pole Zero Diagram with ω_z 70.

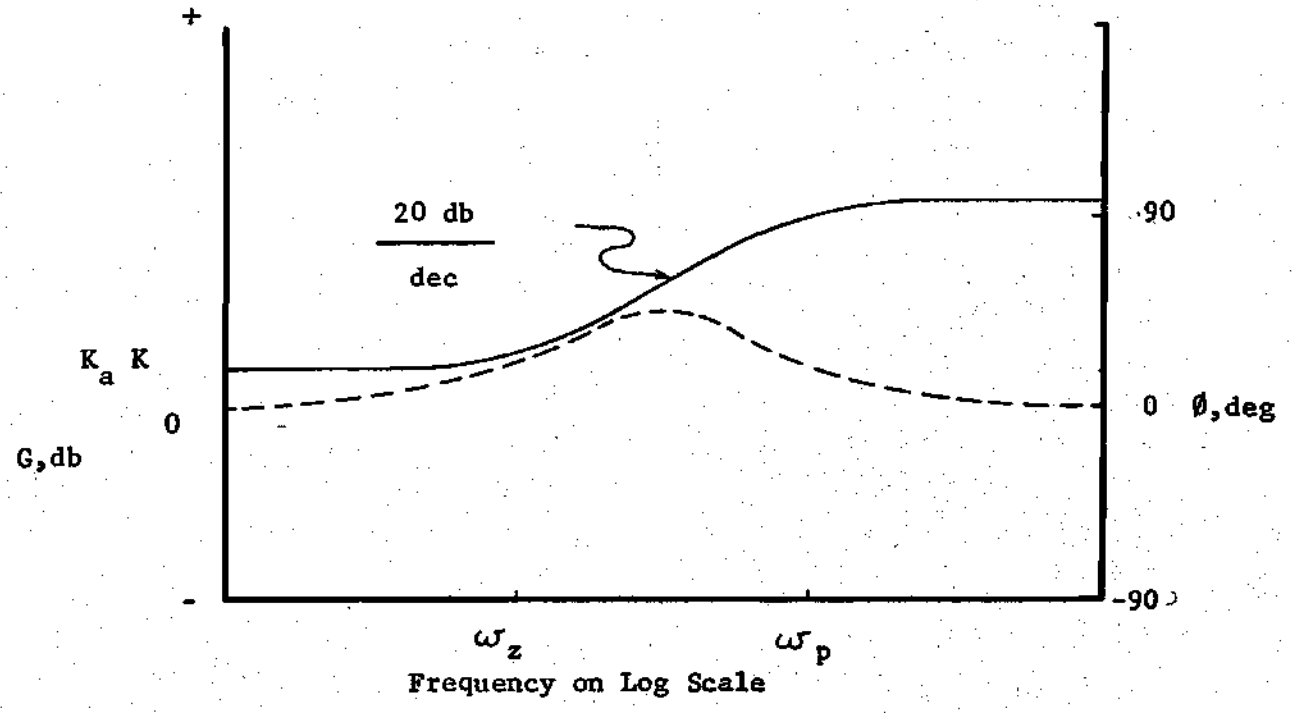

Figure 14b. Network 4 Bode Plot with $\omega_z > 0$.

and 14b, respectively, is where the zero lies in the left hand plane. This is a lead-lag configuration with the phase angle verses frequency plot demonstrating phase lead at low frequencies, reaching its maximum between the break frequencies of the pole and the zero and returning to zero at high frequencies.

With the zero at the origin, this network is a differentiator. The pole-zero diagram and Bode plot for this situation are shown in Figures 15a and 15b, respectively. Note that the magnitude verses frequency plot immediately starts increasing at a rate of 20 db/dec, and levels off after the break frequency of the pole is reached.

It can be seen from an examination of the expressions for K and ω_z in equation (3.36), that when ω_z is less than zero, i. e. when the zero lies in the right hand plane, K becomes negative. This implies a reversal of output polarity. The pole-zero diagram and Bode plot for this situation are shown in Figures 16a and 16b, respectively. It can be seen that the magnitude verses frequency plot in identical with that of Figure 14a, where the zero is in the left hand plane. However, the phase angle verses frequency plot indicates that the zero now contributes a phase lag rather than a phase lead.

3.6 Network 5 - The Integrator or The Lag-Lead

The schematic for network 5 is shown in Figure 17a. Viewing the schematic, the system can be put directly into block diagram form. The block diagram is shown in Figure 17b.

Block "a" is the transfer function of the left input circuit to amplifier 1, its electrical equivalent being shown in Figure 18a. Using the results given by equation (3.5) and substituting appropriate quantities

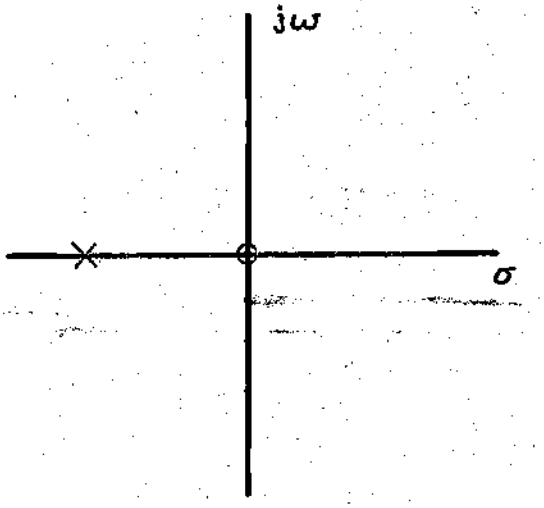

Figure 15a. Network 4 Pole-Zero Diagram with $\omega_z = 0$.

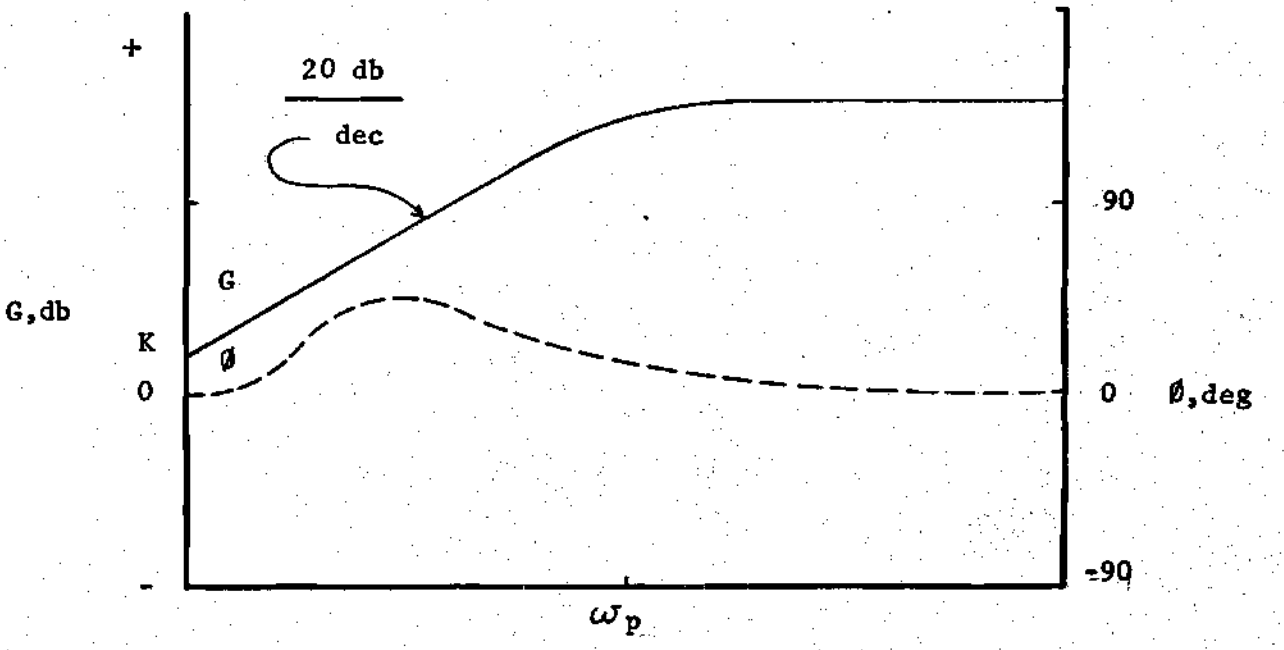

Frequency on Log Scale

Figure 15b. Network 4 Bode Plot with $\omega_z = 0$.

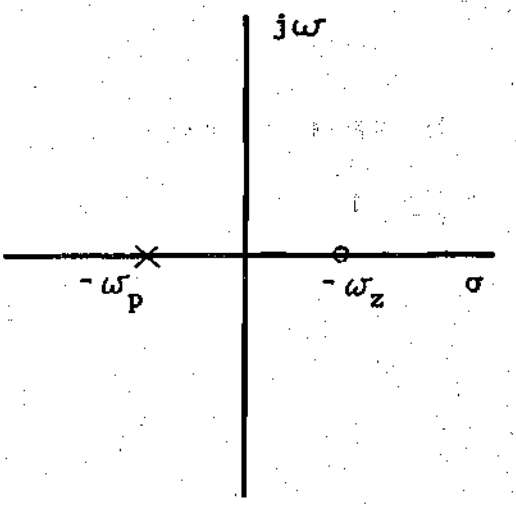

Figure 16a. Network 4 Pole Zero Diagram with $\omega_z < 0$.

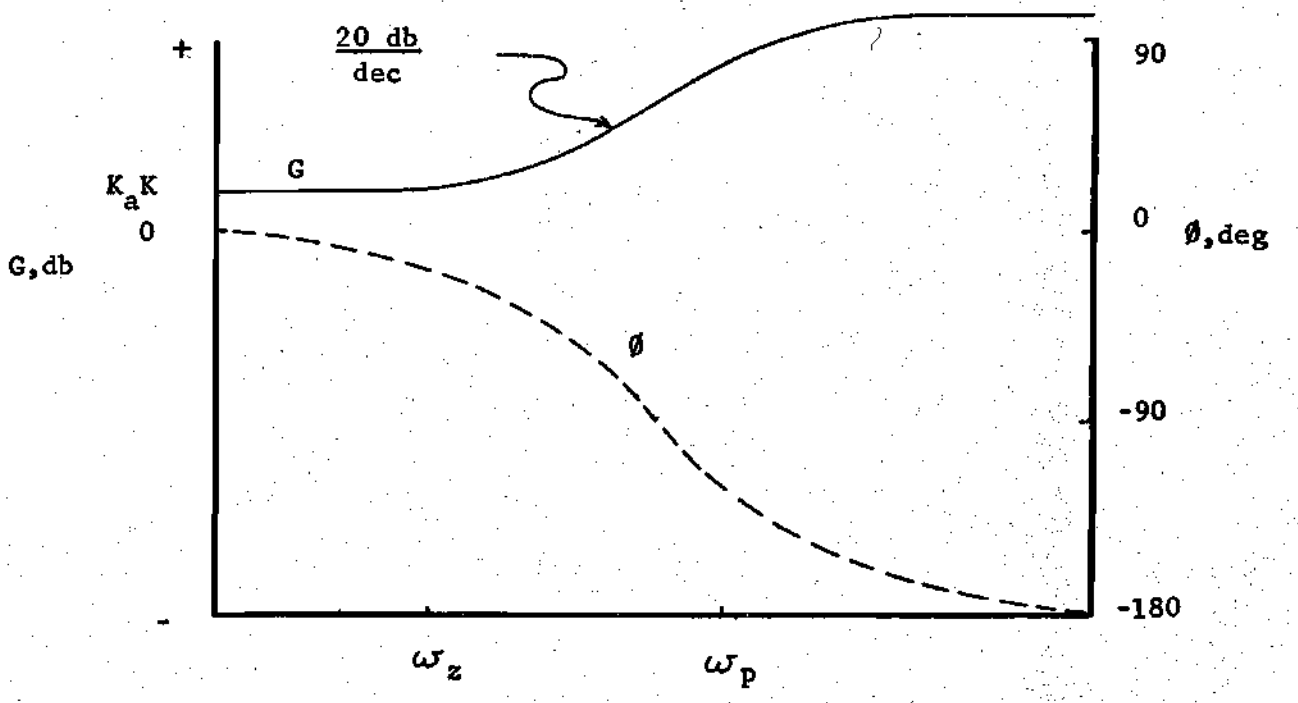

Figure 16b. Network 4 Bode Plot with $_z < 0$.

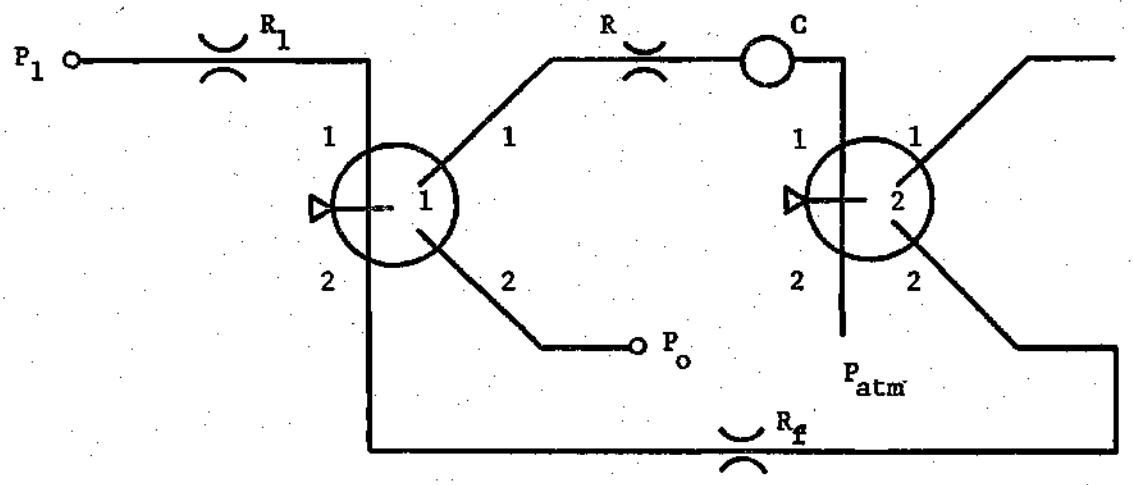

Figure 17a. Network 5 Schematic.

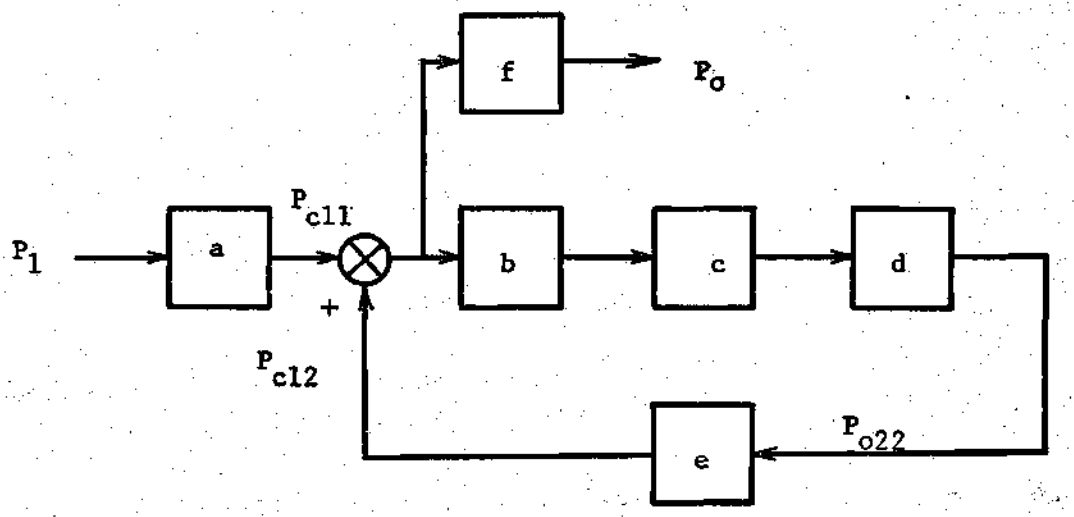

Figure 17b. Network 5 Block Diagram.

gives

$$a = \frac{P_{c11}}{P_1} = \frac{1/R_1 \left(\frac{1}{R_c} + \frac{1}{R_1} \right) e^{-st_{d_1}}}{\left(\frac{C_c}{\frac{1}{R_c} + \frac{1}{R_1}} \right) S + 1} , \qquad (3.38)$$

where t_{d1} is the signal transit time from input to the interaction region of amplifier 1.

In more convenient form

$$\frac{P_{c11}}{P_1} = \frac{K_1 e^{-st_{d_1}}}{s/\omega_{p1} + 1} ,$$

where

$$K = \frac{1}{R \left(\frac{1}{R_c} + \frac{1}{R_1} \right)} , \qquad (3.39)$$

and

$$\omega_{p1} = \frac{1}{R_c C_c} + \frac{1}{R C_c} .$$

Block "b" is the transfer function of amplifier 1. Since all of the left output flow is used for the left control flow into amplifier 2, by a previously explained convention the amplifier 1 transfer function is of the form

$$b = \frac{P_{011}}{P_{cd1}} = K_{p1} \qquad (3.40)$$

The single sided utilization of output cuts amplifier gain in half.

Block "c" is the transfer function of the left input circuit to amplifier 2. The electrical equivalent is shown in Figure 18b. Using the results given by equation (3.14) and substituting appropriate quantities gives

$$C = \frac{P_{c21}}{P_{011}} = \frac{1/(R + R_{011}) \left(\frac{1}{R_{c21}} + \frac{1}{R + R_{011}} \right)}{\left(\frac{C + C_{c21}}{\frac{1}{R_{c21}} + \frac{1}{R + R_{011}}} \right) s + 1} \qquad (3.41)$$

Note the inclusion of the left output resistance of amplifier 1 as a series resistance in this circuit. In a more convenient form

$$\frac{P_{c21}}{P_{011}} = \frac{K_2}{s/\omega_{p2} + 1} ,$$

where

$$K_2 = \frac{1}{(R + R_{011}) \left(\frac{1}{R_{c21}} + \frac{1}{R + R_{011}} \right)} , \qquad (3.42)$$

and

$$\omega_{p2} = \frac{1}{R_{c21} (C + C_{c21})} + \frac{1}{(R + R_{011}) (C + C_{c21})} .$$

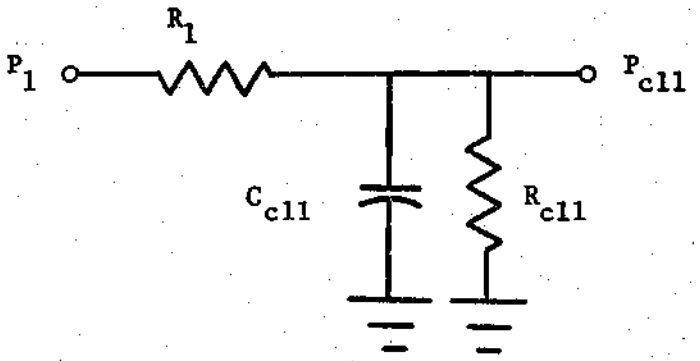

Figure 18a. Network 5 Left Electrical Equivalent Input Circuit to Amplifier 1.

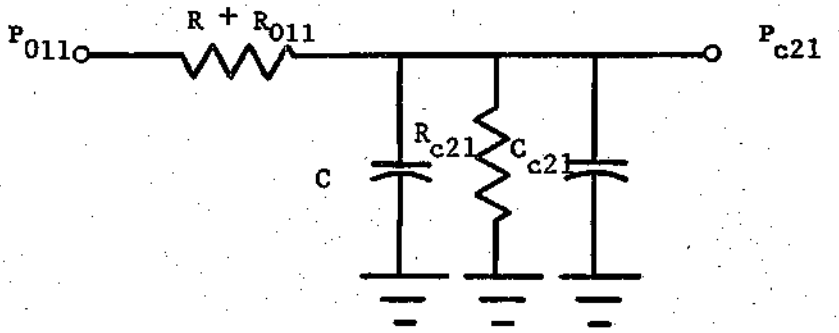

Figure 18b. Network 5 Left Electrical Equivalent Input Circuit to Amplifier 2.

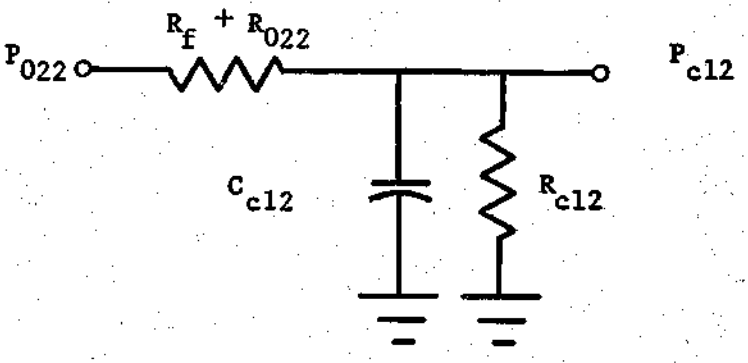

Figure 18c. Network 5 Electrical Equivalent Feedback Circuit.

Block "d" is the amplifier 2 transfer function

$$d = \frac{P_{od22}}{P_{cd2}} = K_{p2} e^{-st_{d2}} \quad , \tag{3.43}$$

where t_{d2} is the signal transit time from the left output of amplifier 1, through amplifier 2 and the feedback loop and through the right input of amplifier 1. Once again the amplifier gain is cut in half because of single sided operation.

Blcok e is the feedback loop transfer function. The electrical equivalent is shown in Figure 18c. Using the results given by equation (3.5) and substituting appropriate quantities gives

$$e = \frac{P_{c12}}{P_{022}} = \frac{1/(R_f + R_{022}) \left(\frac{1}{R_{c12}} + \frac{1}{R_f + R_{022}} \right)}{\left(\frac{C_{c12}}{\frac{1}{R_{c12}} + \frac{1}{R_f + R_{022}}} \right) s + 1} \tag{3.44}$$

In more convenient form

$$\frac{P_{c12}}{P_{022}} = \frac{K_f}{s/\omega_{pf} + 1} \quad ,$$

where

$$K_f = \frac{1}{(R_f + R_{022}) \left(\frac{1}{R_{c12}} + \frac{1}{R_f + R_{022}} \right)} \quad , \tag{3.45}$$

and

$$\omega_{pf} = \frac{1}{R_{c12}\, C_{c12}} + \frac{1}{(R_f + R_{022})\, C_{c12}} .$$

Block f is again the amplifier 1 transfer function, this time with output loading. Single sided output utilization cuts the gain in half. The transfer function is then

$$f = \frac{P_0}{P_{cd1}} = \frac{(K_{a1/2})\, e^{st_{d0}}}{s/\omega_{pa1} + 1} , \qquad (3.46)$$

where t_{d0} is the signal transit time through the interaction region of amplifier 1 to the output.

A reduction of the block diagram yields

$$\frac{P_0}{P_1} = \frac{af}{1 - bcde} , \qquad (3.47)$$

or

$$\frac{P_0}{P_1} = \frac{\left(\frac{K_1\, e^{-st_{d_1}}}{s/\omega_{p1} + 1}\right)\left(\frac{(K_{a1}/2)\, e^{-st_{d0}}}{s/\omega_{pa1} + 1}\right)}{1 - \frac{K_{p1}\, K_{p2}\, K_2\, K_f\, e^{-st_{d_2}}}{(s/\omega_{p2} + 1)\,(s/\omega_{pf} + 1)}} , \qquad (3.48)$$

or

$$\frac{P_0}{P_1} = \frac{(s/\omega_{p2} + 1)\left(\frac{K_1\, e^{-st_{d1}}}{s/\omega_{p1} + 1}\right)\left(\frac{(K_{a1}/2)e^{-st_{d0}}}{s/\omega_{pa1} + 1}\right)}{s/\omega_{p2} + \left(1 - \frac{K_{p1}\, K_{p2}\, K_2\, K_f\, e^{-st_{d2}}}{(s/\omega_{pf} + 1)}\right)} \qquad (3.49)$$

When C_c, C_0 and t_d may be neglected, ω_{p1}, ω_{pa1} and ω_{pf} become infinite. The reduced transfer function is then

$$\frac{P_0}{P_1} = \tfrac{1}{2} \times \left[\frac{(s/\omega_{p2} + 1) \quad K_1 K_{a1}}{s/\omega_{p2} + (1 - K_{p1} K_{p2} K_2 K_f)} \right] . \quad (3.50)$$

If the system parameters are adjusted such that $K_{p1} K_{p2} K_2 K_f = 1$, the reduced transfer function becomes

$$\frac{P_0}{P_1} = \frac{K (s/\omega_z + 1)}{s} ,$$

where

$$K = K_{a1} K_1 \omega_{p2} \quad , \quad ,$$

$$K_1 = \frac{1}{R_1 \left(\frac{1}{R_{c11}} + \frac{1}{R_1}\right)} \quad , \quad (3.51)$$

and

$$\omega_z = \omega_{p2}$$

This is an integrator configuration, the pole being located at the origin. An examination of equation (3.42) shows that the zero may be located anywhere on the real axis of the left hand plane. Pole-zero and Bode diagrams for this case are shown in Figures 19a and 19b respectively. Note that the magnitude verses frequency plot immediately starts decreasing at a rate of 20db/dec.

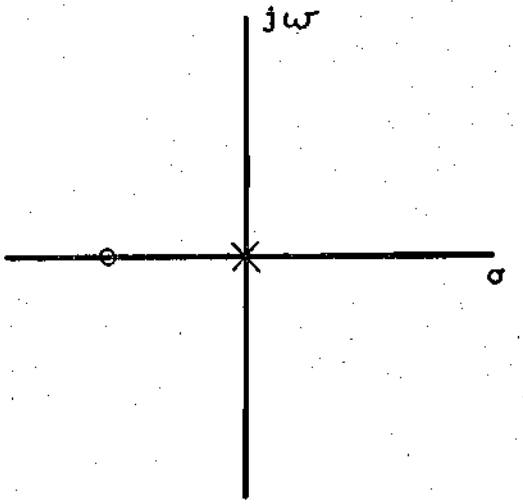

Figure 19a. Network 5 Pole-Zero Diagram with $\omega_p = 0$.

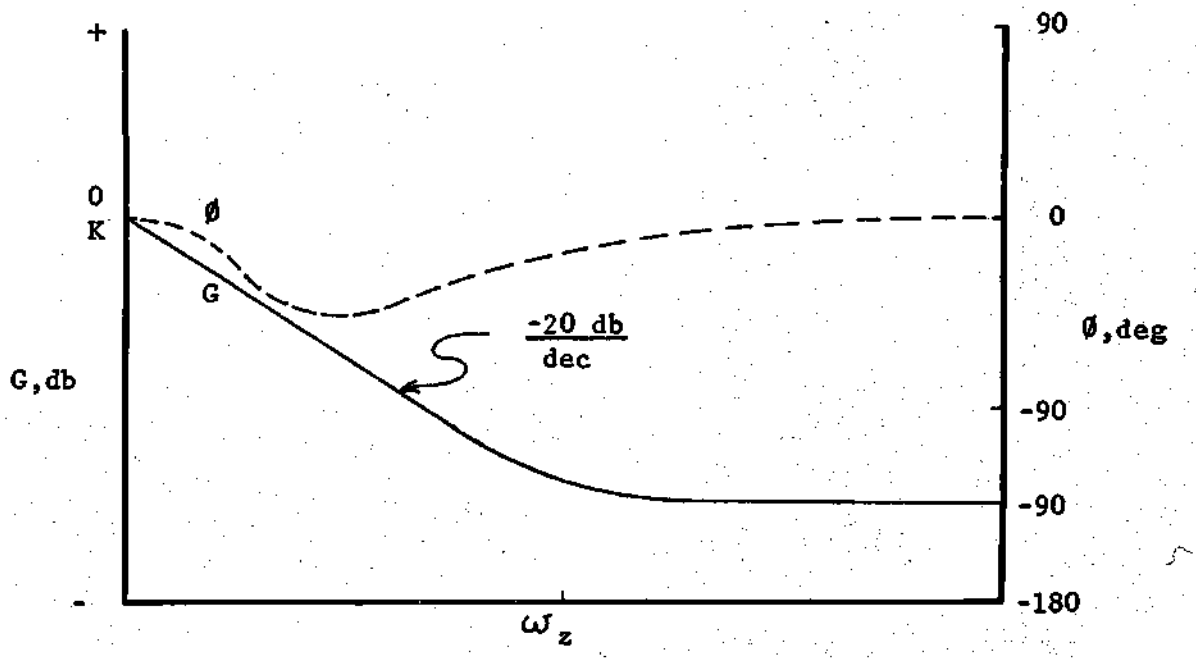

Figure 19b. Network 5 Bode Plot with $\omega_p = 0$.

If the system parameters are adjusted such that $0 < K_{p1} K_{p2} K_2 K_f < 1$, the reduced transfer function takes the form

$$\frac{P_0}{P_1} = K' \left(\frac{s/\omega_z + 1}{s/\omega_p + 1} \right) ,$$

where

$$K' = \frac{K}{\omega_z \left(1 - K_{p1} K_{p2} K_2 K_f \right)} , \qquad (3.52)$$

$$\omega_p = \omega_z \left(1 - K_{p1} K_{p2} K_2 K_f \right)$$

and ω_z and K are defined as in equation (3.51). An examination of the above expression for ω_p shows that the pole always lies to the right of the zero. This is a lag-lead configuration. The pole-zero diagram and Bode plot are similar to those shown in Figures 12a and 12b respectively. In this network, pole and zero locations are completely independent. If the zero location is chosen first, a gain adjustment can locate the pole in any arbitrary position to the right of the zero. It should be cautioned that if $K_{p1} K_{p2} K_2 K_f > 1$, the break frequency of the pole is negative, rendering the system unstable.

CHAPTER IV

THE NETWORKS

4.1 Preliminary Comments

This chapter deals with the reduced transfer functions for those fluidic networks which are obtained by various combinations of the simple configurations discussed in Chapter III. Figures 20 through 26 show the fluidic schematics of these networks, whereas for each, the pole-zero diagram and Bode plot are shown in Figures 27 through 36. The complete transfer functions, for which the reduced transfer functions are a special case, are derived in the appendix. Discussion of the networks pole-zero locations are also provided following each Bode plot.

4.2 Network 6 The Differentiator or Real Poles and Real Zero Configuration

The fluidic schematic is shown in Figure 20a. The reduced transfer function is given by

$$\frac{P_0}{P_i} = \tfrac{1}{2} K K_i K_{a3} \left[\frac{\left(\frac{K_{p1}}{p2} - \frac{K_{p2}}{p1} \right) s + (K_{p1} - K_{p2})}{(s/\omega_{p1} + 1)\,(s/\omega_{p2} + 1)} \right] \quad (4.1)$$

where

$$K = \frac{1}{(R + R_{01})\left(\frac{1}{R_{c3}} + \frac{1}{R + R_{01}} \right)} ,$$

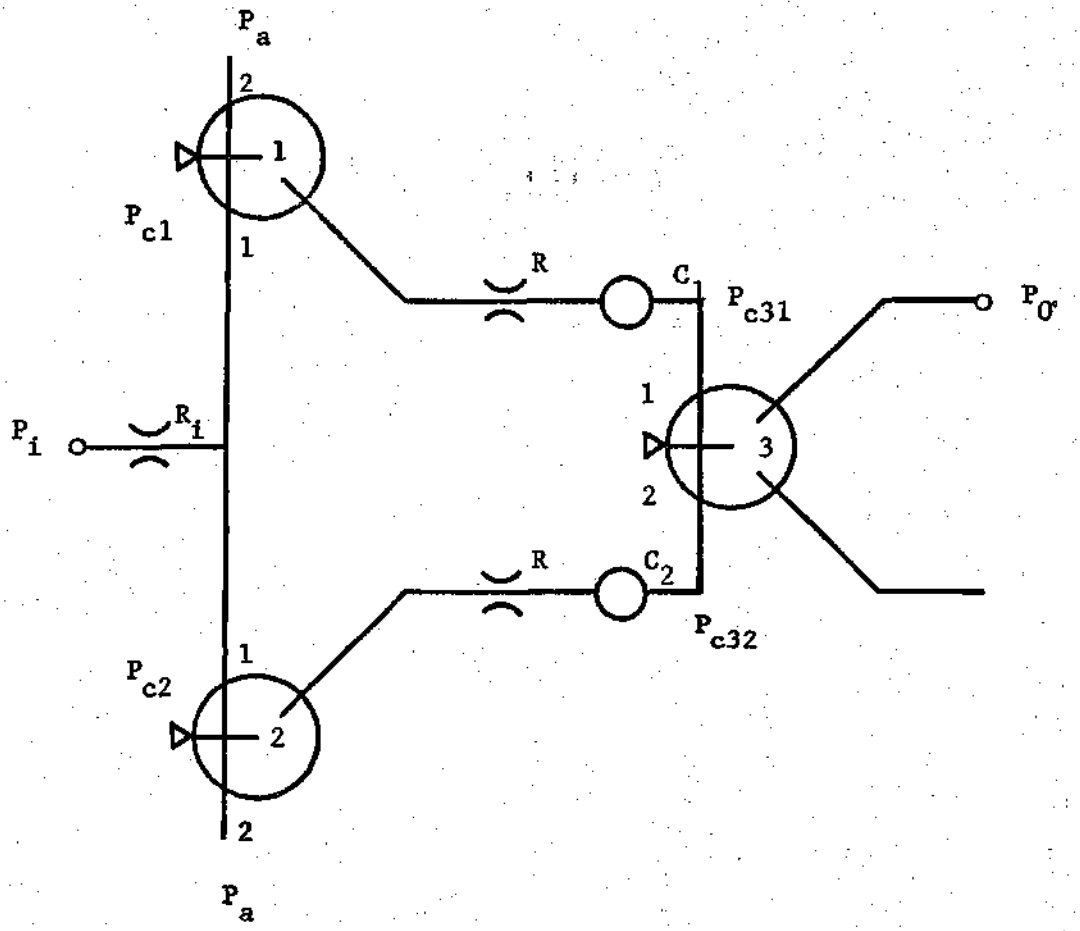

Figure 20a. Network 6 Schematic.

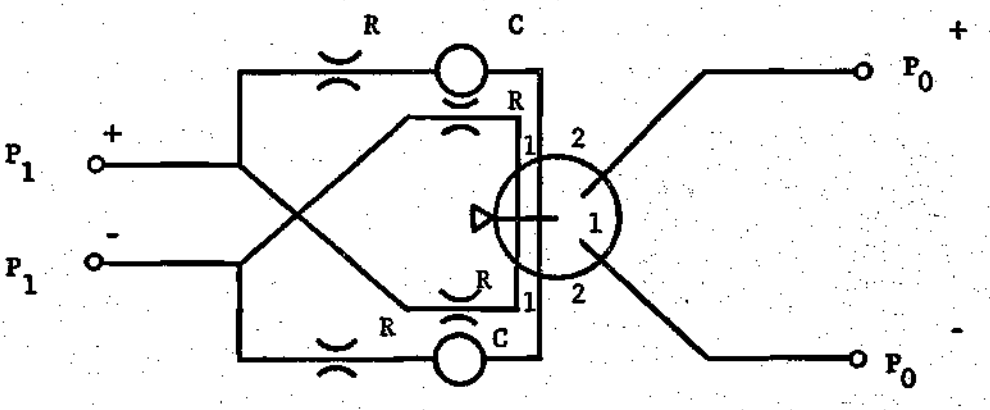

Figure 20b. Network 7 Schematic.

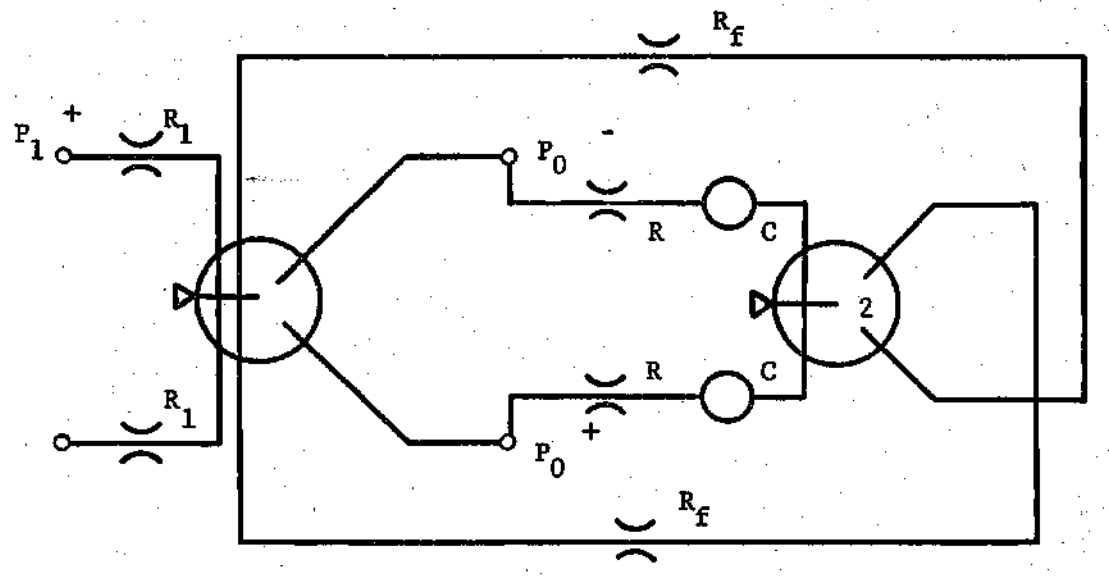

Figure 21a. Network 8 Schematic.

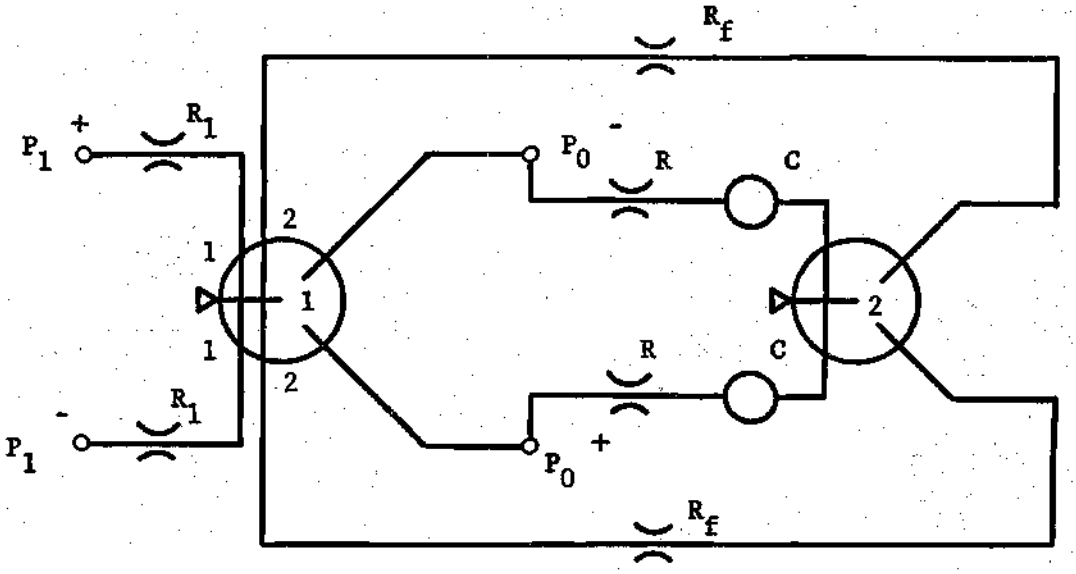

Figure 21b. Network 9 Schematic.

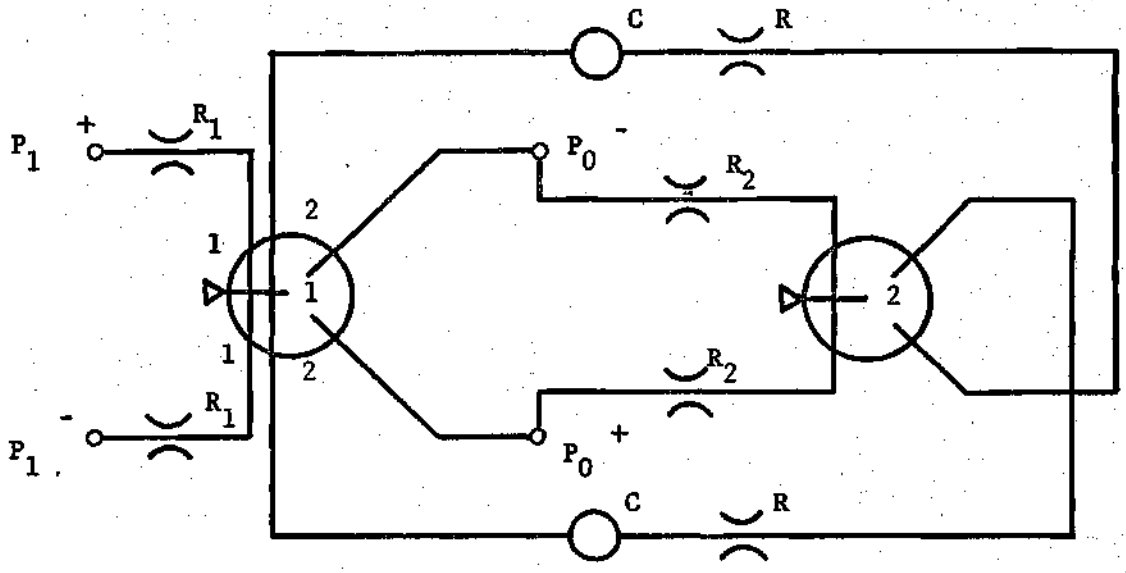

Figure 22a. Network 10 Schematic.

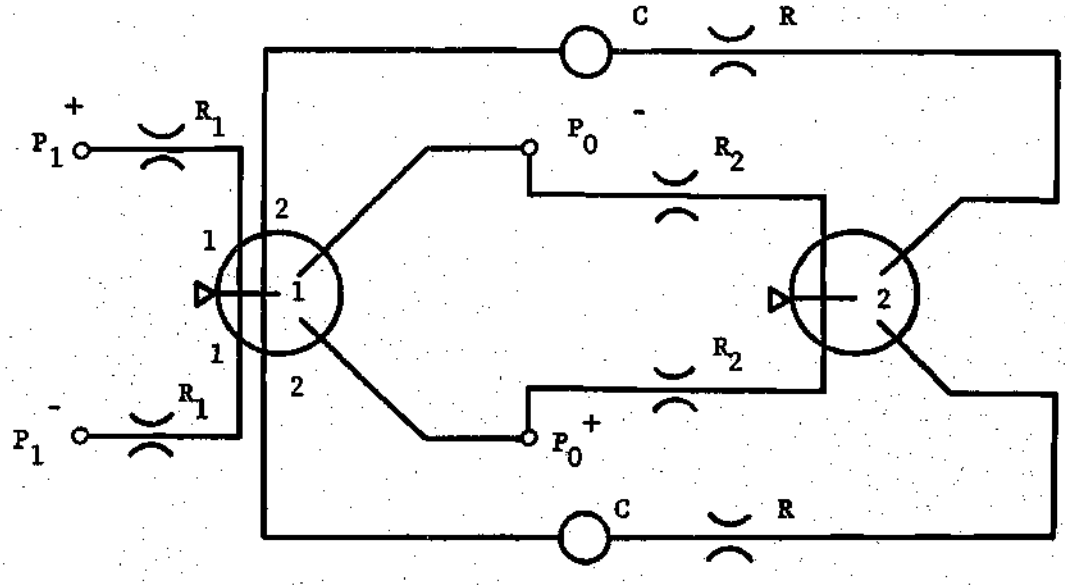

Figure 22b. Network 11 Schematic.

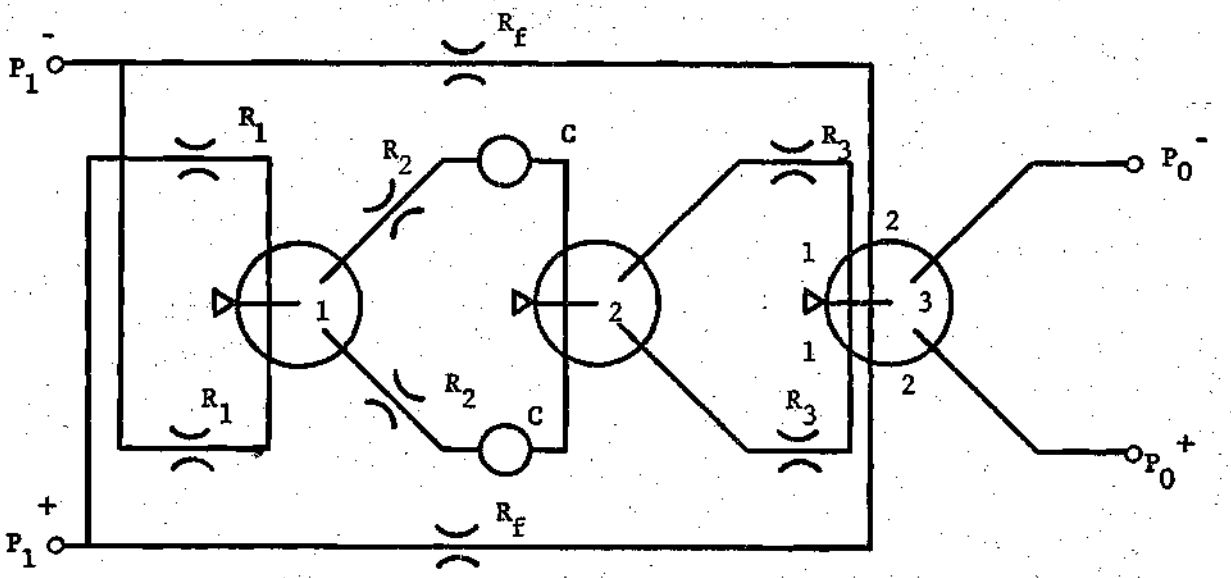

Figure 23a. Network 12 Schematic.

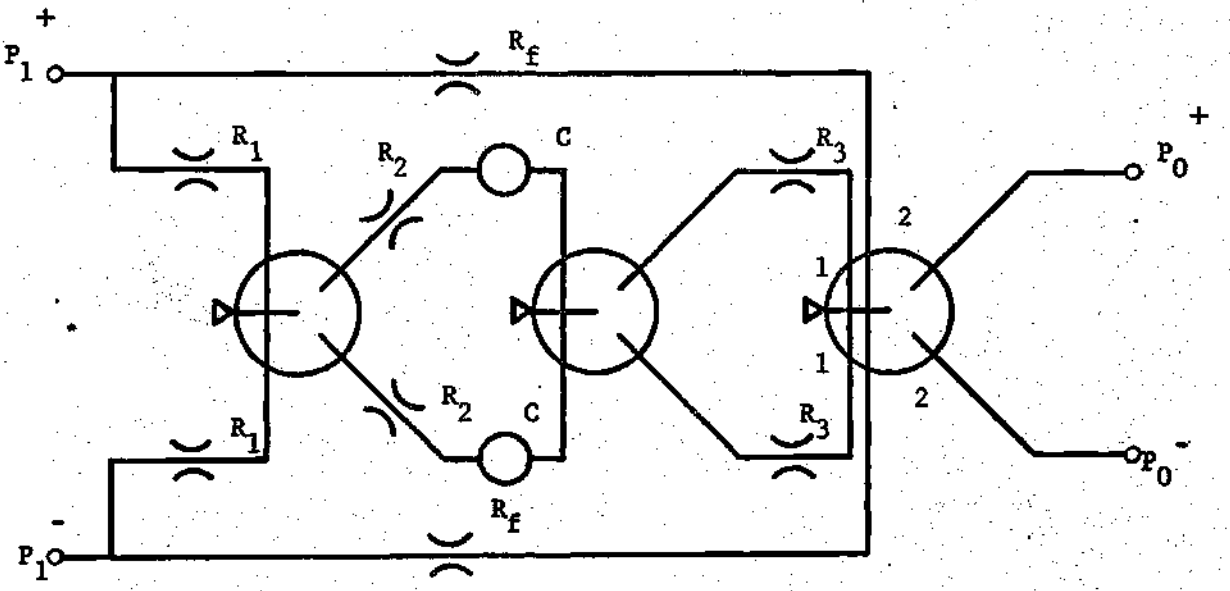

Figure 23b. Network 13 Schematic.

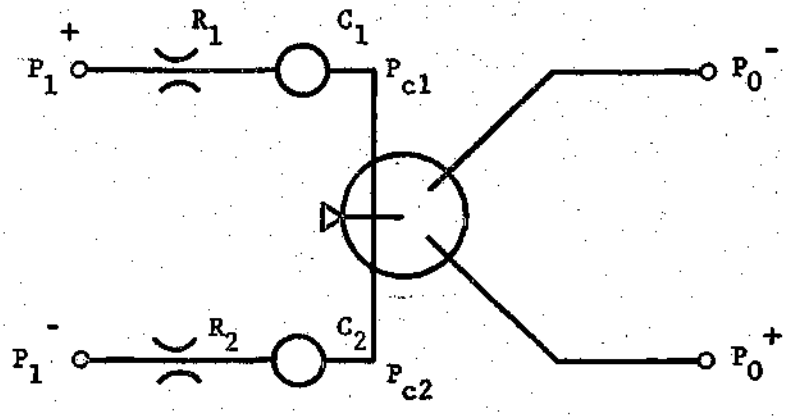

Figure 24a. Network 14 Schematic.

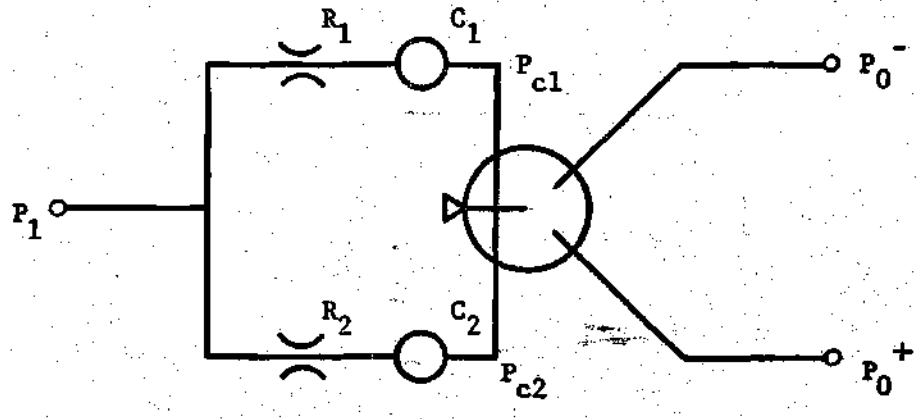

Figure 24b. Network 15 Schematic.

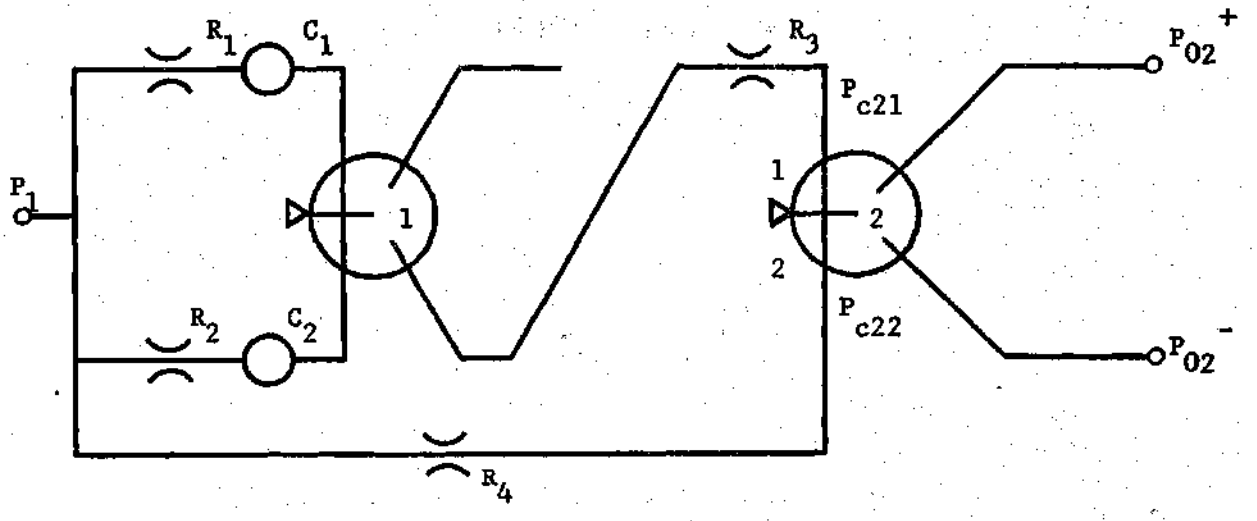

Figure 25a. Network 16 Schematic.

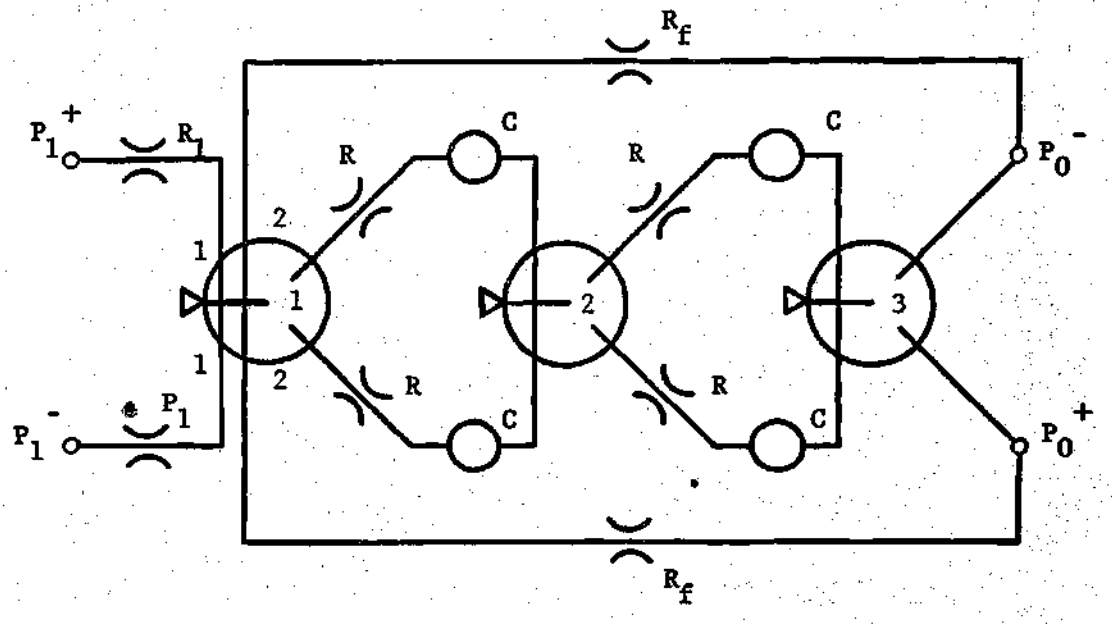

Figure 25b. Network 17 Schematic.

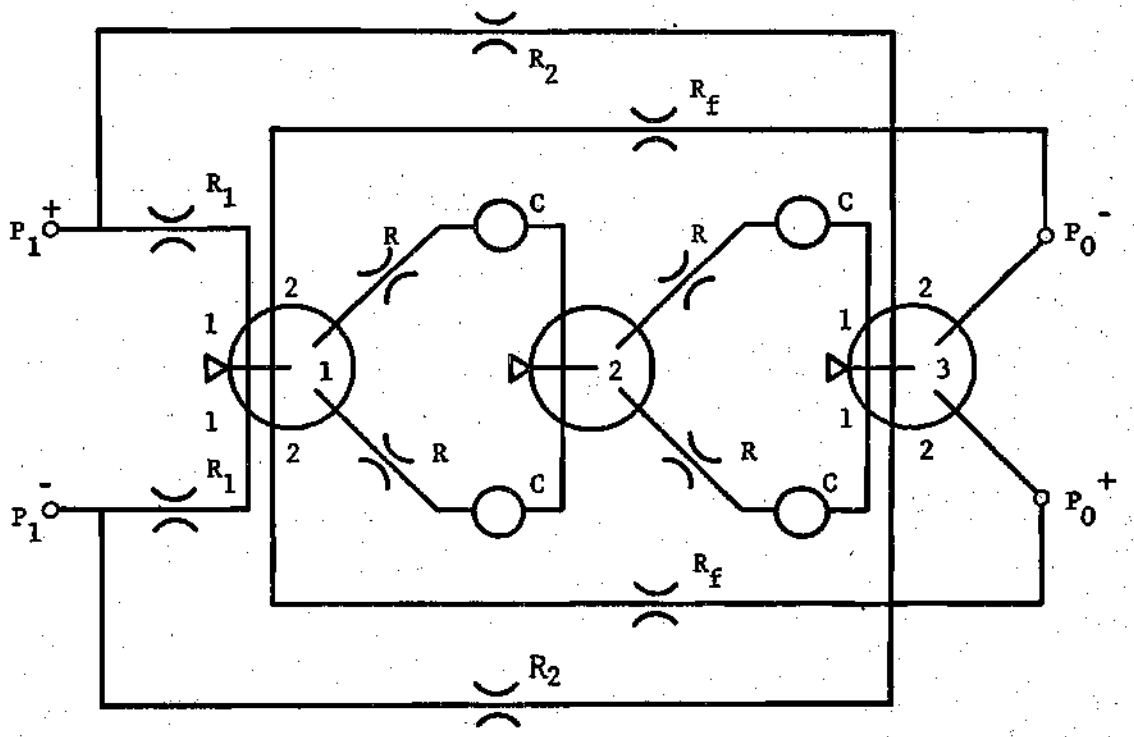

Figure 26. Network 18 Schematic.

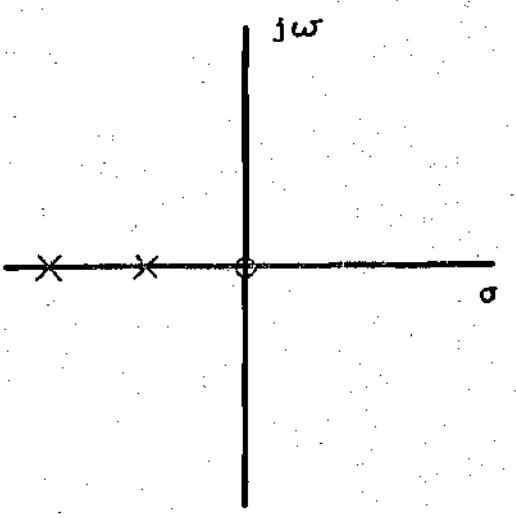

Figure 27a. Network 6 Pole-Zero Diagram with $K_{p1}=K_{p2}$.

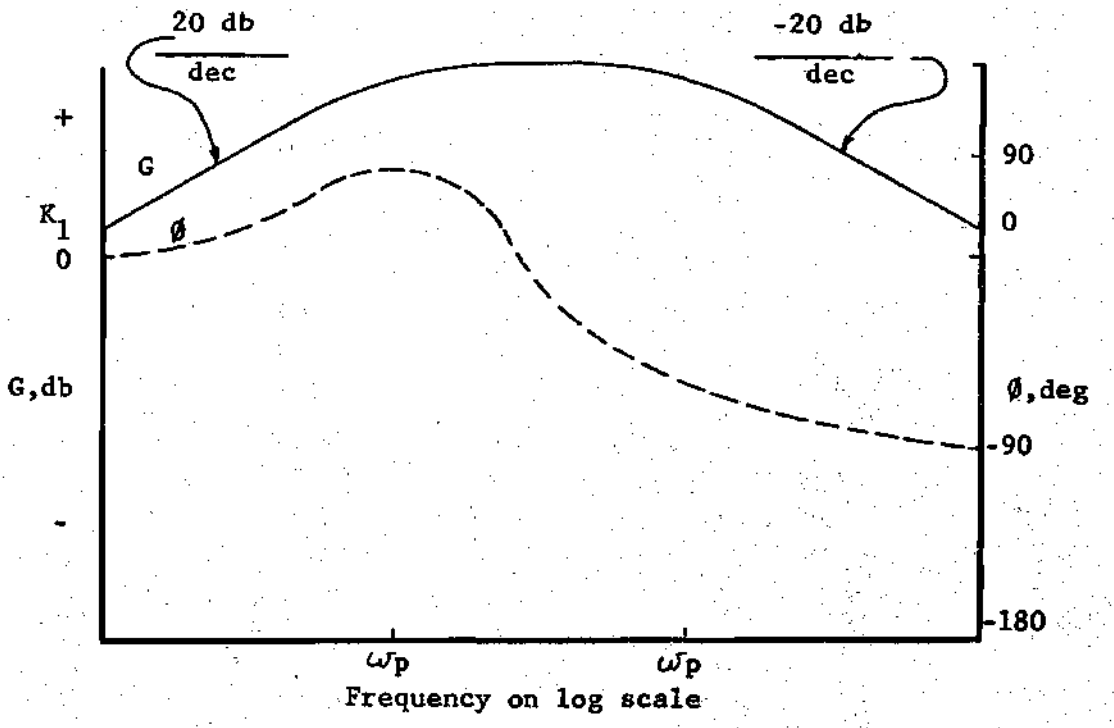

Figure 27b. Network 6 Bode Plot with $K_{p1}=K_{p2}$.

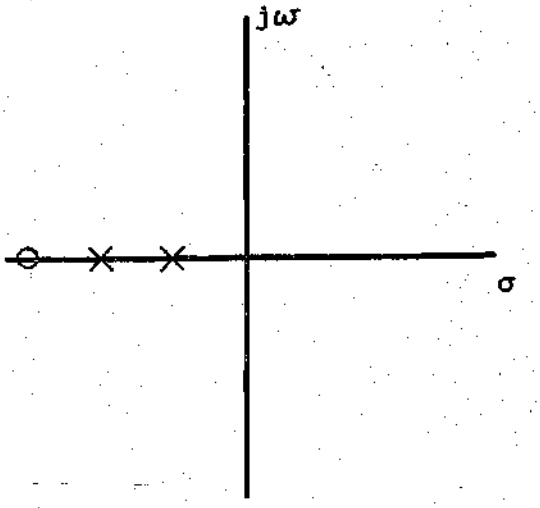

Figure 28a. Network 6 Pole Zero Diagram for Case 1.

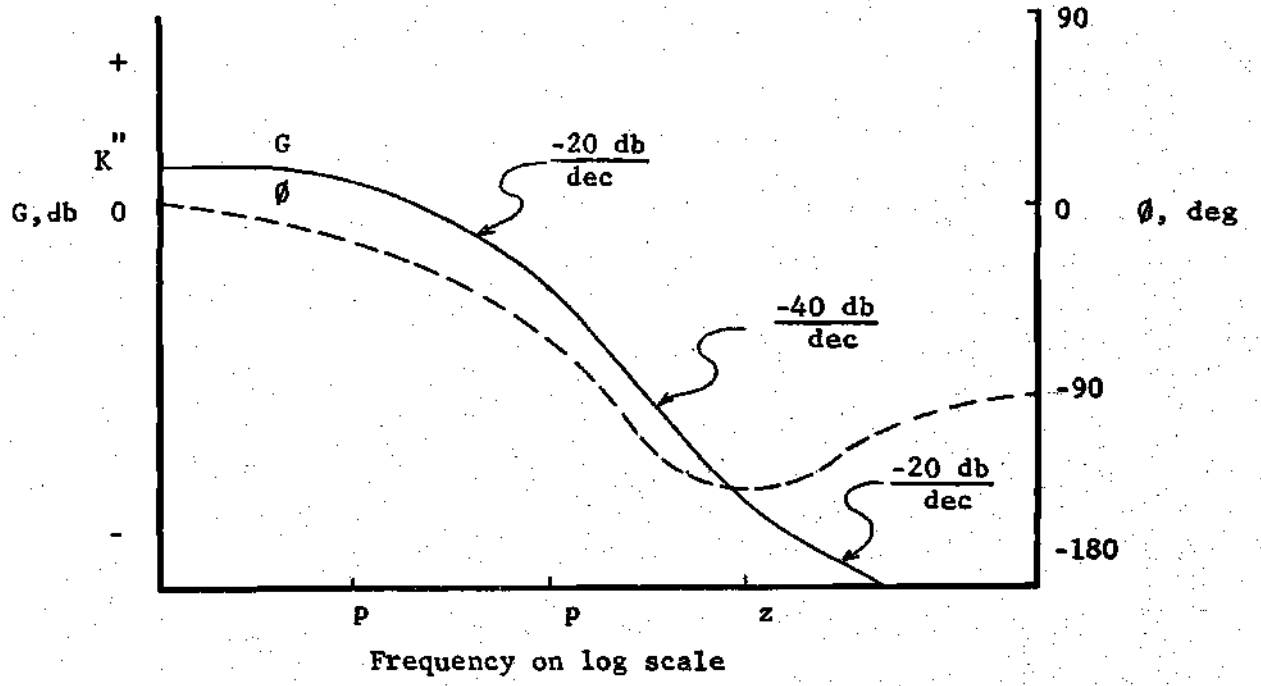

Figure 28b. Network Bode Plat for Case 1.

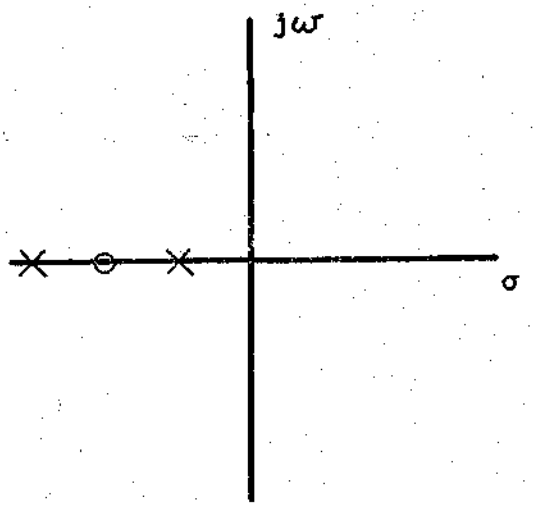

Figure 29a. Network 6 Pole Zero Diagram for Case 2.

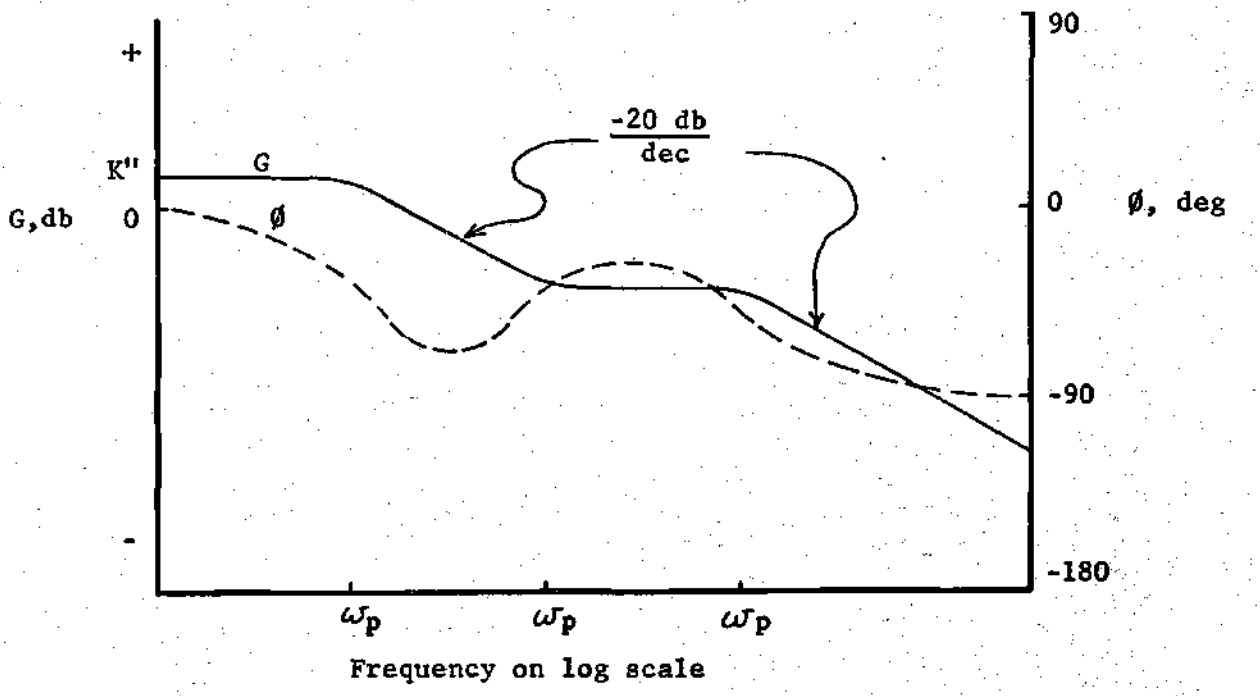

Figure 29b. Network 6 Bode Plot for Case 2.

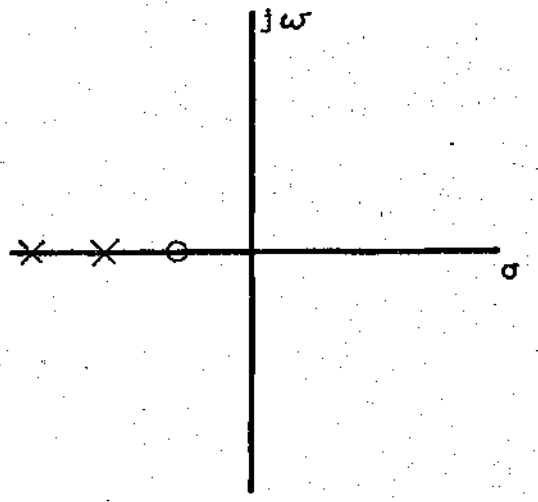

Figure 30a. Network 6 Pole Zero Diagram for Case 3.

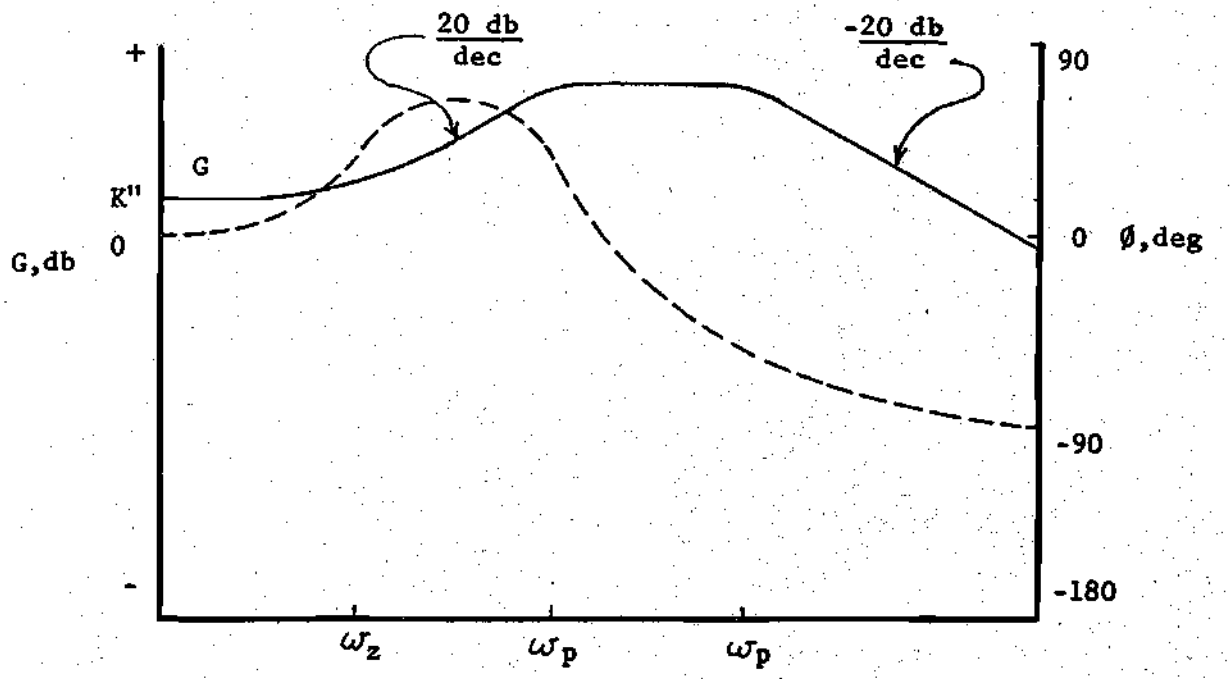

Figure 30b. Network 6 Bode Plot for Case 3.

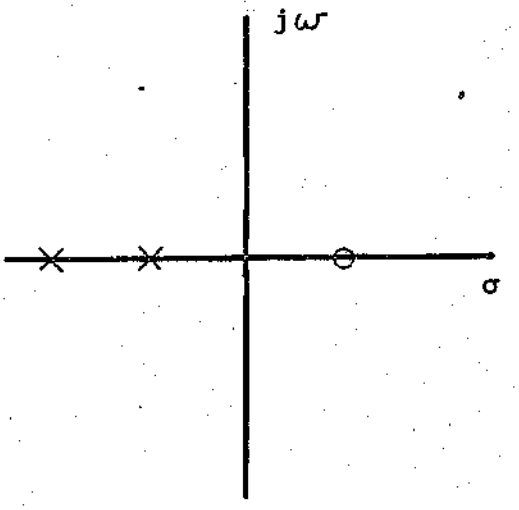

Figure 31a. Network 6 Pole Zero Diagram for Case 4.

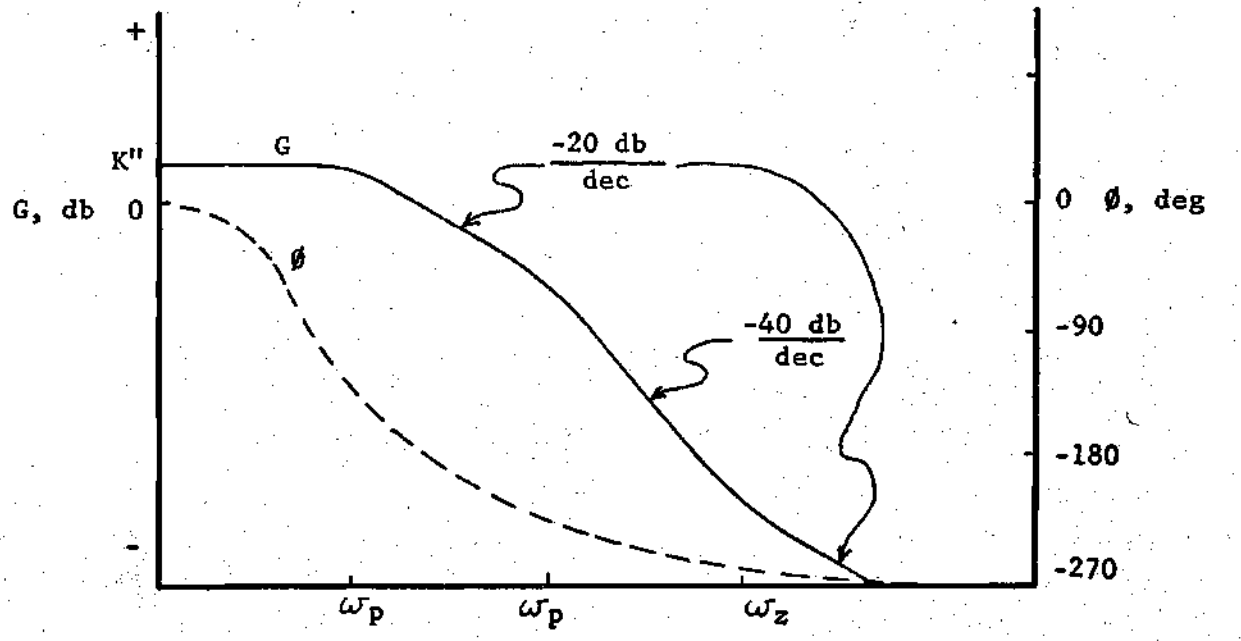

Figure 31b. Network 6 Bode Plot for Case 4.

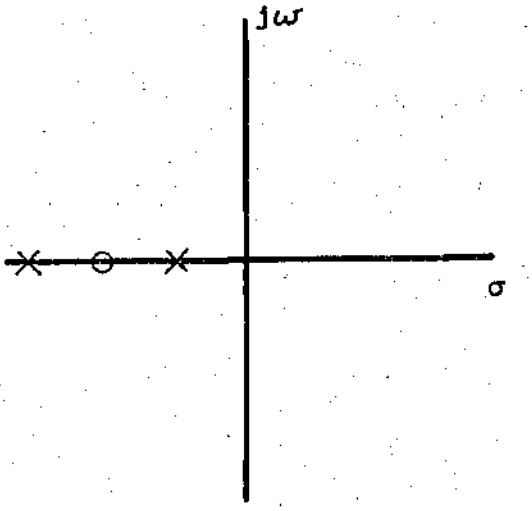

Figure 32a. Network 14 Pole Zero Diagram.

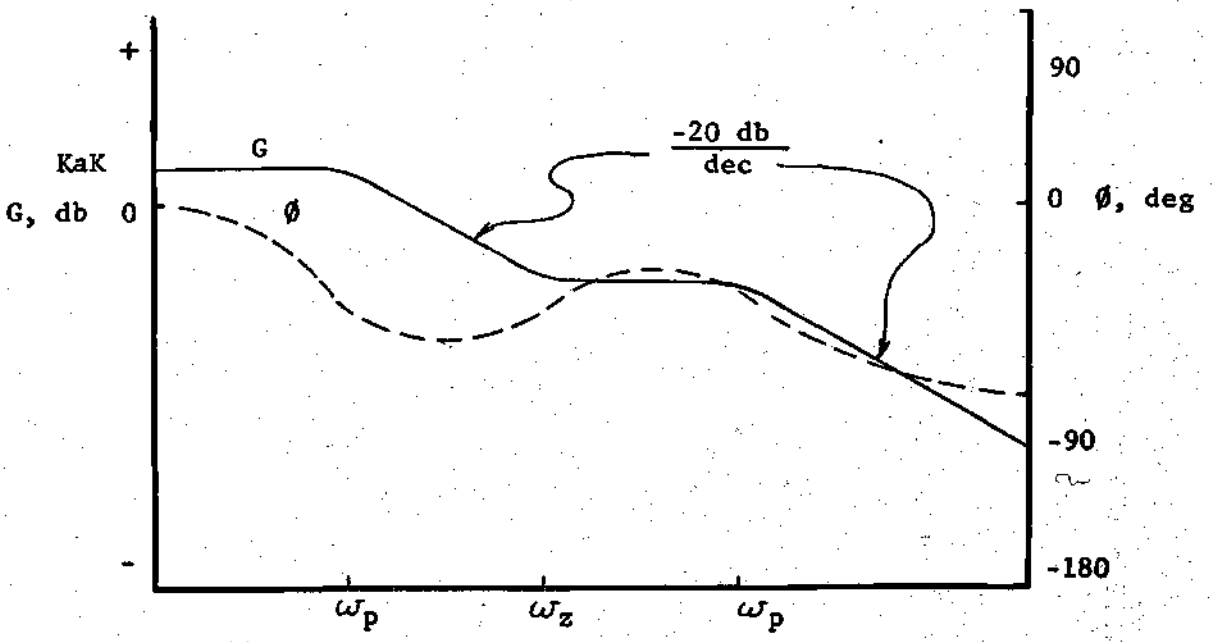

Figure 32b. Network 14 Bode Plot.

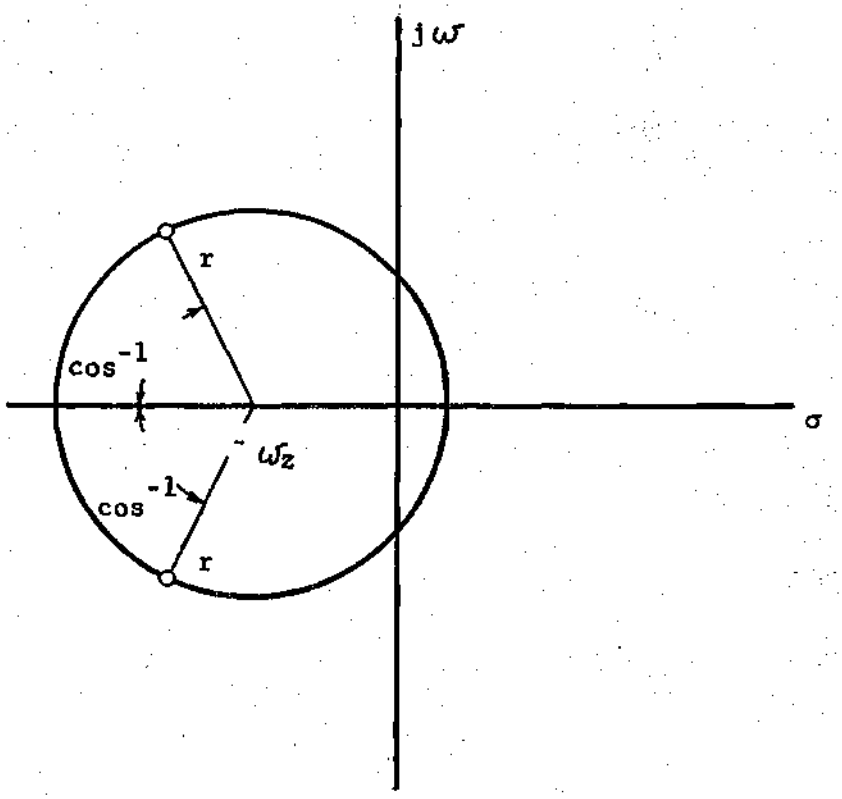

Figure 33. Network 16 Zero Locus.

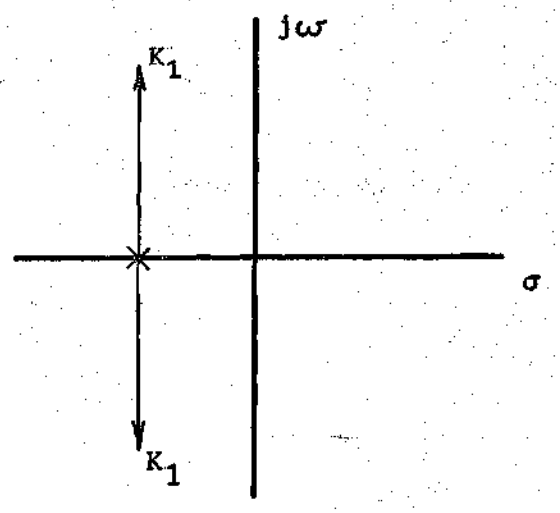

Figure 34a. Network 17 Root Locus.

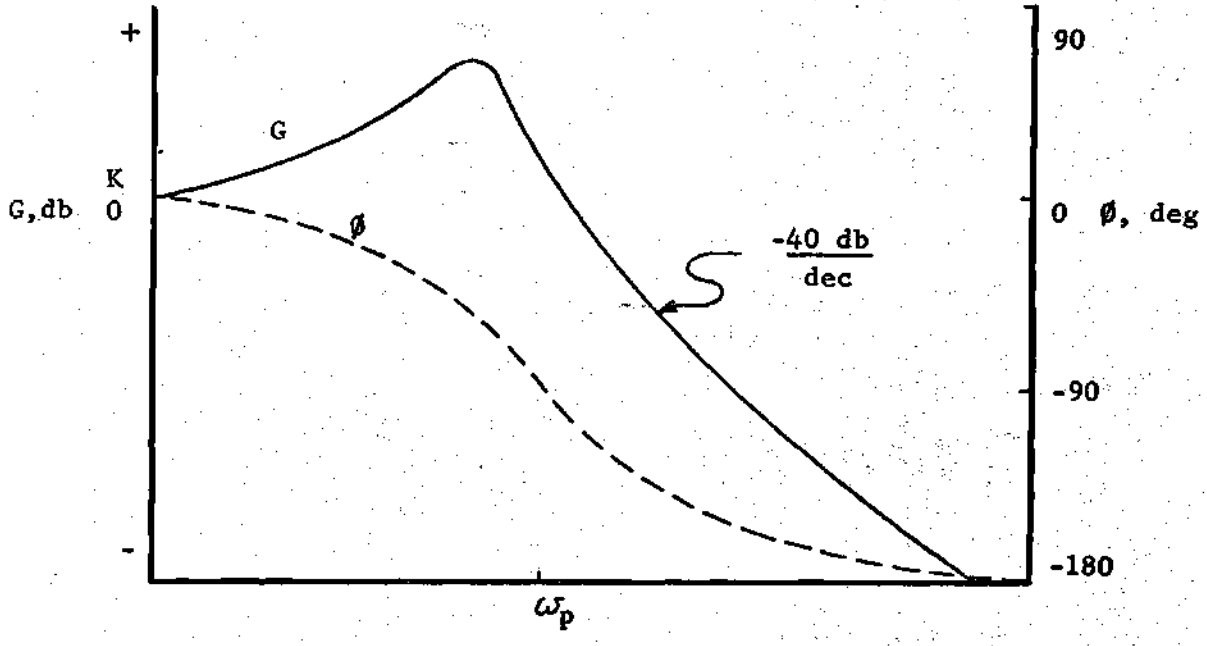

Figure 34b. Network 17 Bode Plot with $\xi < .707$.

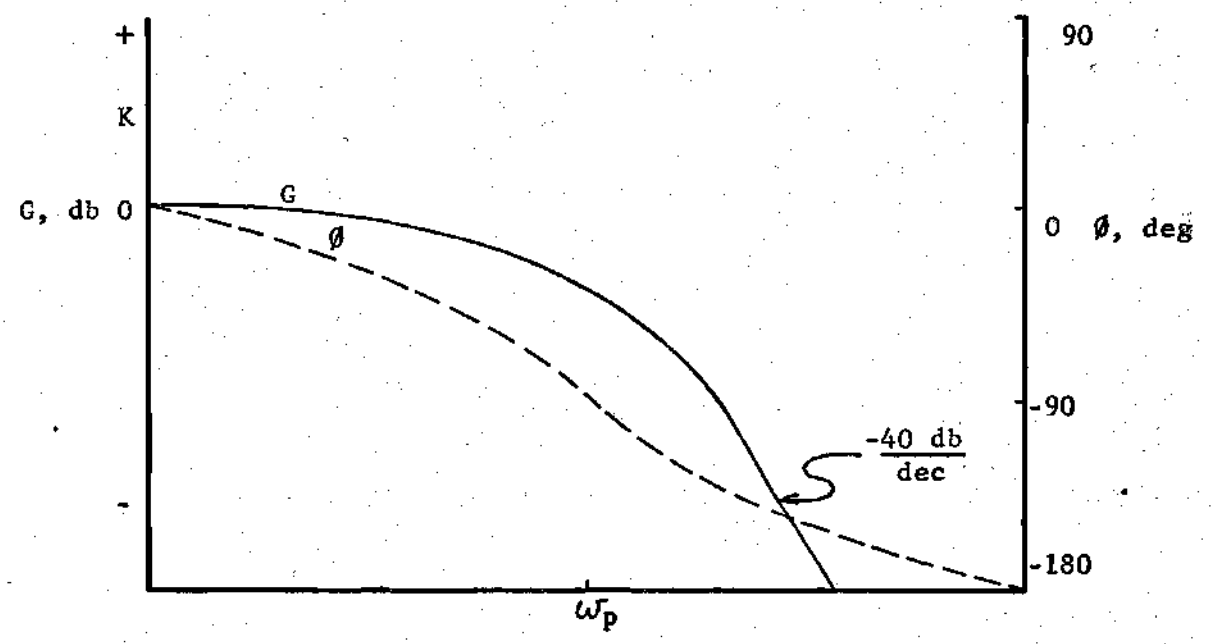

Frequency on log scale

Figure 35a. Network 17 Bode Plot with ξ =.707.

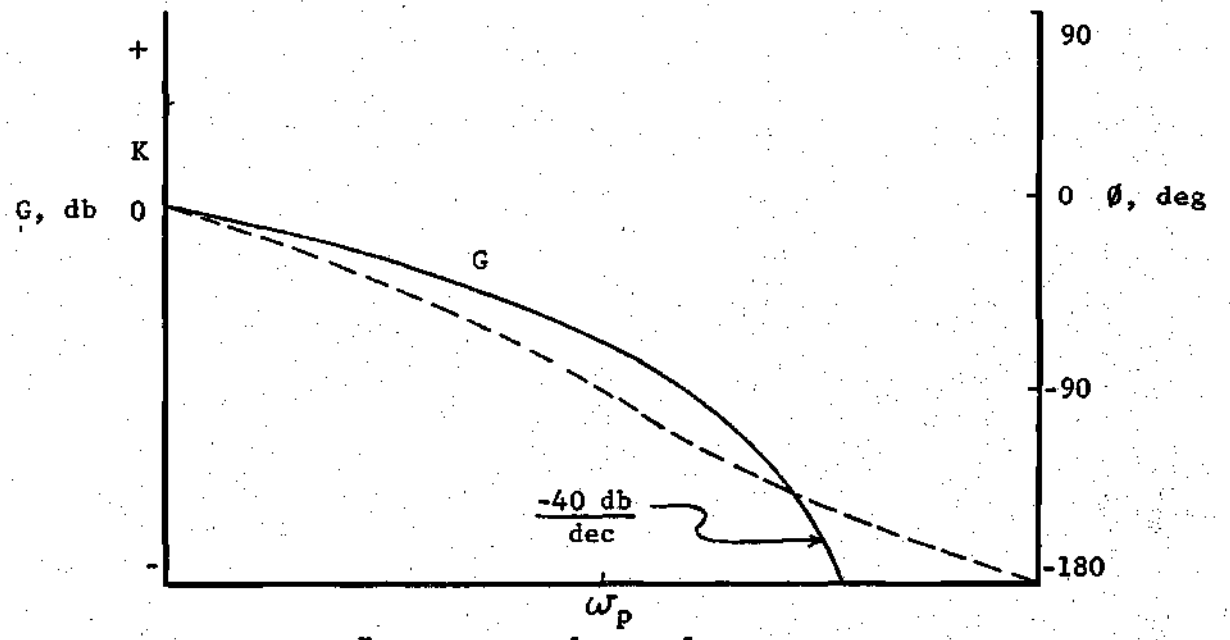

Frequency on log scale

Figure 35b. Network 17 Bode Plot with $\xi > .707$.

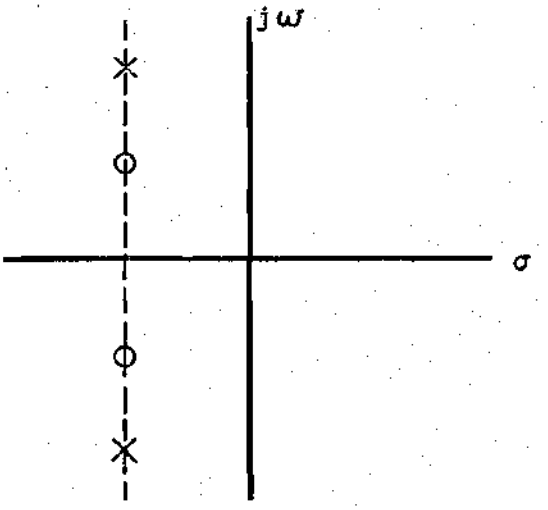

Figure 36a. Network 18, Case 1 Pole-Zero Diagram.

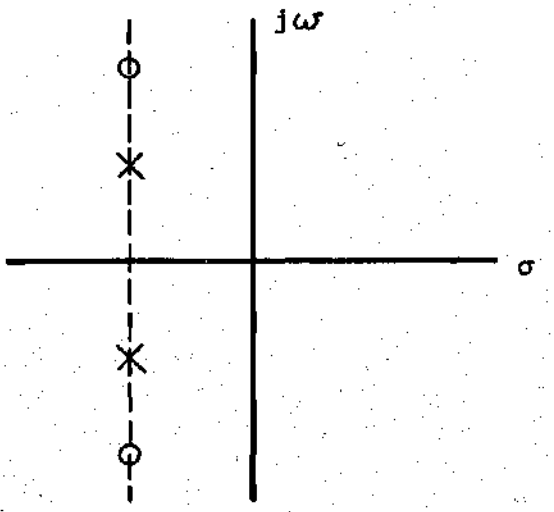

Figure 36b. Network 18, Case 2 Pole-Zero Diagram.

$$K_i = \frac{1}{R_i \left(\frac{1}{R_{c1}} + \frac{1}{R_i} \right)} , \qquad (4.2)$$

$$\omega_{p1} = \frac{1}{(R + R_{01}) C_1} + \frac{1}{R_{c3} C_1}$$

$$\omega_{p2} = \frac{1}{(R + R_{01}) C_2} + \frac{1}{R_{c3} C_2} ,$$

$$R_{c1} = R_{c11} = R_{c21} ,$$

$$R_{c3} = R_{c31} = R_{c32} ,$$

and $$R_{01} = R_{02} .$$

If $K_{p1} = K_{p2} = K_p$, the reduced transfer function can be put into the form

$$\frac{P_0}{P_i} = \frac{K' s}{(s/\omega_{p1} + 1)(s/\omega_{p2} + 1)} \qquad (4.3)$$

where

$$K' = \tfrac{1}{2} K_i K K_p K_{a3} \left(\frac{1}{\omega_{p1}} - \frac{1}{\omega_{p2}} \right) , \qquad (4.4)$$

and all other parameters are defined as in equation (4.2).

The zero for this configuration is located at the origin, while the poles can be located anywhere on the real axis of the left hand plane. This is a differentiator transfer function, with the pole-zero

diagram and Bode plot as shown in Figures 27a and 27b, respectively. Note the differentiator characteristics of the Bode plot, where the magnitude ratio is initially increasing at a rate of 20 db/dec and the phase angle is initially leading.

If $K_{p1} \neq K_{p2}$, the reduced transfer function has the form

$$\frac{P_0}{P_i} = \frac{K'' (s/\omega_z + 1)}{(s/\omega_{p1} + 1)(s/\omega_{p2} + 1)} ,$$

where

$$K'' = \tfrac{1}{2} K_i K K_{a3} (K_{p1} - K_{p2}), \tag{4.5}$$

$$z = \frac{\omega_{p1} \omega_{p2} (K_{p1} - K_{p2})}{K_{p1} \omega_{p1} - K_{p2} \omega_{p2}} ,$$

and all other parameters are defined as in equation (4.2).

It is seen from equation (4.5) that the zero can be located anywhere on the real axis of either plane. There are several possible combinations of pole-zero positioning.

Case 1 occurs when the zero lies to the left of the two poles, in other words, when

$$\omega_{p1} < \omega_{p2} < \omega_z < 0, \tag{4.6}$$

or

$$\omega_{p2} < \omega_{p1} < \omega_z < 0.$$

The pole-zero diagram and Bode plot for this configuration are shown in Figures 28a and 28b respectively.

Case 2 occurs when the zero lies between the two poles, or

$$\omega_{p1} < \omega_z < \omega_{p2} < 0,$$

or (4.7)

$$\omega_{p2} < \omega_z < \omega_{p1} < 0.$$

The pole-zero diagram and Bode plot for this configuration are shown in Figures 29a and 29b respectively.

Case 3 occurs when the zero lies to the right of the two poles, but in the left hand plane, or

$$\omega_p < \omega_{p1} < \omega_{p2} < 0,$$

or (4.8)

$$\omega_z < \omega_{p2} < \omega_{p1} < 0.$$

The pole-zero diagram and Bode plot for the configuration are shown in Figures 30a and 30b respectively.

Case 4 occurs when the zero lies to the right of the two poles and in the right hand plane, or

$$\omega_{p1} < \omega_{p2} < 0 < \omega_z ,$$

or (4.9)

$$\omega_{p2} < \omega_{p2} < 0 < \omega_z.$$

The pole-zero diagram and Bode plot for this configuration are shown in Figures 31a and 31b respectively. Note that the magnitude versus frequency plot is the same as for case 2, but the zero now contributes a phase lag.

Note from equation (4.5) that the generation of a right hand plane zero requires that K_{p2} to be greater than K_{p1}. This situation also produces a negative overall system gain, K''. The physical significance of this is an output initially 180 degrees out of phase with input.

4.3 Network 7 - The Differentiator

The fluidic schematic is shown in Figure 20b. The reduced transfer function is given by

$$\frac{P_{od}}{P_{id}} = \frac{K' s}{(s/\omega_p + 1)} \quad ,$$

where

$$K' = \frac{K_a K}{\omega_p} \quad , \tag{4.10}$$

$$K = \frac{1}{R\left(\frac{1}{R_c} + \frac{1}{R}\right)} \quad ,$$

$$\omega_p = \frac{1}{R_c} + \frac{1}{R_c C} \quad ,$$

and

$$R_c = R_{c11} = R_{c12} \quad .$$

The zero is located at the origin. The pole can be located anywhere on the real axis of the left hand plane. This is a differentiator configuration. The pole-zero diagram and Bode plot are similar to those given in Figures 15a and 15b respectively.

4.4 Network 8 - The Lag-Lead

The fluidic schematic is shown in Figure 21a. The reduced transfer function is given by

$$\frac{P_{od}}{P_{id}} = K \left(\frac{s/\omega_z + 1}{s/\omega_p + 1} \right) \quad ,$$

where

$$K = \frac{K_1 K_{a1}}{1 + 2 K_{a1} K_{p2} K_2 K_f} \quad ,$$

$$K_1 = \frac{1}{R_1 \left(\frac{1}{R_{c11}} + \frac{1}{R} \right)} \quad , \qquad (4.11)$$

$$K_2 = \frac{1}{R \left(\frac{1}{R_{c2}} + \frac{1}{R} \right)} \quad ,$$

$$K_f = \frac{1}{(R_f + R_{02}) \left(\frac{1}{R_{c12}} + \frac{1}{R_f + R_{02}} \right)} \quad ,$$

$$\omega_z = \frac{1}{R_{c2}\, C} + \frac{1}{R\, C}$$

and

$$\omega_p = \frac{\omega_z}{1 + 2\, K_{a1}\, K_{p2}\, K_f} \quad .$$

The zero can be located anywhere on the real axis of the left hand plane. The pole is always to the right of the zero and can be located as close to the origin as desired, providing sufficient gain is available. The network therefore has a lag-lead configuration. The pole-zero diagram and Bode plot are similar to those shown in Figures 12a and 12b respectively.

4.5 Network 9 - The Lead-Lag

The fluidic schematic is shown in Figure 21b. The reduced transfer function is given by

$$\frac{P_{od}}{P_{id}} = K \left(\frac{s/\omega_z + 1}{s/\omega_p + 1} \right)$$

where (4.12)

$$K = \frac{K_1\, K_{a1}}{1 - 2K_{a1}\, K_{p2}\, K_2\, K_f} \quad ,$$

$$\omega_p = \frac{\omega_z}{1 - 2\, K_{a1}\, K_{p2}\, K_2\, K_f} \quad ,$$

and all other parameters are defined as in equations (4.11).

The zero can be located anywhere on the real axis of the left hand plane. The pole always lies to the left of the zero. This is therefore a lead-lag configuration. Care must be taken to insure that the factor $2\ K_{a1}\ K_{p2}\ K_2\ K_f$ does not exceed unity and thus render the system unstable. The pole-zero diagram and Bode Plot are similar to those shown in Figures 14a and 14b respectively.

4.6 Network 10 - The Lag-Lead

The fluidic schematic is shown in Figure 22a. The reduced transfer function is given by

$$\frac{P_{od}}{P_{id}} = K \left(\frac{s/\omega_z + 1}{s/\omega_p + 1} \right) ,$$

where

$$K = \frac{K_1\ K_{a1}}{1 + 2K_{a1}\ K_{p2}\ K_2\ K_f} ,$$

$$K_1 = \frac{1}{R_1 \left(\frac{1}{R_{c11}} + \frac{1}{R_1} \right)} , \qquad (4.13)$$

$$K_2 = \frac{1}{R_2 \left(\frac{1}{R_{c2}} + \frac{1}{R_2} \right)} ,$$

$$K_f = \frac{1}{(R + R_{02}) \left(\frac{1}{R_{c12}} + \frac{1}{R + R_{02}} \right)} ,$$

$$\omega_z = \frac{1}{(R + R_{02})\ C} + \frac{1}{R_{c12}\ C} \quad ,$$

and

$$\omega_p = \frac{\omega_z}{1 + 2\ K_{a1}\ K_{p2}\ K_2\ K_f} \quad .$$

The zero can be located anywhere on the real axis of the left hand plane. The pole always lies to the right of the zero and can be located as close to the origin as desired, providing sufficient gain is available. The pole-zero and Bode plots are similar to those shown in Figures 12a and 12b respectively.

4.7 Network 11 - The Lead-Lag

The fluidic schematic is shown in Figure 22b. The reduced transfer function is given by

$$\frac{P_{od}}{P_{id}} = K \left(\frac{s/\omega_z + 1}{s/\omega_p + 1} \right)$$

where

$$K = \frac{K_1\ K_{a1}}{1 - 2\ K_{a1}\ K_{p2}\ K_2\ K_f} \quad , \qquad (4.14)$$

$$\omega_p = \frac{\omega_z}{1 - 2\ K_{a1}\ K_{p2}\ K_2\ K_f} \quad ,$$

and all other parameters are defined as in equations (4.13).

The zero can be located anywhere on the real axis of the left hand plane. The pole always lies to the left of the zero. This is a lead-lag configuration. Care must be taken that the factor $2\ K_{a1}\ K_{p2}\ K_2\ K_f$ does not exceed unity and thus render the system unstable. The pole-zero diagram and Bode plot are similar to those shown in Figures 14a and 14b respectively.

4.8 Network 12 - The Lead-Lag

The fluidic schematic is shown in Figure 23a. The reduced transfer function is given by

$$\frac{P_{od}}{P_{id}} = K \left(\frac{s/\omega_z + 1}{s/\omega_p + 1} \right) ,$$

where

$$K = K_{a3}\ K_f \left(1 - \frac{4K_1\ K_2\ K_{p1}\ K_{p2}\ K_3}{K_f} \right)$$

$$K_1 = \frac{1}{R_1 \left(\frac{1}{R_{c1}} + \frac{1}{R_1} \right)} , \qquad (5.15)$$

$$K_2 = \frac{1}{(R + R_{01}) \left(\frac{1}{R_{c2}} + \frac{1}{R_2 + R_{01}} \right)} ,$$

$$K_3 = \frac{1}{(R_3 + R_{02})\left(\frac{1}{R_{c31}} + \frac{1}{R_3 + R_{02}}\right)} ,$$

$$K_f = \frac{1}{R_f\left(\frac{1}{R_{c32}} + \frac{1}{R_f}\right)} ,$$

$$\omega_p = \frac{1}{(R_2 + R_{01})C} + \frac{1}{R_{c2}C} ,$$

and

$$\omega_z = \omega_p \left(1 - \frac{4 K_1 K_{p1} K_2 K_{p2} K_3}{K_f}\right) .$$

The pole can be located anywhere on the real axis of the left hand plane. The zero always lies to the right of the pole. The zero cannot be located at the origin, however. For the configuration to occur, the factor $4 K_1 K_{p1} K_2 K_{p2} K_3 / K_f$ must equal unity. The system gain is then zero. The Pole-Zero diagram and Bode plot for the case of a left hand plane zero are similar to those shown in Figures 14a and 14b respectively, and, for a right hand plane zero, in Figures 15a and 15b respectively.

4.9 Network 13 - The Lag-Lead

The fluidic schematic is shown in Figure 23a. The reduced transfer function is given by

$$\frac{P_{od}}{P_{id}} = K \left(\frac{s/\omega_z + 1}{s/\omega_p + 1}\right) , \qquad (5.16)$$

where

$$K = K_{a3} K_4 \left(\frac{1 + 4 K_1 K_{p1} K_2 K_{p2} K_3}{K_f} \right) ,$$

$$\omega_z = \omega_p \left(\frac{1 + 4 K_1 K_{p1} K_2 K_{p2} K_3}{K_f} \right) ,$$

and all other parameters are as defined in equation (5.15).

The pole can be located anywhere on the real axis of the left hand plane. The zero always lies to the left of the pole. This is a lag-lead configuration. The Pole-Zero diagram and Bode plot are similar to those shown in Figures 12a and 12b respectively.

4.10 Network 14 - Real Poles-Real Zero

The fluidic schematic is shown in Figure 24a. The reduced transfer function is given by

$$\frac{P_{od}}{P_{id}} = K_a K \frac{s/\omega_z + 1}{(s/\omega_{p1} + 1)(s/\omega_{p2} + 1)} ,$$

where

$$\omega_{p1} = \frac{1}{R_1 C_1} + \frac{1}{R_c C_1} ,$$

$$\omega_{p2} = \frac{1}{R_2 C_2} + \frac{1}{R_c C_2} , \qquad (5.17)$$

$$\omega_z = \frac{R_1 R_2}{C_1 R_1 + C_2 R_2} \left[\frac{1}{R_2}\left(\frac{1}{R_c}+\frac{1}{R_1}\right)+\frac{1}{R_1}\left(\frac{1}{R_c}+\frac{1}{R_2}\right)\right],$$

and

$$K = \frac{\frac{1}{R_1}\left(\frac{1}{R_c}+\frac{1}{R_2}\right)+\frac{1}{R_2}\left(\frac{1}{R_c}+\frac{1}{R_1}\right)}{2\left(\frac{1}{R_c}+\frac{1}{R_2}\right)\left(\frac{1}{R_c}+\frac{1}{R_1}\right)} .$$

The poles can be anywhere on the real axis of the left hand plane, Restrictions on zero positioning can now be obtained.

Let

$$\rho_1 = \frac{1}{R_1}\left(\frac{1}{R_c}+\frac{1}{R_2}\right)$$

and

$$\rho_2 = \frac{1}{R_2}\left(\frac{1}{R_c}+\frac{1}{R_1}\right),$$

then

$$\omega_{p1} = \frac{R_1 \rho_1}{C_2} ,$$

$$\omega_{p2} = \frac{R_2 \rho_2}{C_1} , \qquad (5.18)$$

and

$$\omega_z = \frac{\rho_1 + \rho_2}{C_1/R_2 + C_2/R_1} ,$$

or

$$\omega_z = \frac{(\rho_1 + \rho_2)\omega_{p1}\omega_{p2}}{\rho_2\omega_{p1} + \rho_1\omega_{p2}} \quad .$$

It can be seen by inspection of the above result that ω_z must lie between ω_1 and ω_2. The Pole-Zero diagram and Bode plot are shown in Figures 32a and 32b respectively.

4.11 Network 15 - Real Poles-Real Zero

The fluidic schematic is shown in Figure 24b. The reduced transfer function is given by

$$\frac{P_{od}}{P_1} = K_a K \frac{s/\omega_z + 1}{(s/\omega_{p1} + 1)(s/\omega_{p2} + 1)} , \qquad (5.19)$$

where

$$K = \frac{\frac{1}{R_1}(\frac{1}{R_c} + \frac{1}{R_2}) - \frac{1}{R_2}(\frac{1}{R_c} + \frac{1}{R_1})}{(\frac{1}{R_c} + \frac{1}{R_2})(\frac{1}{R_c} + \frac{1}{R_1})},$$

$$\omega_z = \frac{R_1R_2}{R_2C_2 - R_1C_1} \frac{1}{R_1}(\frac{1}{R_c} + \frac{1}{R_2}) - \frac{1}{R_2}(\frac{1}{R_c} + \frac{1}{R_1}) ,$$

and all other parameters are defined as in equation (5.17).

The poles can be located anywhere on the real axis of the left hand plane. Once again, defining ω_1, ω_2, ω and $\quad_2$ as in equation (5.18), and using the above expression for ω_z yields the result

$$\omega_z = \frac{(\rho_1 - \rho_2)\,\omega_{p1}\omega_{p2}}{\rho_1\omega_{p2} - \rho_2\omega_{p1}} \quad . \tag{5.20}$$

It can be seen by inspection of the above result, that the zero can take on all real values. Its possible locations are to the left of the poles, between the poles, to the right of the poles but in the left hand plane, or in the right hand plane. These possibilities correspond to cases 1, 2, 3 and 4 of netowrk 6, and the Pole-Zero and Bode plots correspond to those shown in Figures 27a, 27b, 28a, 28b, 29a, 29b, 30a and 30b.

4.12 Network 16 - Real Poles-Complex Zeros

The fluidic schematic is shown in Figure 25a. The reduced transfer function is given by

$$\frac{P_{od2}}{P_1} = K_{a2}K_4(1-K') \quad \frac{\frac{s^2}{\omega_o^2} + \frac{2\xi s}{\omega_o} + 1}{(s/\omega_{p1}+1)(s/\omega_{p2}+1)} \quad ,$$

where

$$K_4 = \frac{1}{R_4\left(\frac{1}{R_{c22}} + \frac{1}{R_4}\right)} \quad , \tag{5.21}$$

$$K' = \frac{K_{a2} K K_{p1} K_3}{K_4 K_{a2}} \quad ,$$

$$K = \frac{\frac{1}{R_1}\left(\frac{1}{R_{c1}} + \frac{1}{R_2}\right) - \frac{1}{R_2}\left(\frac{1}{R_{c1}} + \frac{1}{R_1}\right)}{\left(\frac{1}{R_{c1}} + \frac{1}{R_2}\right)\left(\frac{1}{R_{c1}} + \frac{1}{R_1}\right)} \quad ,$$

$$K_3 = \frac{1}{(R_3 + R_{01})\left(\frac{1}{R_{c21}} + \frac{1}{R_3 + R_{01}}\right)} \quad ,$$

$$\omega_{p1} = \frac{1}{R_1(C_1 + C_{c1})} + \frac{1}{R_{c1}(C_1 + C_{c1})} \quad ,$$

$$\omega_{p2} = \frac{1}{R_2(C_2 + C_{c1})} + \frac{1}{R_{c1}(C_2 + C_{c1})} \quad ,$$

$$\omega_o = \left[\omega_{p1}\omega_{p2}(1-K')\right]^{\frac{1}{2}} \quad ,$$

$$\zeta = \left[\frac{\omega_o}{2(1-K')}\right]\left[\frac{1}{\omega_{p1}} + \frac{1}{\omega_{p2}} - \frac{K'}{\omega_z}\right] ,$$

and

$$\omega_z = \frac{R_1R_2}{R_2C_2-R_1C_1}\left[\frac{1}{R_1}\left(\frac{1}{R_{c1}}+\frac{1}{R_2}\right) - \left(\frac{1}{R_{c1}}+\frac{1}{R_1}\right)\right] .$$

Since the expressions for ω_{p1}, ω_{p2} and ω_z are the same as for these parameters in network 11, the same restrictions apply. The poles can lie anywhere on the real axis of the left hand, while the zero can have any real value.

It can be shown [12] that the locus of zeros is a circle on the s-plane, with center at $-\omega_z$ and radius given by

$$r = \left[(\omega_z - \omega_{p1})(\omega_z - \omega_{p2})\right]^{\frac{1}{2}} . \qquad (5.22)$$

A real-values radius and therefore complex roots will only occur only if both poles lie to one side of the zero. The locus of zeros is shown in Figure 33.

4.13 Network 17 - Complex Poles

The fluidic schematic is shown in Figure 25b. The reduced transfer function is given by

$$\frac{P_{od}}{P_{1d}} = \frac{K}{\frac{s^2}{\omega_x^2} + \frac{2\xi s}{\omega_x} + 1} ,$$

where

$$K = \frac{4K_{p1}K_{p2}K_{a3}K_1K_2K_3}{1 + K_L} ,$$

$$K_L = 4K_{p1}K_{p2}K_{a3}K_2K_3K_f ,$$

$$K_1 = \frac{1}{R_1 (\frac{1}{R_{c11}} + \frac{1}{R_1})} , \qquad (5.23)$$

$$K_2 = \frac{1}{(R + R_{01})(\frac{1}{R_c} + \frac{1}{R + R_{01}})} ,$$

$$K_3 = \frac{1}{(R + R_{02})(\frac{1}{R_c} + \frac{1}{R + R_{02}})} ,$$

$$K_f = \frac{1}{R_f (\frac{1}{R_{c12}} + \frac{1}{R_f})} ,$$

$$R_{01} = R_{02} ,$$

$$R_c = R_{c2} = R_{c3} ,$$

$$\omega_x = \omega_p \, (1 + K_L)^{\frac{1}{2}} ,$$

$$\omega_p = \frac{1}{RC} + \frac{1}{R_c C} ,$$

and

$$= (K_L)^{-\frac{1}{2}} .$$

The real component of the second order root is given by

$$R_e \{s\} = \omega_x \xi = \omega_p (1+K_L) \quad \frac{1}{(1+K_L)^{\frac{1}{2}}} = \omega_p . \qquad (5.24)$$

Therefore, the root locus is a straight vertical line located at $-\omega_p$ in the s-plane. Increasing K_L causes a more oscillatory response to a step input. The root locus is shown in Figure 34a. The Bode plot for the underdamped case, that is, a damping ratio of less than .707, is given in Figure 34b. The Bode plots for the cases where the damping ratio equals .707 and is greater than .707 are given in Figures 35a and 35b respectively.

4.14 Network 18 - Complex Poles-Complex Zeros

The lundic schematic is shown in Figure 26. The reduced transfer function is given by

$$\frac{P_{od}}{P_{1d}} = K \frac{\frac{s^2}{\omega_0^2} + \frac{2\xi_0 s}{\omega_0} + 1}{\frac{s^2}{\omega_x^2} + \frac{2\xi_x s}{\omega_x} + 1} ,$$

where

$$K = \frac{K_{a3} K_g (1 + \frac{K_1 K_L}{K_g K_f})}{1 + K_L} ,$$

$$K_L = 4K_{p1} K_{p2} K_{a3} K_2 K_3 K_f , \qquad (5.24)$$

$$K_1 = \frac{1}{R_1 (\frac{1}{R_{c11}} + \frac{1}{R_1})} ,$$

$$K_2 = \frac{1}{(R + R_{01})(\frac{1}{R_{c2}} + \frac{1}{R + R_{01}})} ,$$

$$K_3 = \frac{1}{(R + R_{02})(\frac{1}{R_{c3}} + \frac{1}{R + R_{02}})} ,$$

$$K_f = \frac{1}{R_f(\frac{1}{R_{c12}} + \frac{1}{R_f})} ,$$

$$K_g = \frac{1}{R_2 (\frac{1}{R_{c32}} + \frac{1}{R_2})} ,$$

$$R_{01} = R_{02} ,$$

$$R_c = R_{c2} = R_{c3},$$

$$\omega_0 = \omega_p(1 + \frac{K_I K_L}{K_g K_f})^{\frac{1}{2}} ,$$

$$\omega_x = \omega_p(1 + K_L)^{\frac{1}{2}} ,$$

$$\xi_0 = (1 + \frac{K_I K_L}{K_g K_f})^{-\frac{1}{2}} ,$$

$$\xi_x = (1 + K_L)^{-\frac{1}{2}},$$

and

$$\omega_p = \frac{1}{RC} + \frac{1}{R_c C} .$$

It can be seen that

$$\omega_0 \zeta_0 = \omega_x \zeta_x = \omega_p. \tag{5.25}$$

Therefore, the complex poles and zeros lie on a vertical line located at $-\omega_p$ in the s-plane. Increasing K_L lowers both ζ_0 and ζ_x. There are two possible Pole-Zero configurations. Case 1 occurs when the zeros lie closer to the real axis. The Pole-Zero diagram is shown in Figure 36a. Case 2 occurs when the poles lie closer to the real axis. The Pole-Zero diagram is shown in Figure 36b.

CHAPTER V

EXPERIMENTAL PROGRAM

5.1 Purpose of the Experimental Work

The dynamic testing of a few selected networks is conducted in order to demonstrate the relative accuracies of reduced and complete transfer functions. The results are not intended to be experimental validation of the amplifier model, the verity of which is well established.

5.2 Apparatus

A schematic of the dynamic test apparatus is shown in Figure 37. The pneumatic signal generator is an electrical to pneumatic signal converter. The electrical signal is supplied by an electrical function generator. The input and output pressures are measured by Pitran transducers. A dual channel oscilloscope is used, with input pressure pictured on the horizontal axis and output pressure on the vertical. In all the networks tested, a Corning Model 19807 center dump proportional amplifier is used. All external resistors are laminar restrictors.

5.3 Test Procedure

In all tests, the amplifier supply pressure, P_s, is set at 6 psig. P_c, the bias level, is set at 10 percent P_s by adjusting the supply pressure control valve attached to the pneumatic signal generator.

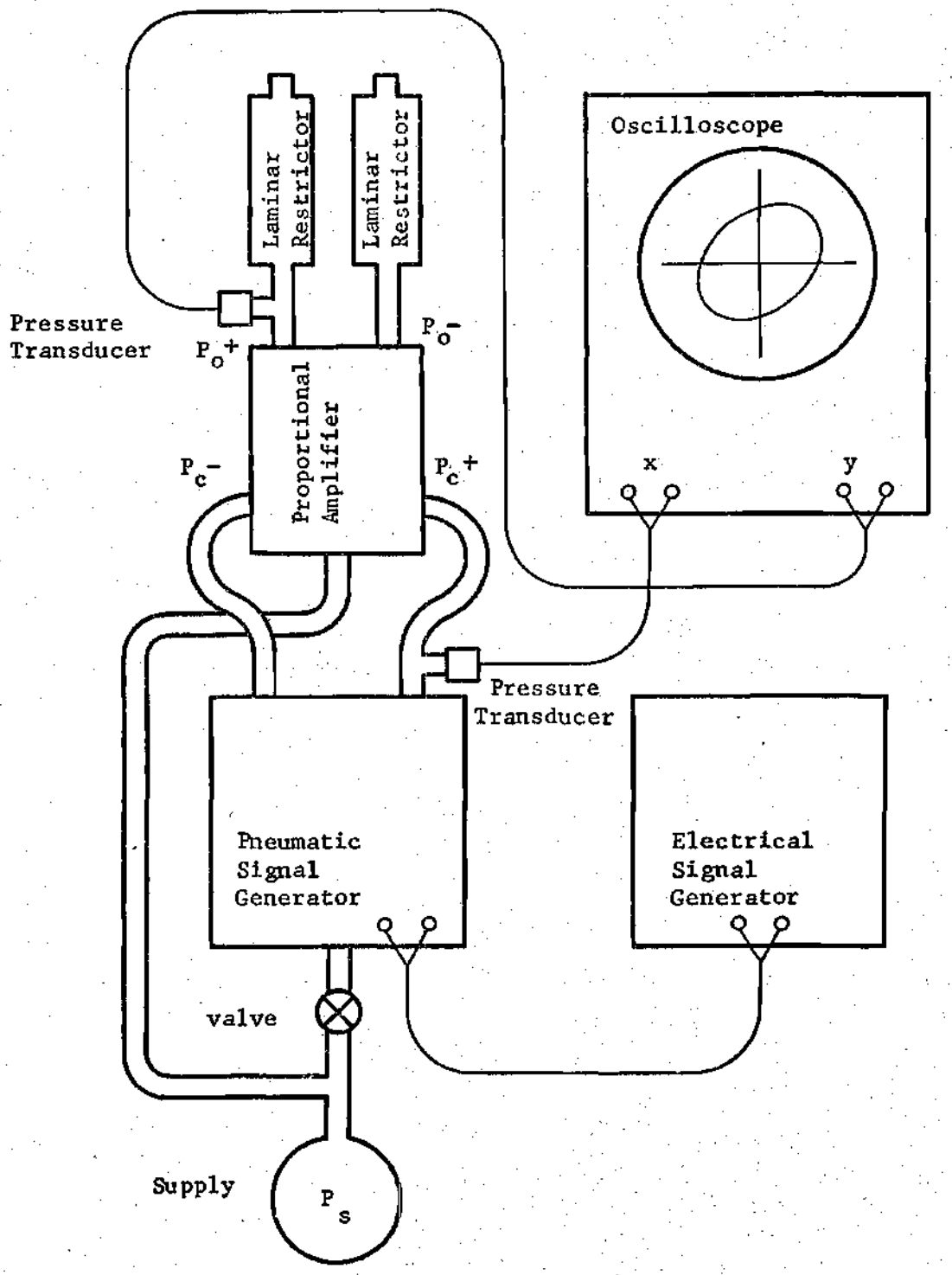

Figure 37. Schematic of Dynamic Test Apparatus.

With the electric signal generator set at 1 to 2 Hz, the pattern on the oscilloscope is a straight line. As the input frequency is increased, the linear pattern becomes an ellipse. Such a pattern is shown in Figure 38, where B/C gives the system amplitude ratio, G, and $\sin^{-1}$ A/B gives the phase angle, . When the major axis of ellipse lies in the first and third quadrants, the phase angle lies between 0° and -90°. When the phase angle equals 90°, the major axis is vertical. A phase angle between -90° and -180° causes the major axis to fall in second and fourth quadrants.

If the initial linear pattern is adjusted so that B/C = 1, then G is the same as the magnitude ratio, M, where the magnitude ratio is defined as the amplitude ratio at a given frequency divided by the dc amplitude ratio, which is the overall system gain.

5.4 The Network Transfer Functions

Appropriate pressure versus flow curves are generated and all system parameters are evaluated at the operating point pressures, as explained in a previous section. Since experimentally obtained system output amplitudes can be conveniently read as magnitude ratios, overall system gain constants are irrelevant. For this reason each overall system gain is taken as unity. The complete and reduced transfer functions for each experimentally tested network are then obtained. Reasonably short connector lengths keep amplifier and connecting line dynamics to a minimum.

The amplifier transfer function is given by

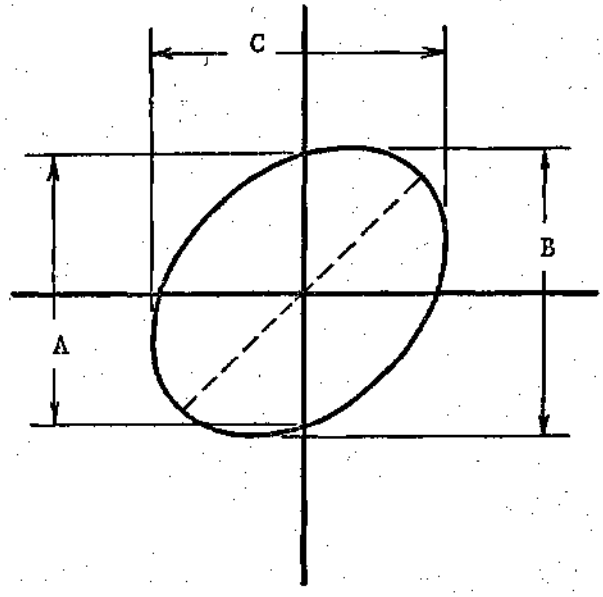

Figure 38. The Oscilloscope Elliptical Pattern.

$$\frac{P_{od}}{P_{cd}} = \frac{e^{-(.00036)s}}{(.0030)\ s + 1} \qquad (5.1)$$

Magnitude and phase angle versus frequency plots of this transfer function are compared with experimental data in Figures 39 and 40. The pole break frequency as predicted analytically is significantly lower than the value indicated by test results.

The reduced transfer function for network 1 is given by

$$\frac{P_0}{P_1} = \frac{1}{(.0153)\ s + 1} \qquad (5.2)$$

and the complete transfer function by

$$\frac{P_0}{P_1} = \frac{e^{-(.00064)s}}{(.0153)s + 1} \qquad (5.3)$$

Magnitude and phase angle versus frequency plots of these transfer functions are compared with experimental results in Figures 41 and 42. Here again, the pole break frequency as predicted analytically is lower than the value indicated by test results. Note that the reduced transfer function phase angle plot levels off to -90° at higher frequencies. Neither experimental data nor values predicted by the

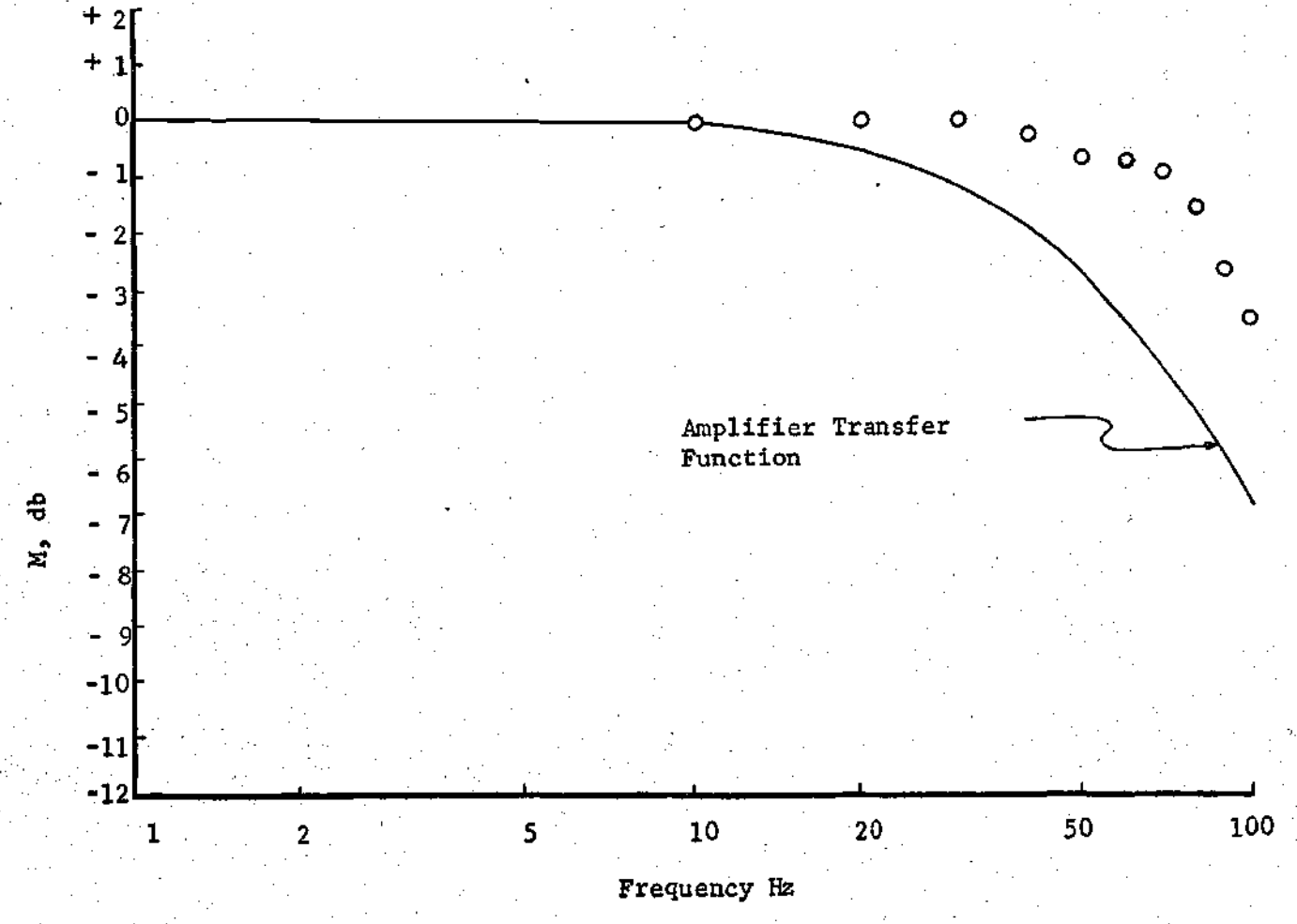

Figure 39. Amplifier Magnitude Ratio Versus Frequency.

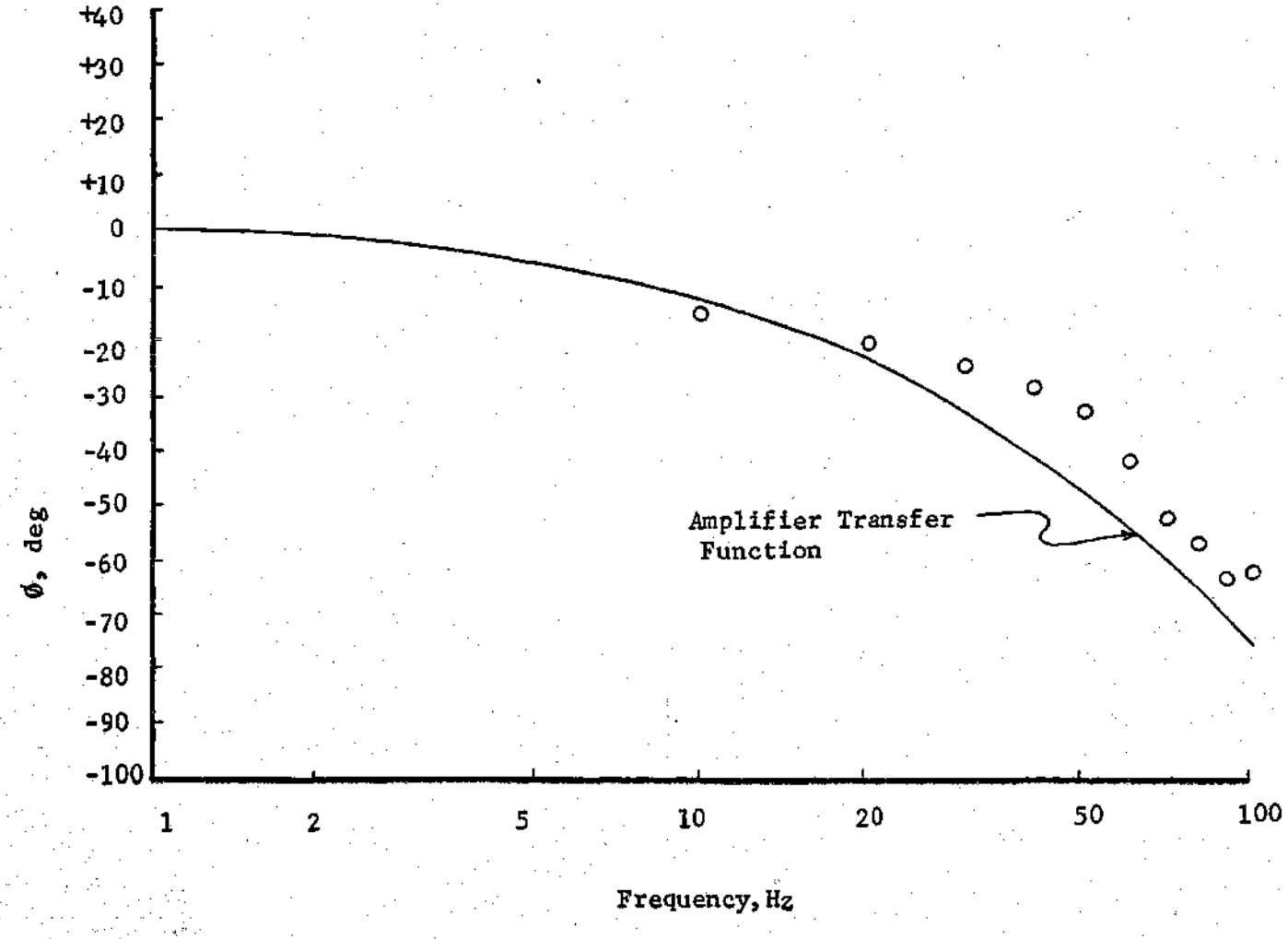

Figure 40. Amplifier Phase Angle Versus Frequency.

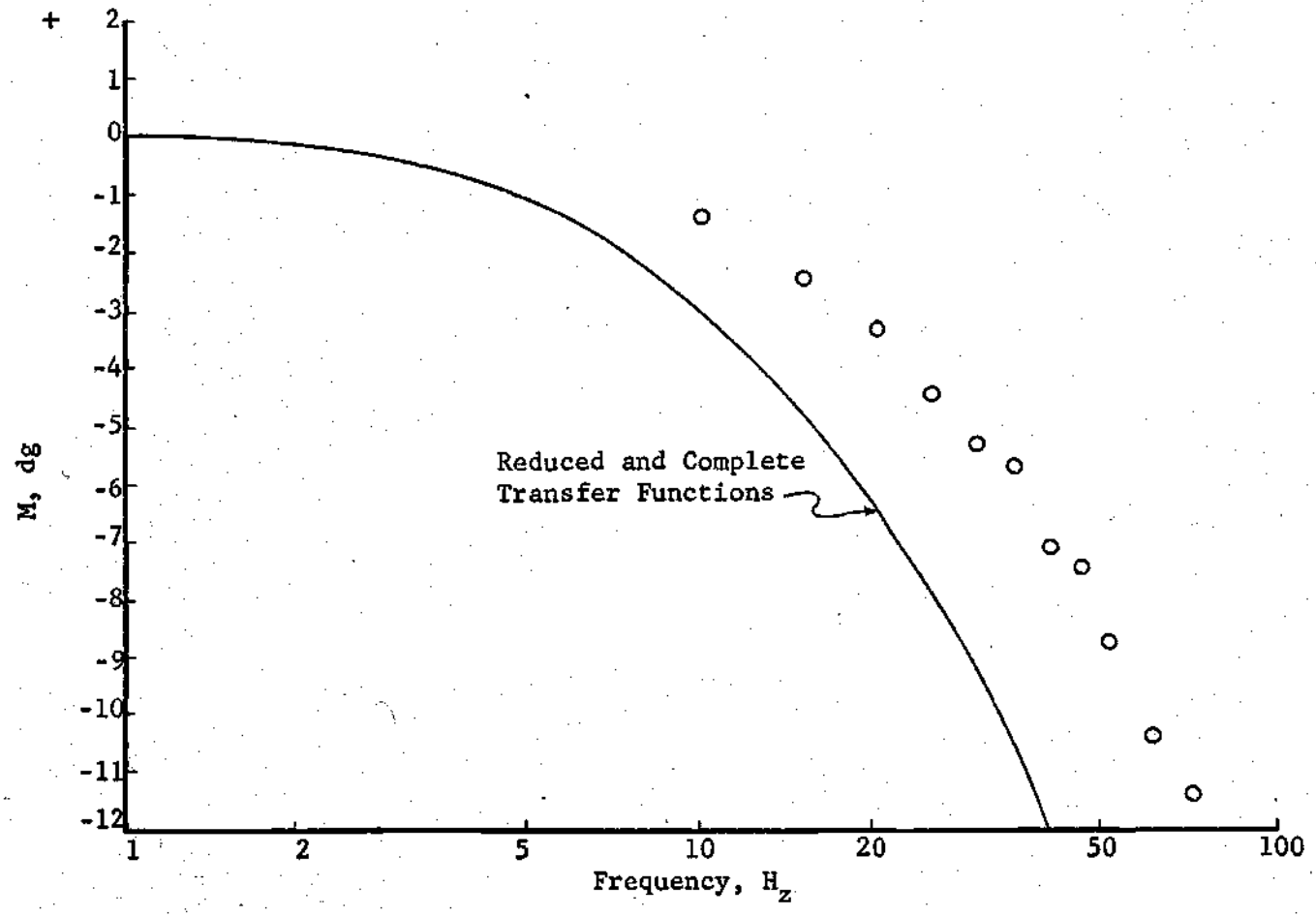

Figure 41. Network 1 (Passive Lag) Magnitude Ratio Versus Frequency.

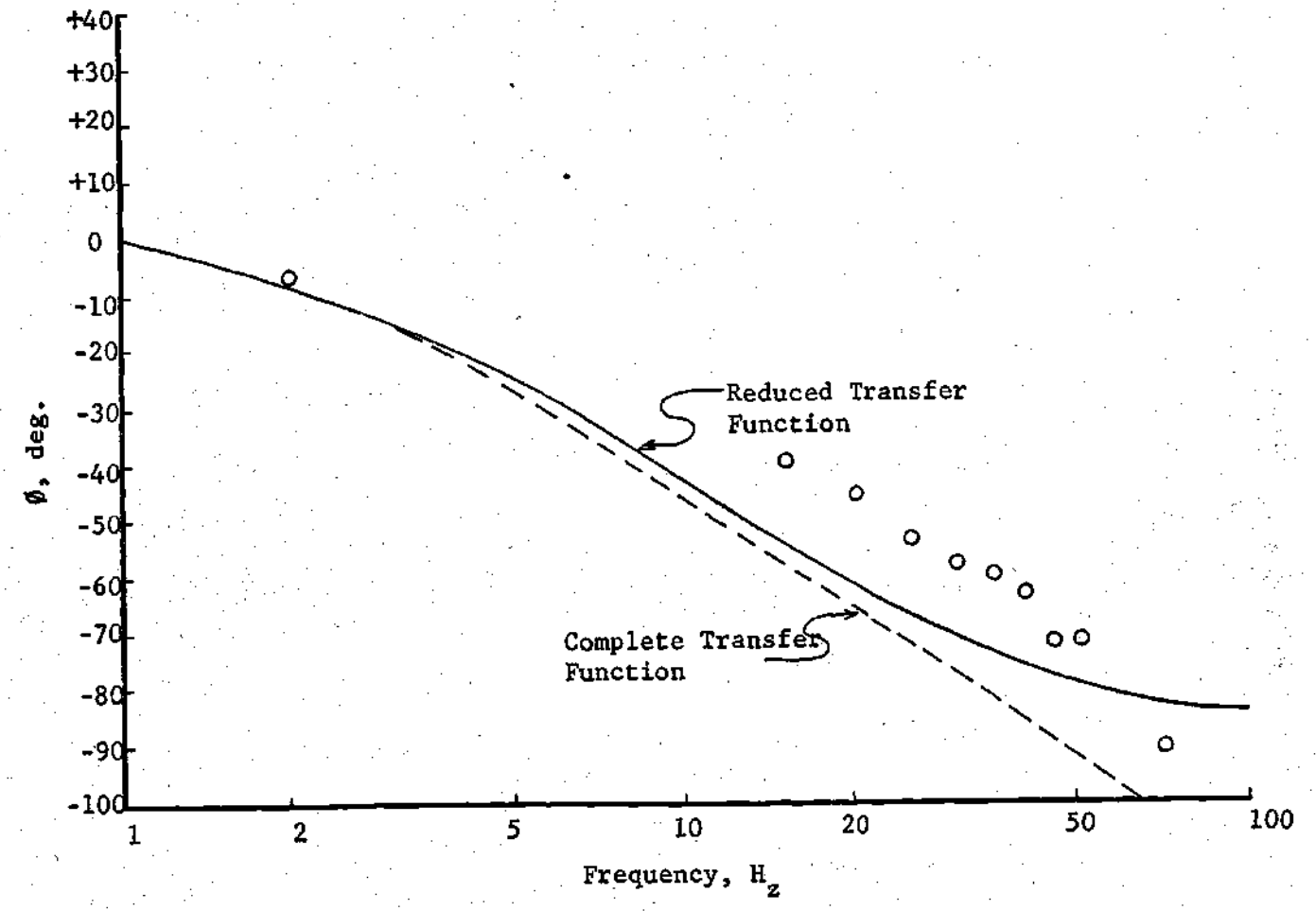

Figure 42. Network 1 (Passive Lag) Phase Angle Versus Frequency.

complete transfer function have this characteristic, both tend to keep decreasing with frequency.

The reduced transfer for network 3 is given by

$$\frac{P_{0d}}{P_{cd}} = \frac{(.0082)s + 1}{(.0139)s + 1} \tag{5.4}$$

and the complete transfer function by

$$\frac{P_{0d}}{P_{cd}} = \frac{[(.0099)s+1]e^{-(.00087)s}}{[(.0168)s+1][(.0030)s+1][(.0031)s+1]} \tag{5.5}$$

functions are compared with experimental data in Figures 43 and 44. The magnitude predictions of the complete transfer function are not very accurate, analytically derived pole break frequencies once again being too low. The experimentally obtained phase angle plot does at least have some agreement with complete transfer function values. The phase angle contribution by transport delay keeps the phase angle decreasing, while the reduced transfer function calls for it to return to zero at higher frequencies.

The reduced transfer function for network 4 is given by

$$\frac{P_{0d}}{P_1} = \frac{(.0149)s+1}{(.0095)s+1} \tag{5.6}$$

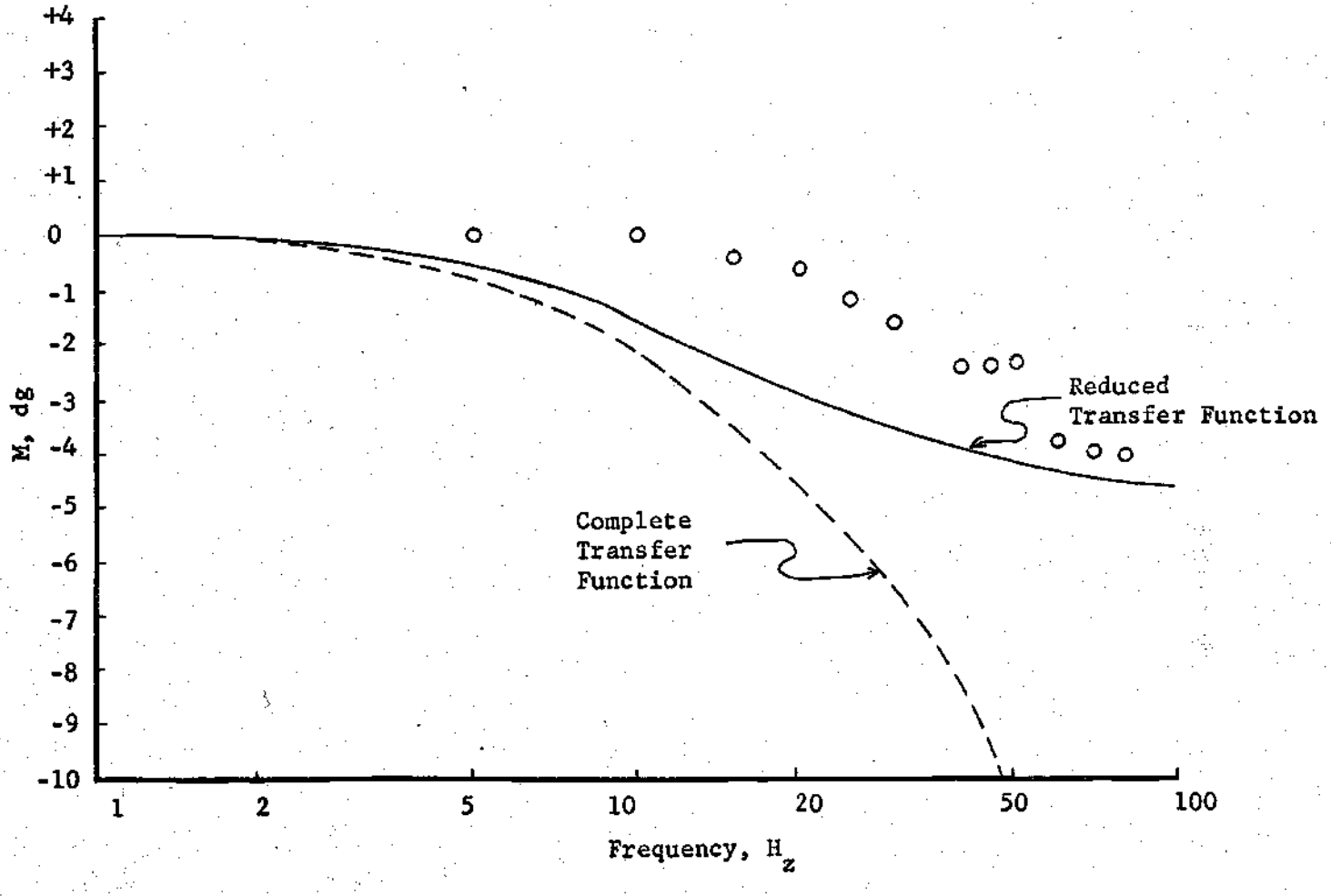

Figure 43. Network 3 (Lag-Lead) Magnitude Ratio Versus Frequency.

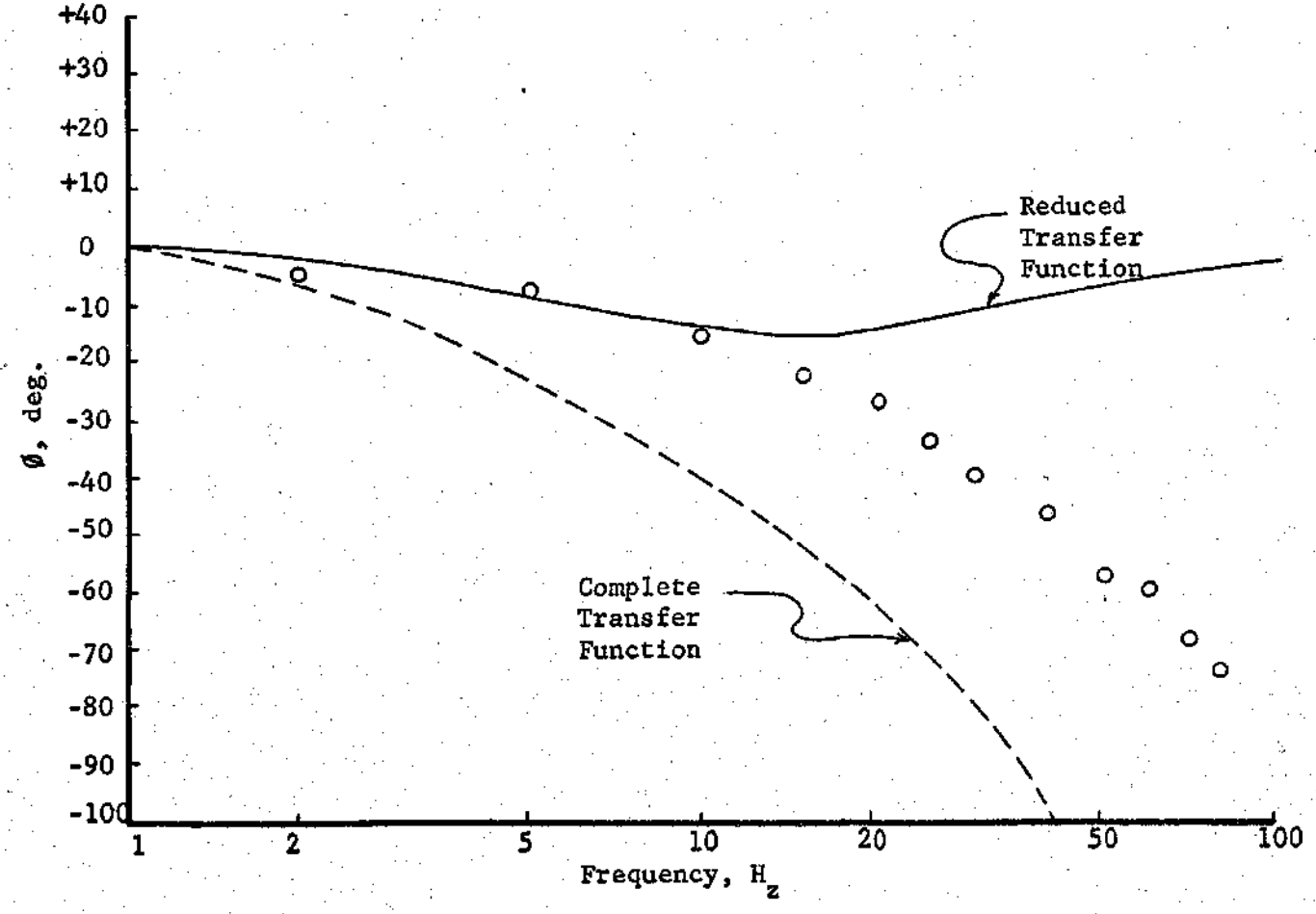

Figure 44. Network 3 (Lag-Lead) Phase Angle Versus Frequency.

and the complete transfer function by

$$\frac{P_{0d}}{P_1} = \frac{[(.0149)s+1]\, e^{-(.00087)s}}{[(.0095)s+1][(.0030)s+1]} \qquad (5.7)$$

Magnitude and phase angle versus frequency plots of these transfer functions are compared with experimental data in Figures 45 and 46. The complete transfer function magnitude predictions are reasonably accurate, but some error once again stems from low pole break frequency values. Note that phase lead is never actually achieved, due to the effects of transport delay.

5.5 Discussion of Results

In the systems tested, only fair agreement between experimental results and response are predicted by the complete transfer function exists. Analytical pole break frequencies are too low in all cases. These discrepancies can at least in part be attributed to inaccuracies in the evaluation of amplifier input and output resistances.

These quantities are obtained experimentally, as previously discussed. The flow instrumentation, a Brooks rotameter with a 0 to 10 SCFH scale, may contribute some inaccuracy. The flow rates measured are on the lower end of the instrument's scale. At flow rates approaching zero, the meter is quite inaccurate, the float being unstable. The only slightly higher readings used might then be suspect.

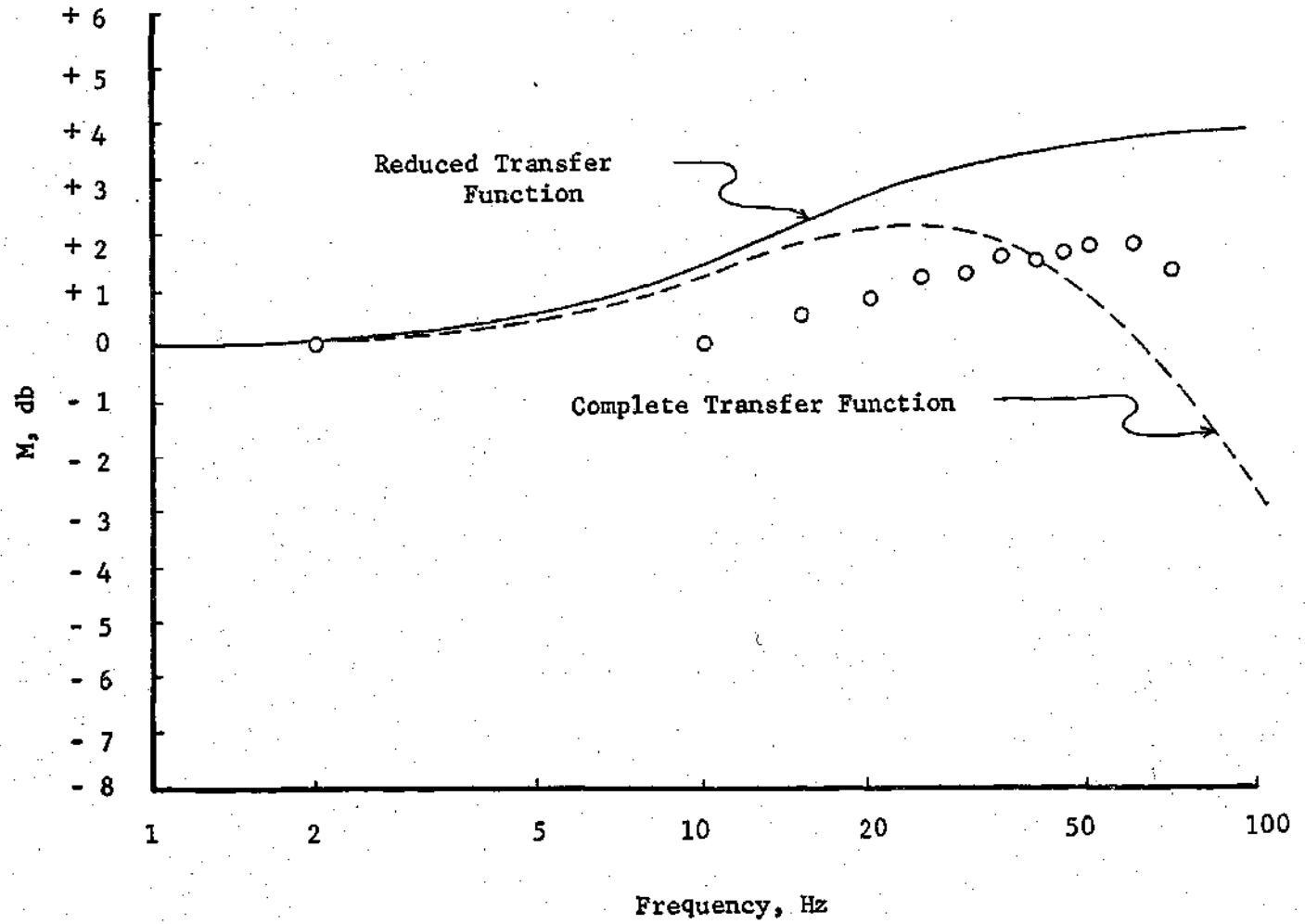

Figure 45. Network 4 (Lead-Lag) Magnitude Ratio Versus Frequency.

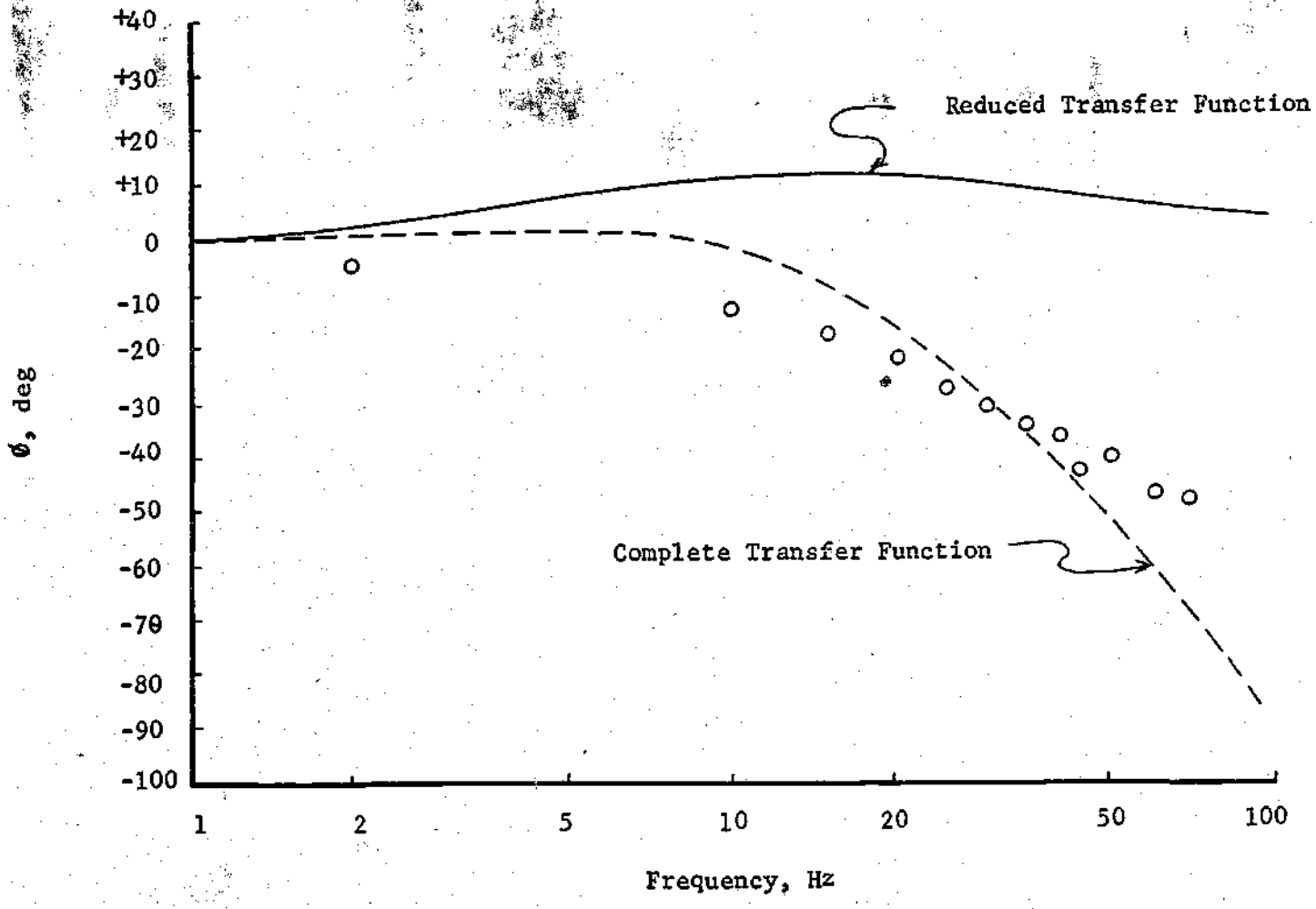

Figure 46. Network 4 (Lead-Lag) Phase Angle Versus Frequency.

The evaluation of output resistance using a manufacturer supplied output pressure versus output flow curve for an amplifier of similar geometry, where the supply pressure is 5 psig, yields the value $R_o = .51$ lbf-sec/in^5. Evaluating the same parameter using the experimentally derived output pressure-flow curve, where the supply pressure is 6 psig, yields the value $R_o = .80$ lbf-sec/in^5. In spite of the difference in supply pressure, the smaller value of R_o is perhaps more realistic, in view of the doubtful nature of the rotameter reading at low flow rates.

The amplifier pole break frequency is given by

$$\omega_{pa} = \frac{1}{2R_o C_t} + \frac{1}{2R C_t}$$

Since R_ℓ, the load resistance, has a value of 28 lbf-sec/in^5, it can be seen that the amplifier pole frequency is very sensitive to the output resistance, R_o. Using the lower value of R_o causes the pole frequency to increase by about 50 percent. This corrects a major part of the experimental error.

Since R_c is also a relatively small quantity, similar reasoning indicates that inaccuracy in its evaluation could be responsible for error in the prediction of other network pole and zero break frequencies.

CHAPTER VI

CONCLUSIONS AND RECOMMENDATIONS

Networks have been presented for the implementation of elementary transfer functions. These may be combined in series to produce any rational, finite transfer function with no fewer poles than zeros and only left hand plane poles. They should serve as an ample basis for analog fluidic system design.

The use of the lumped electrical equivalent amplifier model in the analysis of the basic networks is a convenient procedure and lends great physical insight into the workings of fluidic systems. A well known and widely used amplifier model is accepted without question in this study. However, a careful examination of certain aspects of the model casts some doubt on its analytical rigor and indicates a need for further investigation. These doubts center around the lumped parameter representation of the connecting line.

While connecting line dynamics are not explicitly discussed, a connecting line model is included in the electrical equivalent amplifier circuit. This model, shown for an input connector is given in Figure 47a. C_c is the connecting line capacitance and R_c is the resistance of the amplifier control port and line combined. The e^{-st_d} term represents pure transport delay. The transfer function for this lumped parameter system is given by

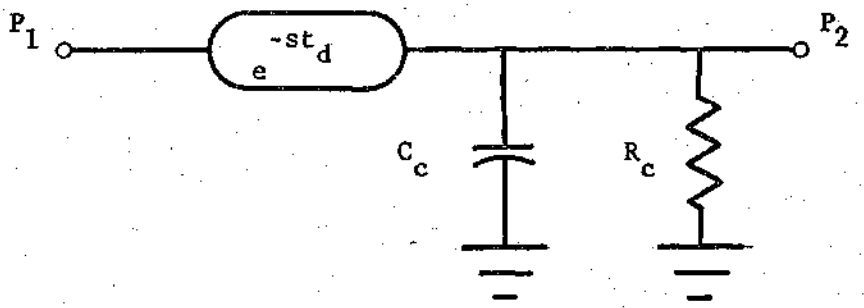

Figure 47a. The Lumped Connecting Line Model.

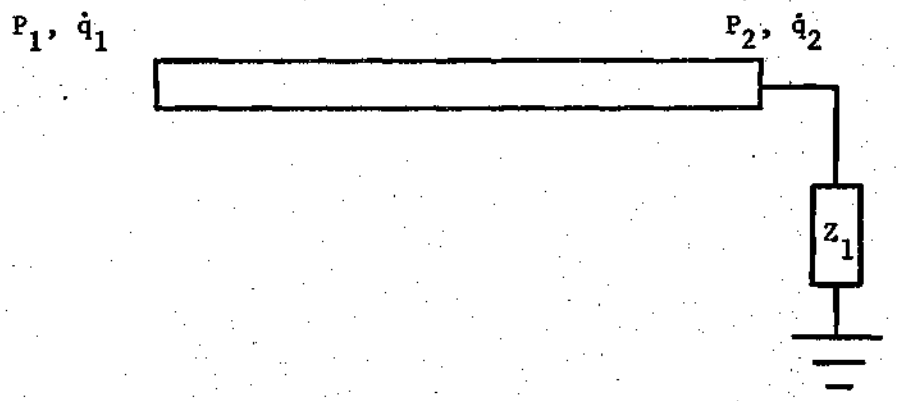

Figure 47b. A Distributed Connecting Line Model.

$$\frac{P_2}{P_1} = e^{-st_d} \qquad (6.1)$$

The magnitude ratio is constant at unity and the phase angle linearly decreases with frequency, as discussed previously.

A distributed parameter representation of the undamped connecting line is pictured in Figure 47b. A mathematical description of the system is given by Takahashi[13] as

$$\begin{bmatrix} P_2 \\ \dot{q}_2 \end{bmatrix} = \begin{bmatrix} \cosh\Gamma & -Z_c \sinh\Gamma \\ -Z^{-1} \sinh\Gamma & \cosh\Gamma \end{bmatrix} \begin{bmatrix} P_1 \\ \dot{q}_1 \end{bmatrix},$$

where Z_c, the characteristic impedance of the line is given by

$$Z_c = Z\sqrt{Z/\gamma}$$

with

$$Z = \frac{\rho}{A} s, \qquad (6.2)$$

$$\gamma = \frac{A}{P} s,$$

and

$$\Gamma = st_d.$$

In addition,

$$\dot{q}_2 = \frac{P_2}{Z_\ell} \quad , \tag{6.3}$$

where Z_ℓ is the load impedance. Combining equations (6.2) and (6.3) yields the transfer function

$$\frac{P_2}{P_1} = \frac{1}{\cos\omega t_d + j \frac{Z_c}{Z_\ell} \sin\omega t_d} \quad . \tag{6.4}$$

If $Z_c/Z_\ell = 1$, then

$$\frac{P_2}{P_1} = \frac{1}{\cos\omega t_d + j \sin\omega t_d} = e^{-st_d}, \tag{6.5}$$

which is the same as the lumped parameter transfer function given in equation (6.1). For a typical input connector however, $Z_c/Z_\ell << 1$, and the transfer function is very nearly

$$\frac{P_2}{P_1} = \frac{1}{\cos\omega t_d} = \sec\omega t_d \tag{6.6}$$

The magnitude ratio given by equation (6.6) is the absolute value of $\sec\omega t_d$ and goes to infinity at $\omega t_d = \pi/2, 3\pi/2, \ldots (2n+1)2$.

The phase angle decreases by discrete jumps of 180 degrees at these critical values of ωt_d. For those frequencies and geometries of interest in this study, ωt_d always lies below $\pi/2$. Therefore, the above transfer function predicts zero phase lag and an increasing magnitude ratio with increasing frequency, within the realm of typical operation. This is in conflict with the predictions of the amplifier model. This discrepancy is unexplained. However, the well established position of the amplifier model as an analytical technique justifies its use in this study. In addition, although not conclusive, the experimental results of this study favor the lumped parameter representation with transport delay operator. Experimental phase angle versus frequency data for all networks tested indicates an ever decreasing phase angle at higher frequencies. This can only be the result of transport delay.

When system parameters are carefully evaluated, the complete transfer functions provide a reasonably accurate picture of network response. However, it can be seen from the experimental results that the reduced transfer functions can only be accurate at very low frequencies. Even then, for some configurations, the reduced transfer function is not adequate. A case in point is network 4, a lead-lag configuration. The experimental results, shown in Figure 46, demonstrate that phase lead is never achieved by this network, even though predicted by the reduced transfer function. Again, in Figure 44, for a lag-lead network, the experimental phase versus frequency plot keeps decreasing at higher frequencies, while the

reduced transfer function calls for a return to zero.

Since the reduced transfer function is the transfer function to be implemented, it is seen that certain configurations are difficult to physically produce. If the designer is limited to the use of breadboarded circuits, as tested in this study, this is true. The inevitably long connectors result in large values of input and output capacitance and large transport delay constants.

However, in some commercial applications, miniaturized, integrated circuit blocks are used, with the result that amplifier and connecting line (in this case, connecting passage) dynamics are kept to an absolute minimum. For these systems, reduced and complete transfer function will be nearly identical.

In addition to their superior frequency response, circuit blocks are rugged and inexpensive when mass produced. However, many applications call for the production of only a single network or a small quantity. The use of integrated circuit blocks may not be economically feasible in such a situation.

The solution might be in the development of variable parameter circuit blocks. Variable capacitors could be used to regulate RC factors, it being easier to vary a volume than a laminar resistance. An alternative for some transfer functions would be to use those networks that require gain admustment for pole-zero location. Gain can be adjusted by adjusting amplifier supply pressure. The development of such networks would facilitate the use of truly high performance fluidic systems in situations where they were formally not economically feasible.

APPENDIX

THE COMPLETE TRANSFER FUNCTIONS

A.1 Network 6

Viewing the fluidic schematic, shown in Figure 20a, using the results of equations (3.39) and (3.42), and substituting appropriate parameters, gives

$$\frac{P_{c31}}{P_i} = \left(\frac{K_{i1}}{s/\omega_{Pi1}+1}\right)\left(K_{P1}e^{-st_{d1}}\right)\left(\frac{K_1}{s/\omega_{P1}+1}\right). \tag{A.1}$$

Similarly,

$$\frac{P_{c32}}{P_i} = \left(\frac{K_{i2}}{s/\omega_{Pi2}+1}\right)\left(K_{P2}e^{-st_{d2}}\right)\left(\frac{K_2}{s/\omega_{P2}+1}\right). \tag{A.2}$$

Typically,

$$\begin{aligned} R_{c11} &= R_{c21} = R_{c1}\,, \\ R_{c31} &= R_{c32} = R_{c3}\,, \\ R_{01} &= R_{02}\,, \\ \text{and} \quad C_{c11} &= C_{c21} = C_{c1}\,. \end{aligned} \tag{A.3}$$

The parameters of equations (A.1) and (A.2) are then defined as

$$K_{i1} = K_{i2} = K_i = \frac{1}{R_i\left(\frac{1}{R_{c1}} + \frac{1}{R_i}\right)} ,$$

$$K_1 = K_2 = K = \frac{1}{(R + R_{01})\left(\frac{1}{R_{c3}} + \frac{1}{R + R_{01}}\right)} ,$$

$$\omega_{Pi1} = \omega_{Pi2} = \omega_{Pi} = \frac{1}{R_i C_{c1}} + \frac{1}{R_{c1} C_{c1}} , \qquad (A.4)$$

$$\omega_{P1} = \frac{1}{(R + R_{01})(C_1 + C_{c1})} + \frac{}{R_{c3}(C_1 + C_{c1})} ,$$

and $$\omega_{P2} = \frac{1}{(R + R_{01})(C_2 + C_{c1})} + \frac{1}{R_{c3}(C_2 + C_{c1})} .$$

With reference to Figure 20a, t_{d1} is the signal transit time from input to interaction chamber 3, through amplifier 1. t_{d2} is the signal transit time to interaction chamber 3, through amplifier 2. t_{d3} is the signal transit time through interaction chamber 3, to output.

A use of

$$P_{cd3} = P_{c31} - P_{c32} , \qquad (A.5)$$

and

$$\frac{P_o}{P_{cd3}} = \frac{K_{a3} e^{-st_{d3}}}{s/\omega_{Pa3} + 1} , \qquad (A.6)$$

the complete transfer function can be written as

$$\frac{P_o}{P_i} = \frac{K_{P1} K_i K (s/\omega_{P2} + 1) e^{-st_{d1}} - K_{P2} K_i K (s/\omega_{P1} + 1) e^{-st_{d2}}}{(s/\omega_{Pi} + 1)(s/\omega_{P1} + 1)(s/\omega_{P2} + 1)}$$

$$\times \frac{(K_{a3}/2) e^{-st_{d3}}}{s/\omega_{Pa3} + 1} . \qquad (A.7)$$

When amplifier and connecting line dynamics may be neglected, the result is

$$\frac{P_o}{P_i} = \frac{1}{2} K_1 K K_{a3} \frac{(\frac{K_{P1}}{\omega_{P2}} - \frac{K_{P2}}{\omega_{P1}})s + (K_{P1} - K_{P2})}{(s/\omega_{P1} + 1)(s/\omega_{P2} + 1)} \qquad (A.8)$$

A.2 Network 7

Viewing the fluidic schematic shown in Figure 20b, yields directly

$$\frac{P_{cd1}}{P_{1d}} = \frac{P_{cd12} - P_{cd11}}{P_{1d}} \qquad (A.9)$$

where, by the results of equation (3.39) and substituting appropriate parameters

$$\frac{P_{cd11}}{P_{1d}} = \frac{-K_1}{s/\omega_{P1} + 1} ,$$

with

$$K_1 = \frac{1}{R(\frac{1}{R_{c11}} + \frac{1}{R})} , \qquad (A.10)$$

and $$\omega_{P1} = \frac{1}{R_{c11}C_{c11}} + \frac{1}{RC_{c11}} .$$

By the results of equation (3.42) and substituting appropriate parameters

$$\frac{P_{cd12}}{P_{1d}} = \frac{K_2}{s/\omega_{P2} + 1} , \qquad (A.11)$$

where $$K_2 = \frac{1}{R(\frac{1}{R_{c12}} + \frac{1}{R})} ,$$

and $$\omega_{P2} = \frac{1}{R_{c12}(C + C_{c12})} + \frac{1}{R(C + C_{c12})} .$$

Therefore

$$\frac{P_{cd1}}{P_{1d}} = \frac{K_2}{s/\omega_{P2} + 1} - \frac{K_1}{s/\omega_{P1} + 1} . \qquad (A.12)$$

It will be assumed that the input signal path lengths are approximately equal. Transport delay for the entire network can then be described by the single constant, t_{d1}. It is further assumed that

$$R_{c11} = R_{c12} = R_c . \qquad (A.12)$$

Therefore

$$K_1 = K_2 = K . \qquad (A.13)$$

The complete transfer function may then be written as

$$\frac{P_{od}}{P_{1d}} = K \frac{(s/\omega_{P1} + 1) - (s/\omega_{P2} + 1)}{(s/\omega_{P1} + 1)(s/\omega_{P2} + 1)} \frac{K_{a1} e^{-st_{d1}}}{s/\omega_{P1} + 1} . \qquad (A.14)$$

Note in the fluidic schematic the reversal of positive and negative output ports. This gives rise to the negative sign in front of the above result. Neglecting amplifier and connecting line dynamics yields

$$\frac{P_{od}}{P_{1d}} = \frac{KK_{a1}}{\omega_{P2}} \left(\frac{S}{s/\omega_{P2} + 1}\right) . \qquad (A.15)$$

A.3 Network 8

Viewing the fluidic schematic, shown in Figure 21a, the system can be directly put into block diagram form. The block diagram is shown in Figure 48. Using the results of equations (3.39) and (3.42) and substituting appropriate parameters yields

$$a = \frac{K_1 e^{-st_{d1}}}{s/\omega_{P1} + 1} , \tag{A.16}$$

where

$$K_1 = \frac{1}{R_1(\frac{1}{R_{c11}} + \frac{1}{R_1})} ,$$

and $$\omega_P = \frac{1}{R_{c11}C_{c11}} + \frac{1}{R_1 C_{c11}} .$$

$$b = \frac{K_{a1} e^{-st_{do}}}{s/\omega_{Pa1} + 1} . \tag{A.17}$$

$$c = \frac{K_2}{s/\omega_{P2} + 1} , \tag{A.18}$$

where $$K_2 = \frac{1}{R(\frac{1}{R_{c2}} + \frac{1}{R})} ,$$

and $$\omega_{P2} = \frac{1}{R_{c2}(C + C_{c2})} + \frac{1}{R(C + C_{c2})} .$$

$$d = 2K_{P2} e^{-st_{d2}} . \tag{A.19}$$

$$e = \frac{K_f}{s/\omega_{Pf} + 1} , \tag{A.20}$$

where $$K_f = \frac{1}{(R_f + R_{02})(\frac{1}{R_{c12}} + \frac{1}{R_f + R_{02}})} ,$$

and

$$\omega_{Pf} = \frac{1}{R_{c12}C_{c12}} + \frac{1}{(R_f + R_{02})C_{c12}} .$$

t_{d1} is the signal transit time from input, to interaction chamber 1.

t_{d0} is the signal transit time through interaction chamber 1, to output

t_{d2} is the signal transit time from output, through amplifier 2, and to interaction chamber 1.

A reduction of the block diagram yields

$$\frac{P_{0d}}{P_{1d}} = \frac{ab}{1 + bcde} . \tag{A.21}$$

The complete transfer can be written as

$$\frac{P_{0d}}{P_{1d}} = \frac{(\frac{K_1 e^{-st_{d1}}}{s/\omega_{P1} + 1})(\frac{K_{a1} e^{-st_{d0}}}{s/\omega_{Pa1} + 1})}{1 + (\frac{K_{a1} e^{-st_{d0}}}{s/\omega_{Pa1} + 1})(\frac{K_2}{s/\omega_{P2} + 1})(2K_{P2} e^{-st_{d2}})(\frac{K_f}{s/\omega_{Pf} + 1})} , \tag{A.22}$$

or

$$\frac{P_{0d}}{P_{1d}} = \frac{(s/\omega_{P2} + 1)(\frac{K_1 e^{-st_{d1}}}{s/\omega_{P1} + 1})(\frac{K_{a1} e^{-st_{d0}}}{s/\omega_{Pa1} + 1})}{(s/\omega_{P2} + 1) + K_2(\frac{K_{a1} e^{-st_{d0}}}{s/\omega_{Pa1} + 1})(2K_{P2} e^{-st_{d2}})(\frac{K_f}{s/\omega_{Pf} + 1})} . \tag{A.23}$$

When amplifier and connecting line dynamics may be neglected, this simplifies to

$$\frac{P_{0d}}{P_{1d}} = \frac{K_1 K_{a1}(s/\omega_{p2} + 1)}{(s/\omega_{p2} + 1) + 2K_{a1}K_2K_{p2}K_f} . \qquad (A.24)$$

A.4 Network 9

It can be seen from its fluidic schematic, shown in Figure 21b, that network 9 is simply network 8 with a positive instead of a negative feedback. The complete transfer function can then be written directly as

$$\frac{P_{0d}}{P_{1d}} = \frac{(s/\omega_{p2} + 1)\left(\frac{K_1 e^{-st_{d1}}}{s/\omega_{p1} + 1}\right)\left(\frac{K_{a1} e^{-st_{d0}}}{s/\omega_{pa1} + 1}\right)}{(s/\omega_{p2}+1) - K_2\left(\frac{K_{a1} e^{-st_{d0}}}{s/\omega_{pa1}+1}\right)(2K_{p2}e^{-st_{d2}})\left(\frac{K_f}{s/\omega_{pf} + 1}\right)} . \qquad (A.25)$$

When amplifier and connecting line dynamics may be neglected

$$\frac{P_{0d}}{P_{1d}} = \frac{K_1 K_{a1}(s/\omega_{p2} + 1)}{(s/\omega_{p2} + 1) - 2K_{a1}K_2K_{p2}K_f} . \qquad (A.26)$$

A.5 Network 10

An inspection of the network 10 schematic, shown in Figure 22a, shows that it is very similar to network 8. The difference is that the capacitor, C, now lies in the feedback loop. The block diagram of Figure 48 may be used, and all block transfer functions are identical, except those of blocks "c" and "e".

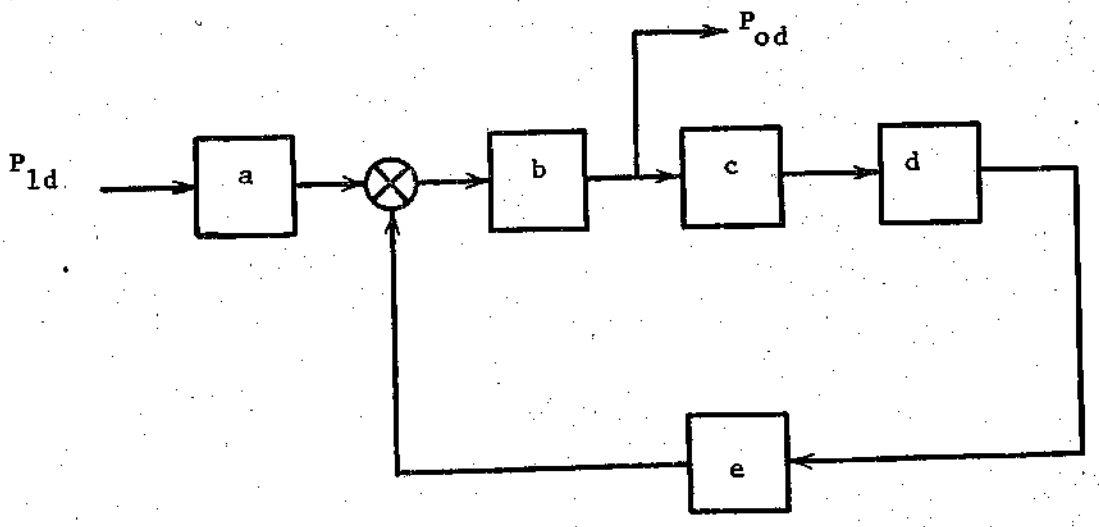

Figure 48. Network 8 Block Diagram.

Using the results of equations (3.39) and (3.42) and substituting appropriate quantities yields

$$c = \frac{K_2}{s/\omega_{p2} + 1}, \tag{A.27}$$

where

$$K_2 = \frac{1}{R_2\left(\frac{1}{R_{c2}} + \frac{1}{R_2}\right)},$$

and

$$\omega_{p2} = \frac{1}{R_{c2}C_{c2}} + \frac{1}{R_2C_{c2}}.$$

$$e = \frac{K_f}{s/\omega_{pf} + 1}, \tag{A.28}$$

where

$$K_f = \frac{1}{(R + R_{02})\left(\frac{1}{R_{c12}} + \frac{1}{R + R_{02}}\right)},$$

and

$$\omega_{pf} = \frac{1}{R_{c12}(C + C_{c12})} + \frac{1}{(R + R_{02})(C + C_{c12})}.$$

The complete transfer function can be written as

$$\frac{P_{0d}}{P_{1d}} = \frac{(s/\omega_{pf} + 1)\left(\frac{K_1}{s/\omega_{p1} + 1}\right)\left(\frac{K_{a1}e^{-st_{d1}}}{s/\omega_{pa1} + 1}\right)}{(s/\omega_{pf} + 1) + K_f\left(\frac{K_{a1}e^{-st_{d1}}}{s/\omega_{pa1} + 1}\right)\left(\frac{K_2}{s/\omega_{p2} + 1}\right)(2K_{p2}e^{-st_{d2}})}. \tag{A.29}$$

When amplifier and connecting line dynamics may be neglected

$$\frac{P_{0d}}{P_{1d}} = \frac{K_1 K_{a1}(s/\omega_{Pf} + 1)}{(s/\omega_{Pf} + 1) + 2K_{a1}K_2K_{P2}K_f} . \qquad (A.30)$$

A.6 Network 11

It can be seen from its fluidic schematic, shown in Figure 22b, that network 11 is simply network 10 with positive instead of negative feedback. The complete transfer function can then be written directly as

$$\frac{P_{0d}}{P_{1d}} = \frac{(s/\omega_{Pf} + 1)\left(\frac{K_1}{s/\omega_{P1} + 1}\right)\left(\frac{K_{a1}e^{-st_{d1}}}{s/\omega_{Pa1} + 1}\right)}{(s/\omega_{Pf} + 1) - K_f\left(\frac{K_{a1}e^{-st_{d1}}}{s/\omega_{Pa1} + 1}\right)\left(\frac{K_2}{s/\omega_{P2} + 1}\right)(2K_{P2}e^{-st_{d2}})} \qquad (A.31)$$

When amplifier and connecting line dynamics may be neglected

$$\frac{P_{0d}}{P_{1d}} = \frac{K_1 K_{a1}(s/\omega_{Pf} + 1)}{(s/\omega_{Pf} + 1) - 2K_{a1}K_2K_{P2}K_f} . \qquad (A.32)$$

A.7 Network 12

Viewing the fluidic schematic, shown in Figure 23a, the system can be directly put into block diagram form. The block diagram is shown in Figure 49. Using the results of equations (3.39) and (3.42) and substituting appropriate quantities yields

$$a = \frac{K_1 e^{-st_{d1}}}{s/\omega_{P1} + 1} , \qquad (A.33)$$

where

$$K_1 = \frac{1}{R_1\left(\frac{1}{R_{c1}} + \frac{1}{R_1}\right)} ,$$

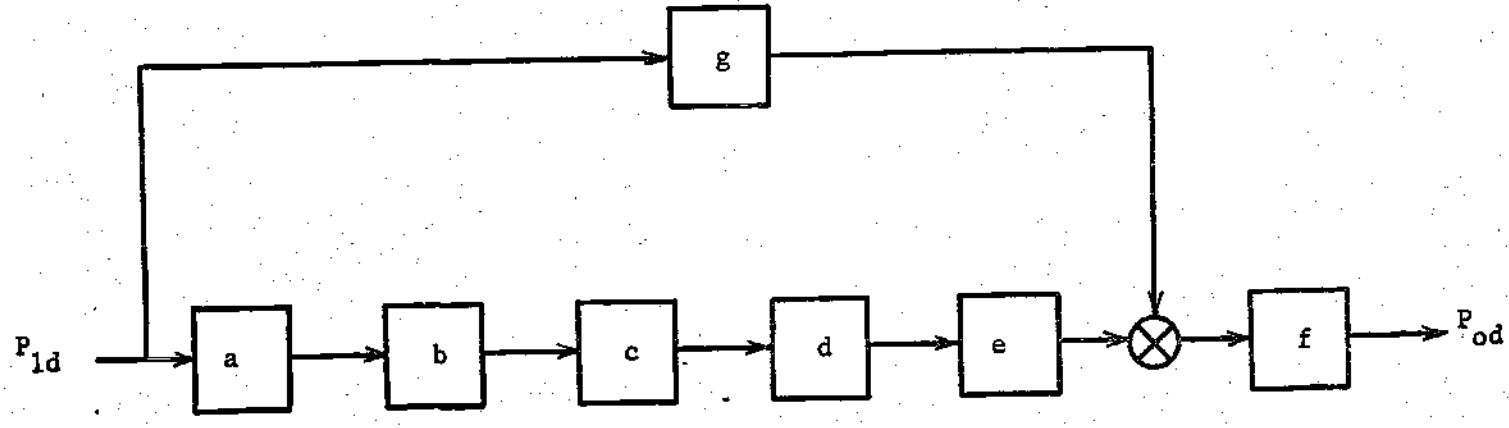

Figure 49. Network 12 Block Diagram.

and $$\omega_{P1} = \frac{1}{R_{c1}C_{c1}} + \frac{1}{R_1 C_{c1}} .$$

$$b = 2K_{P1} . \tag{A.34}$$

$$c = \frac{K_2}{s/\omega_{P2} + 1} , \tag{A.35}$$

where $$K_2 = \frac{1}{(R_2 + R_{01})(\frac{1}{R_{c2}} + \frac{1}{R_2 + R_{01}})} ,$$

and $$\omega_{P2} = \frac{1}{R_{c2}(C + C_{c2})} + \frac{1}{(R_2 + R_{01})(C + C_{c2})} .$$

$$d = 2K_{P2} , \tag{A.36}$$

$$e = \frac{K_3}{s/\omega_{P3} + 1} , \tag{A.37}$$

where $$K_3 = \frac{1}{(R_3 + R_{02})(\frac{1}{R_{c3}} + \frac{1}{R_3 + R_{02}})} ,$$

and $$\omega_{P3} = \frac{1}{R_{c3}C_{c3}} + \frac{1}{(R_3 + R_{02})C_{c3}} .$$

$$g = \frac{K_f e^{-st_{df}}}{s/\omega_{Pf} + 1} , \tag{A.38}$$

where $$K_f = \frac{1}{R_f(\frac{1}{R_{c32}} + \frac{1}{R_f})} ,$$

and $$\omega_{Pf} = \frac{1}{R_{c32}C_{c32}} + \frac{1}{R_f C_{c32}} .$$

t_{d1} is the signal transit time from input, through amplifiers 1 and 2, to interaction chamber 3. t_{df} is the signal transit time through the feedforward loop, to interaction chamber 3. t_{d3} is the signal transit time through interaction chamber 3, to output.

A reduction of the block diagram yields

$$\frac{P_{0d}}{P_{1d}} = abcdef - fg \ . \tag{A.39}$$

The complete transfer may then be written directly as

$$\frac{P_{0d}}{P_{1d}} = \frac{4K_1K_2K_{P1}K_{P2}K_{a3}K_3 e^{-s(t_{d1}+t_{d3})}}{(s/\omega_{P1}+1)(s/\omega_{P2}+1)(s/\omega_{P3}+1(s/\omega_{Pa3}+1)} \tag{A.40}$$

$$- \frac{K_{a3}K_f e^{-s(t_{d3}+t_{df})}}{(s/\omega_{Pa3}+1)(s/\omega_{Pf}+1)} \ ,$$

or

$$\frac{P_{0d}}{P_{1d}} = \frac{4K_1K_2K_{P1}K_{P2}K_{a3}K_3(s/\omega_{Pf}+1)e^{-s(t_{d1}+t_{d3})} - K_{a3}K_f(s/\omega_{P1}+1)(s/\omega_{P2}+1)(s/\omega_{P3}+1)e^{-s(t_{d3}+t_{df})}}{(s/\omega_{P1}+1)(s/\omega_{P2}+1)(s/\omega_{P3}+1)(s/\omega_{Pa3}+1)(s/\omega_{Pf}+1)} \tag{A.41}$$

When amplifier and connecting line dynamics may be neglected

$$\frac{P_{0d}}{P_{1d}} = \frac{4K_1K_2K_3K_{P1}K_{P2}K_{a3} - K_{a3}K_f(s/\omega_{P2}+1)}{(s/\omega_{P2}+1)} \ . \tag{A.42}$$

A.8 Network 13

It can be seen from its fluidic schematic, shown in Figure 23b, that network 13 is simply network 12 with a positive instead of a negative

feedforward loop. The complete transfer function can then be written directly as

$$\frac{P_{0d}}{P_{1d}} = \frac{4K_1K_2K_3K_{P1}K_{P2}K_{a3}(s/\omega_{Pf}+1)e^{-s(t_{d1}+t_{d3})} + K_{a3}K_f(s/\omega_{P1}+1)(s/\omega_{P2}+1)(s/\omega_{P3}+1)e^{-s(t_{d3}+t_{df})}}{(s/\omega_{P1}+1)(s/\omega_{P2}+1)(s/\omega_{P3}+1)(s/\omega_{Pa3}+1)(s/\omega_{Pf}+1)} \tag{A.43}$$

When amplifier and connecting line dynamics may be neglected

$$\frac{P_{0d}}{P_{1d}} = \frac{4K_1K_2K_3K_{P1}K_{P2}K_{a3} + K_{a3}K_f(s/\omega_{P2}+1)}{(s/\omega_{P2}+1)} \tag{A.44}$$

A.9 Network 14

The schematic is shown in Figure 24a. Using the results of equation (3.9) and substituting appropriate quantities yields

$$P_{c1} = \frac{P_1^+}{R_1(C_1+C_c)s + \frac{R_1}{R_c} + 1}, \tag{A.45}$$

and

$$P_{c2} = \frac{P_1^-}{R_1(C_2+C_c)s + \frac{R_2}{R_c} + 1}.$$

Using $$P_{cd} = P_{c1} - P_{c2} \quad \text{and} \quad P_1^+ = -P_1^- \tag{A.46}$$

results in

$$P_{cd} = \frac{P_1^+}{R_1(C_1+C_c)s + \frac{R_1}{R_c} + 1} + \frac{P_1^+}{R_2(C_2+C_c)s + \frac{R_2}{R_c} + 1}. \tag{A.47}$$

Since $$P_{1d} = 2P_1^+, \tag{A.48}$$

$$\frac{P_{cd}}{P_{1d}} = \frac{R_1(C_1+C_c)s + \frac{R_1}{R_c} + 1 + R_2(C_2+C_c)s + \frac{R_2}{R_c} + 1}{2[R_1(C_1+C_c)s + \frac{R_1}{R_c}+1][R_2(C_2+C_c)s + \frac{R_2}{R_c} + 1} \qquad (A.49)$$

The complete transfer function is then

$$\frac{P_{Od}}{P_{1d}} = \frac{\frac{1}{R_1}(\frac{1}{R_c} + \frac{1}{R_2}) + \frac{1}{R_2}(\frac{1}{R_c} + \frac{1}{R_1})}{2(\frac{1}{R_c} + \frac{1}{R_2})(\frac{1}{R_c} + \frac{1}{R_1})} \times \frac{\frac{(C_1+C_c)/R_2 + (C_2+C_c)/R_1}{\frac{1}{R_1}(\frac{1}{R_c} + \frac{1}{R_2}) + \frac{1}{R_2}(\frac{1}{R_c} + \frac{1}{R_1})} s+1}{\frac{C_1 + C_c}{(\frac{1}{R_c}+\frac{1}{R_1})} s+1 \quad \frac{C_2+C_c}{(\frac{1}{R_c}+\frac{1}{R_2})} s+1} \times$$

$$\frac{K_a e^{-s_{td}}}{s/\omega_{Pa} + 1} \quad . \qquad (A.50)$$

A.10 Network 15

The schematic is shown in Figure 24b. Using the results of equation (3.9) and substituting appropriate quantities yields

$$P_{c1} = \frac{P_1}{R_1(C_1 + C_c)s + \frac{R_1}{R_c} + 1} \qquad (A.51)$$

and

$$P_{c2} = \frac{P_1}{R_2(C_2 + C_c)s + \frac{R_2}{R_c} + 1} \; . \qquad (A.52)$$

A use of

$$P_{cd} = P_{c1} - P_{c2} \; , \qquad (A.53)$$

gives

$$P_{cd} = \frac{P_1}{R_1(C_1 + C_c)s + \frac{R_1}{R_c}+1} - \frac{P_1}{R_2(C_2+C_c)s + \frac{R_2}{R_c} + 1} \qquad (A.54)$$

or

$$\frac{P_{cd}}{P_1} = \frac{R_2(C + C_c)s + \frac{R_2}{R_c} + 1 - R_1(C + C_c)s - \frac{R_1}{R_c} - 1}{[R_1(C + C_c)s + \frac{R_1}{R_c} + 1][R_2(C + C_c)s + \frac{R_2}{R_c} + 1]} \quad . \tag{A.55}$$

The complete transfer function is then

$$\frac{P_{Od}}{P_1} = \frac{\frac{1}{R_1}(\frac{1}{R_c} + \frac{1}{R_2}) - \frac{1}{R_2}(\frac{1}{R_c} + \frac{1}{R_1})}{(\frac{1}{R_c} + \frac{1}{R_1})(\frac{1}{R_c} + \frac{1}{R_2})} \times$$

$$\frac{\frac{(C_2 + C_c)/R_1 - (C_1 + C_c)/R_2}{\frac{1}{R_1}(\frac{1}{R_c} + \frac{1}{R_2}) - \frac{1}{R_2}(\frac{1}{R_c} + \frac{1}{R_1})} s + 1}{\left(\frac{C_1 + C_c}{\frac{1}{R_c} + \frac{1}{R_1}}\right)_{s+1} \left(\frac{C_2 + C_c}{\frac{1}{R_c} + \frac{1}{R_2}}\right)_{s+1}} \times \frac{K_a e^{-st_d}}{s/\omega_{Pa} + 1} \quad . \tag{A.56}$$

A.11 Network 16

The fluidic schematic is shown in Figure 25a. It can be seen that the input circuit to amplifier 1 is identical to the input circuit in network 4. Using the results of equation (3.34) yields

$$\frac{P_{cd1}}{P_1} = K\left[\frac{(s/\omega_z + 1)}{(s/\omega_{P1} + 1)(s/\omega_{P2} + 1)}\right]$$

where

$$K = \frac{\frac{1}{R_2}(\frac{1}{R_{c1}} + \frac{1}{R_1}) - \frac{1}{R_1}(\frac{1}{R_{c1}} + \frac{1}{R_2})}{(\frac{1}{R_{c1}} + \frac{1}{R_2})(\frac{1}{R_{c1}} + \frac{1}{R_1})} , \tag{A.57}$$

$$\omega_{P1} = \frac{1}{R_1(C_1 + C_{c1})} + \frac{1}{R_{c1}(C_1 + C_{c1})} ,$$

$$\omega_{P2} = \frac{1}{R_2(C_2 + C_{c1})} + \frac{1}{R_{c1}(C_2 + C_{c1})} ,$$

and $$\omega_z = \frac{R_1R_2}{R_2C_2 - R_1C_1}\left[\frac{1}{R_1}\left(\frac{1}{R_c} + \frac{1}{R_2}\right) - \frac{1}{R_2}\left(\frac{1}{R_c} + \frac{1}{R_1}\right)\right] .$$

It follows that

$$\frac{P_{c21}}{P_1} = K_{P1}K\left[\frac{s/\omega_z + 1}{(s/\omega_{P1} + 1)(s/\omega_{P2} + 1)}\right] \frac{K_3e^{-st_{d3}}}{s/\omega_{P3} + 1} , \quad \text{(A.58)}$$

where

$$K_3 = \frac{1}{(R_3 + R_{01})\left(\frac{1}{R_{c21}} + \frac{1}{R_3 + R_{01}}\right)} ,$$

$$\omega_{P3} = \frac{1}{(R_3 + R_{01})C_{c21}} + \frac{1}{R_{c21}C_{c21}} ,$$

and t_{d3} is the signal transit time from input, through amplifier 1, to interaction chamber 2.

Using the results of equation (3.39) and substituting appropriate quantities yields

$$\frac{P_{c22}}{P_1} = \frac{K_4e^{-st_{d4}}}{s/\omega_{p4} + 1} , \quad \text{(A.59)}$$

where

$$K_4 = \frac{1}{R_4\left(\frac{1}{R_{c22}} + \frac{1}{R_4}\right)} ,$$

$$\omega_{P4} = \frac{1}{R_{c22}C_{c22}} + \frac{1}{R_4C_{c22}} ,$$

and t_{d4} is the signal transit time from input, through resistor R_4, to interaction chamber 2.

Using the amplifier 2 transfer function and the equation

$$\frac{P_{0d2}}{P_1} = \left(\frac{P_{c22} - P_{c21}}{P_1}\right)\left(\frac{P_{0d2}}{P_{cd2}}\right) \qquad (A.60)$$

yields

$$\frac{P_{0d2}}{P_1} = - \frac{KK_{P1}K_3(s/\omega_z + 1)e^{-st_{d3}}}{(s/\omega_{P1} + 1)(s/\omega_{P2} + 1)(s/\omega_{P3} + 1)} - \frac{K_4e^{-st_{d4}}}{s/\omega_{P4} + 1} \times$$

$$\frac{K_{a2}e^{-st_{d2}}}{s/\omega_{Pa2} + 1} , \qquad (A.61)$$

or

$$\frac{P_{0d2}}{P_1} = \frac{-KK_{P1}K_{a2}K_3(s/\omega_z+1)(s/\omega_{P4}+1)e^{-s(t_{d2}+t_{d3})}+K_{a2}K_4(s/\omega_{P1}+1)(s/\omega_{P2}+1)(s/\omega_{P3}+1)e^{-s(t_{d2}+t_{d4})}}{(s/\omega_{P1} + 1)(s/\omega_{P2} + 1)(s/\omega_{P3} + 1)(s/\omega_{P4} + 1)(s/\omega_{Pa2} + 1)} \qquad (A.62)$$

When amplifier and connecting line dynamics may be neglected

$$\frac{P_{0d2}}{P_1} = \frac{-KK_{P1}K_{a2}K_3(s/\omega_z + 1) + K_{a2}K_4(s/\omega_p +1)(s/\omega_{P2} +1)}{(s/\omega_{P1} + 1)(s/\omega_{P2} + 1)} \qquad (A.63)$$

or

$$\frac{P_{0d2}}{P_1} = K_4K_{a2} \frac{\frac{-K_{a2}KK_{P1}K_3}{K_4K_{a2}}(s/\omega_z + 1) + (s/\omega_{P1} +1)(s/\omega_{P2} +1)}{(s/\omega_{P1} + 1)(s/\omega_{P2} + 1)} . \qquad (A.64)$$

$$K' = \frac{K_{a2} K K_{P1} K_3}{K_4 K_{a2}} \tag{A.65}$$

$$\frac{P_{Od}}{P_1} = K_4 K_{a2}(1 - K') \frac{\frac{s^2}{(1 - K')\omega_{P1}\omega_{P2}} + \frac{s}{(1 - K')}\left(\frac{1}{\omega_{P1}} + \frac{1}{\omega_{P2}} - \frac{K'}{\omega_z}\right) + 1}{(s/\omega_{P1} + 1)(s/\omega_{P2} + 1)} \tag{A.66}$$

A.12 Network 17

Viewing the fluidic schematic, shown in Figure 25b, the system can be directly put into block diagram form. The block diagram is shown in Figure 50. Using the results of equations (3.39) and (3.42) and substituting appropriate quantities yields the results

$$a = \frac{K_1 e^{-st_{d1}}}{s/\omega_{P1} + 1} , \tag{A.67}$$

where $$K_1 = \frac{1}{R_1\left(\frac{1}{R_{c11}} + \frac{1}{R_1}\right)} ,$$

and $$\omega_{P1} = \frac{1}{R_{c11}C_{c11}} + \frac{1}{R_1 C_{c11}} .$$

$$b = 2K_{P1} . \tag{A.68}$$

$$c = \frac{K_2}{s/\omega_{P2} + 1} , \tag{A.69}$$

where $$K_2 = \frac{1}{(R + R_{01})\left(\frac{1}{R_{c2}} + \frac{1}{R + R_{01}}\right)} ,$$

and $$\omega_{P2} = \frac{1}{(R + R_{01})(C + C_{c2})} + \frac{1}{R_{c2}(C + C_{c2})} .$$

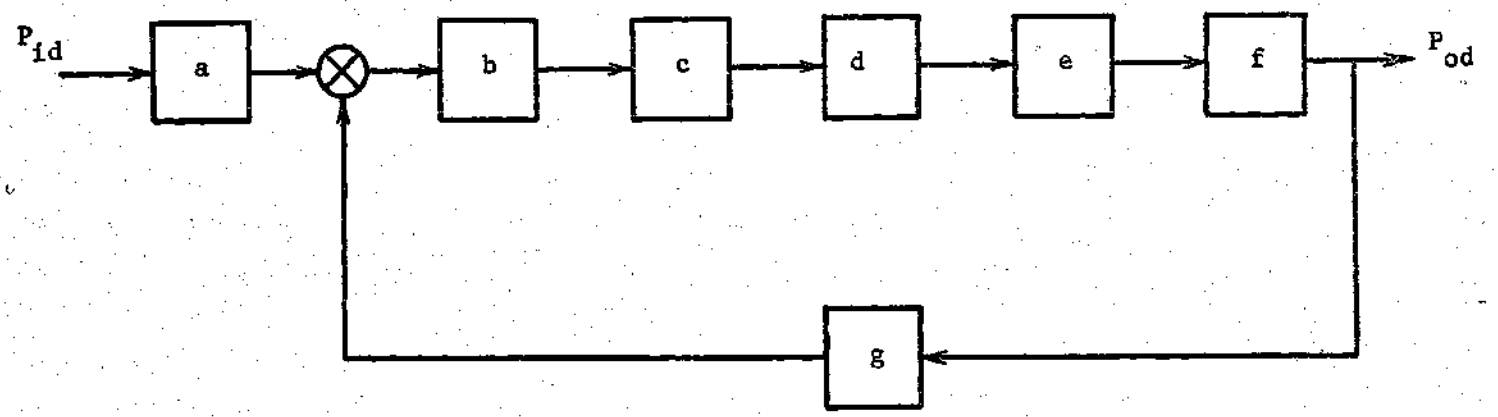

Figure 50. Network 17 Block Diagram.

$$d = 2K_{P2} \,. \tag{A.70}$$

$$e = \frac{K_3}{s/\omega_{P3} + 1} \,, \tag{A.71}$$

where $$K_3 = \frac{1}{(R + R_{02})(\frac{1}{R_{c3}} + \frac{1}{R + R_{02}})} \,,$$

and $$\omega_{P3} = \frac{1}{(R + R_{02})(C + C_3)} + \frac{1}{R_{c3}(C + C_{c3})} \,.$$

$$f = \frac{K_{a3} e^{-st_{d3}}}{(s/\omega_{Pa3} + 1)} \,. \tag{A.72}$$

$$g = \frac{K_f e^{-st_{df}}}{s/\omega_{Pf} + 1} \,, \tag{A.73}$$

where $$K_f = \frac{1}{R_f(\frac{1}{R_{c12}} + \frac{1}{R_f})} \,,$$

and $$\omega_{Pf} = \frac{1}{R_{c12}C_{c12}} + \frac{1}{R_f C_{c12}} \,.$$

t_{d1} is the signal transit time from input, to interaction chamber 1. t_{d3} is the signal transit time through interaction chamber 1 and through amplifiers 1 and 2, to output. t_{df} is the signal transit time from output, through the feedback loop, to interaction chamber 1.

A reduction of the block diagram yields

$$\frac{P_{Od}}{P_1} = \frac{abcdef}{1 + bcdefg} \,, \tag{A.74}$$

or

$$\frac{P_{0d}}{P_1} = \frac{\left(\frac{K_1 e^{-st_{d1}}}{s/\omega_{p1}+1}\right)(2K_{p1})\left(\frac{K_2}{s/\omega_{p2}+1}\right)(2K_{p2})\left(\frac{K_3}{s/\omega_{p3}+1}\right)\left(\frac{K_{a3}e^{-st_{d3}}}{s/\omega_{pa3}+1}\right)}{1 + (2K_{p1})\left(\frac{K_2}{s/\omega_{p2}+1}\right)(2K_{p2})\left(\frac{K_3}{s/\omega_{p3}+1}\right)\left(\frac{K_{a3}e^{-st_{d3}}}{s/\omega_{pa3}+1}\right)\left(\frac{K_f e^{-st_{df}}}{s/\omega_{pf}+1}\right)} \qquad (A.75)$$

or

$$\frac{P_{0d}}{P_1} = \frac{4K_{p1}K_{p2}K_1K_2K_3K_{a3}e^{-st_{d1}}}{(s/\omega_{p1}+1)(s/\omega_{p2}+1)(s/\omega_{p3}+1)(s/\omega_{pa3}+1) + 4K_{p1}K_{p2}K_2K_3K_{a3}K_f\frac{(s/\omega_{p1}+1)e^{-s(t_{d3}+t_{df})}}{(s/\omega_{pf}+1)}} \qquad (A.76)$$

When amplifier and connecting line dynamics may be neglected

$$\frac{P_{0d}}{P_1} = \frac{4K_{p1}K_{p2}K_1K_2K_3K_{a3}}{(s/\omega_{p2}+1)(s/\omega_{p3}+1) + 4K_{p1}K_{p2}K_2K_3K_{a3}K_f}. \qquad (A.77)$$

Typically,

$$R_{01} = R_{02}, \qquad (A.78)$$

and $$R_c = R_{c2} = R_{c3}.$$

Therefore $$\omega_{p2} = \omega_{p3} = \omega_p.$$

Using equation (A.78) in (A.77) yields

$$\frac{P_{0d}}{P_1} = \frac{K(1 + K_L)}{\frac{s^2}{\omega_{p2}} + \frac{s}{\omega_p} + (1 + K_L)} \qquad (A.79)$$

where $$K_L = 4K_{P1}K_{P2}K_2K_3K_{a3}K_f ,$$

and $$K = \frac{4K_{P1}K_{P2}K_1K_2K_3K_{a3}}{1 + K_L} .$$

A.13 Network 18

Viewing the fluidic schematic, shown in Figure 26, the system can be directly put into block diagram form. The block diagram is shown in Figure 51 and a reduced block diagram in Figure 52. Using the results of equations (3.39) and (3.42) and substituting appropriate quantities yields the following results.

$$a = \frac{K_1 e^{-st_{d1}}}{s/\omega_{P1} + 1} \qquad (A.80)$$

where $$K_1 = \frac{1}{R_1(\frac{1}{R_{c11}} + \frac{1}{R_1})}$$

and $$\omega_{P1} = \frac{1}{R_{c11}C_{c11}} + \frac{1}{R_1C_{c11}}$$

$$b = 2K_{P1} . \qquad (A.81)$$

$$c = \frac{K_2}{s/\omega_{P2} + 1} , \qquad (A.82)$$

where $$K_2 = \frac{1}{(R + R_{01})(\frac{1}{R_{c2}} + \frac{1}{R + R_{01}})} ,$$

and $$\omega_{P2} = \frac{1}{(R + R_{01})(C + C_{c2})} + \frac{1}{R_{c2}(C + C_{c2})} .$$

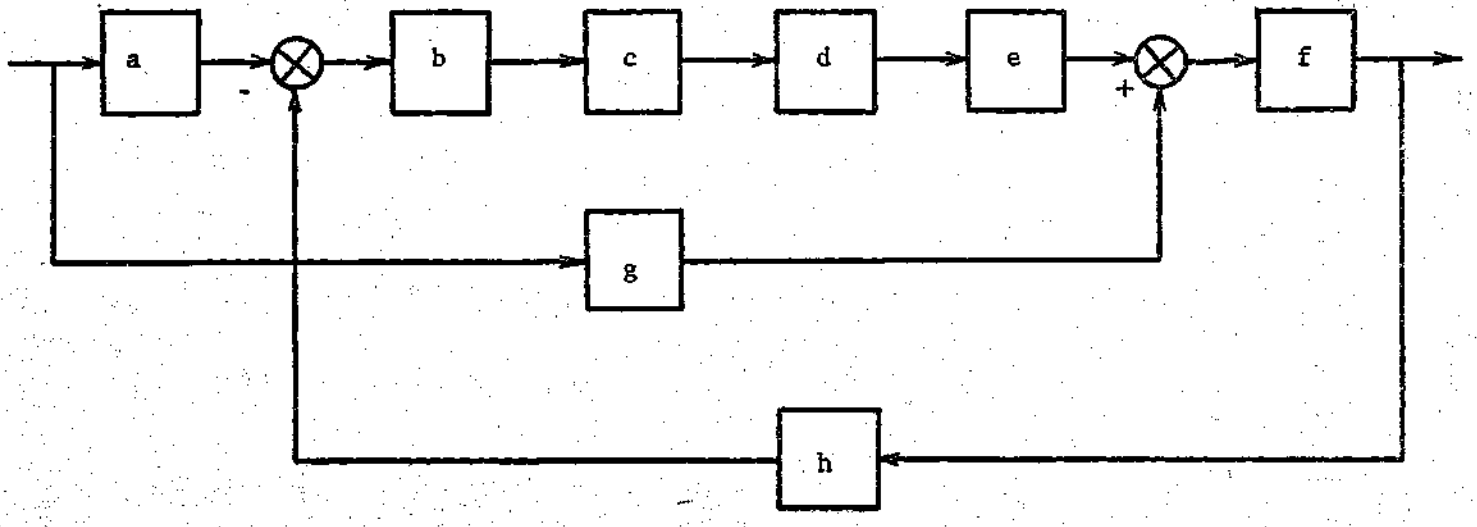

Figure 51. Network 18 Block Diagram.

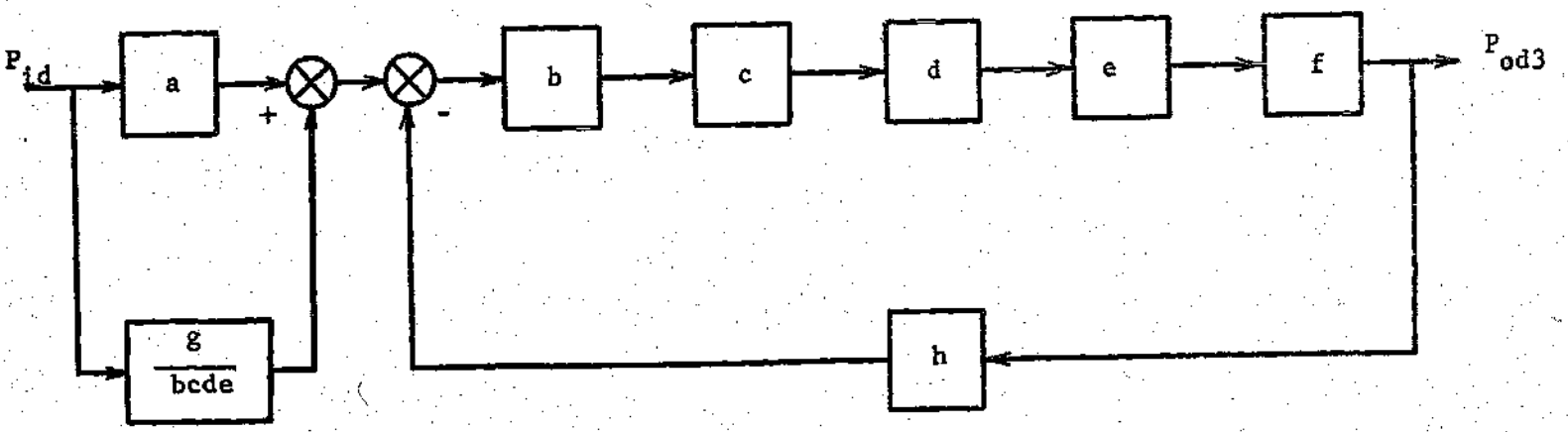

Figure 52. Network 18 Reduced Block Diagram.

$$d = 2K_{P2} . \tag{A.83}$$

$$e = \frac{K_3}{s/\omega_{P3} + 1} , \tag{A.84}$$

where $$K_3 = \frac{1}{(R+R_{02})(\frac{1}{R_{c3}} + \frac{1}{R+R_{02}})} ,$$

and $$\omega_{P3} = \frac{1}{(R+R_{02})(C+C_{c3})} + \frac{1}{R_{c3}(C+C_{c3})} .$$

$$f = \frac{K_{a3}e^{-st_{d3}}}{s/\omega_{Pa3} + 1} . \tag{A.85}$$

$$g = \frac{K_g e^{-st_{dg}}}{s/\omega_{Pg} + 1} , \tag{A.86}$$

where $$K_g = \frac{1}{R_2(\frac{1}{R_{c32}} + \frac{1}{R_2})} ,$$

and $$\omega_{P3} = \frac{1}{R_{c32}C_{c32}} + \frac{1}{R_2 C_{c32}} .$$

$$h = \frac{K_f e^{-st_{df}}}{s/\omega_{Pf} + 1} , \tag{A.87}$$

where $$K_f = \frac{1}{R_f(\frac{1}{R_{c12}} + \frac{1}{R_f})} ,$$

and $$\omega_{Pf} = \frac{1}{R_{c12}C_{c12}} + \frac{1}{R_f C_{c12}} .$$

t_{d1} is the signal transit time from input, to interaction chamber 1.

t_{dg} is the signal transit time through the feedforward loop, to interaction chamber 3. t_{d3} is the signal transit time through interaction chamber 3, to output. t_{df} is the signal transit time from output, through the feedback loop, to interaction chamber 1.

A reduction of the block diagram of Figure 52 yields

$$\frac{P_{od3}}{P_{1d}} = \frac{abcdef + fg}{1 + bcdefh} \tag{A.88}$$

Therefore,

$$\frac{P_{0d}}{P_{1d}} = \frac{\left(\frac{K_1 e^{-st_{d1}}}{s/\omega_{P1}+1}\right)(2K_{P1})\left(\frac{K_2}{s/\omega_{P2}+1}\right)(2K_{P2})\left(\frac{K_3}{s/\omega_{P3}+1}\right)\left(\frac{K_{a3}e^{-st_{d3}}}{s/\omega_{Pa3}+1}\right)+\left(\frac{K_{a3}e^{-st_{d3}}}{s/\omega_{Pa3}+1}\right)\left(\frac{K_g e^{-st_{dg}}}{s/\omega_{Pg}+1}\right)}{1+(2K_{P1})\left(\frac{K_2}{s/\omega_{P2}+1}\right)(2K_{P2})\left(\frac{K_3}{s/\omega_{P3}+1}\right)\left(\frac{K_{a3}e^{-st_{d3}}}{s/\omega_{Pa3}+1}\right)\left(\frac{K_f e^{-st_{dg}}}{s/\omega_{Pf}+1}\right)} \tag{A.89}$$

or

$$\frac{P_{0d}}{P_{1d}} = \frac{4K_{P1}K_{P2}K_1K_{2\ 3}K_{a3}(s/\omega_{Pf}+1)(s/\omega_{Pg}+1)e^{-s(t_{d1}+t_{d3})}}{(s/\omega_{P1}+1)(s/\omega_{P2}+1)(s/\omega_{P3}+1)(s/\omega_{Pa3}+1)(s/\omega_{Pf}+1)(s/\omega_{Pg}+1)}$$

$$\frac{K_{a3}K_g(s/\omega_{P1}+1)(s/\omega_{P2}+1)(s/\omega_{P3}+1)(s/\omega_{Pf}+1)e^{-s(t_{dg}+td_3)}}{+\ 4K_{P1}K_{P2}K_2K_3K_{a3}K_f(s/\omega_{Pg}+1)(s/\omega_{P1}+1)e^{-s(t_{dg}+t_{df})}}. \tag{A.90}$$

When amplifier and connecting line dynamics may be neglected

$$\frac{P_{0d}}{P_{1d}} = \frac{4K_{P1}K_{P2}K_1K_2K_3K_{a3}+K_{a3}K_g(s/\omega_{P2}+1)(s/\omega_{P3}+1)}{(s/\omega_{P2}+1)(s/\omega_{P3}+1)+4K_{P1}K_{P2}K_2K_3K_{a3}K_f}.$$

Typically,

$$R_{c2} = R_{c3} = R_c \,, \tag{A.91}$$

and $$R_{01} = R_{02} \,.$$

Therefore $$\omega_{p2} = \omega_{p3} = \omega_p \,. \tag{A.92}$$

Using the results of equations (A.91) and (A.92) in equation (A.90) yields

$$\frac{P_{0d}}{P_{1d}} = K_g K_{a3} \frac{\dfrac{4K_{p1}K_{p2}K_1K_2K_3}{K_g} + \dfrac{s^2}{\omega_{p2}} + \dfrac{2s}{\omega_p} + 1}{\dfrac{s^2}{\omega_{p2}} + \dfrac{2s}{\omega_p} + 1 + 4K_{p1}K_{p2}K_2K_3K_{a3}K_f} \tag{A.93}$$

BIBLIOGRAPHY

1. Boddy, D. E., "On the Design of Analog Fluidic Circuits," Fluidics Quarterly, Vol. 3, No. 1, p. 1-15 (1971).

2. Parker, G. A. and Addy, M. K., "The Use of Low Gain Amplifiers in Shaping Networks," J.A.C.C., Boulder, p. 559-567 (1969).

3. Doherty, M. C., "Applying Operational Amplifiers," Advances in Instrumentation, Vol. 23, Part II (1968).

4. Young, R. W, "The Jet Beam Deflection Amplifier," Bendix Technical Journal, Vol. 1, No. 4, p. 19-27 (1969).

5. Boothe, W. A., Ringwall, C. G., and Shinn, J. N., "New Fluidic Amplifier Techniques for Speed Control," S.A.E. Aerospace Fluid Power Systems and Equipment Conf., p. 5 (1965).

6. Ostland, O. E. and Bedhuhn, W. G., "Fluidic Yaw Damper System," Air Force Flight Dynamics Tech. Report No. AFFDL-TR-67-24, May 1967.

7. Boothe, W. A., "Feasibility Study of the Application of Fluid Amplifiers to Reactor-Rod Control," N.A.S.A. Rep. CR-54005.

8. Belsterling, C. A., Fluidic Systems Design, Wiley-Interscience, New York, 1971, p. 134.

9. Anderson, B. W., The Analysis and Design of Pneumatic Systems, John Wiley and Sons, New York, 1967, p. 114.

10. Rohman, C. P. and Grogan, E. C., "On the Dynamics of Pneumatic Transmission Lines," Trans. A.S.M.E., Vol. 79, No. 4 (1957).

11. Relsterling, ibid, p. 137.

12. Boddy, ibid, p. 10.

13. Takahashi, Y., Rabins, M. J. and Auslander, D. M., Control and Dynamic Systems, Addison-Wesley, Reading, Mass., 1970, p. 279.